New Applications of Geometric Phase in Optics using Sagnac Interferometer

Thesis submitted for the degree of

Doctor of Philosophy

by

M. Sree Ramana

School of Physics
University of Hyderabad
Hyderabad - 500 046 India

DECLARATION

I hereby declare that the matter embodied in this thesis entitled **"New Applications of Geometric Phase in Optics using Sagnac Interferometer"** is the result of investigations carried out by me in the School of Physics, University of Hyderabad, India, under the supervision of Prof. Surya P. Tewari.

Place: Hyderabad

Date: 6-5-03   **(M. Sree Ramana)**

CERTIFICATE

This is to certify that the work described in this dissertation entitled **"New Applications of Geometric Phase in Optics using Sagnac Interferometer"** has been carried out by **Mr. M. Sree Ramana** under my direct supervision for the full period prescribed under Ph.D. ordinances of the University and the same has not been submitted for any other degree or diploma at this or any other University.

Place: Hyderabad

Date: 6/5/03

07/05/2003

(Dean, School of Physics)

(Prof. Surya P. Tewari)

Acknowledgements

It is indeed a great pleasure to thank all those who have, directly or indirectly, helped in the successful completion of this thesis and I am grateful to everyone who helped me.

At the outset, I wish to thank my guide and guru Prof. Surya P. Tewari who was by my side always, patiently and constantly inspiring, encouraging and guiding me throughout the course. My association with him was a rewarding experience, which I never wish to forget.

I would like to thank the Dean, School of Physics, for making available all the facilities required. I wish to thank all the non-teaching staff for their co-operation. I also wish to thank the authorities of University of Hyderabad, for providing various facilities.

I would like to thank Prof. D. Narayana Rao for his valuable suggestions and co-operation by allowing me to use his lab facilities throughout my course.

I would like to thank Prof. S. Chaturvedi and Dr. Prashanta Panigrahi for spending their time in discussions. I wish to thank all the faculty of School of Physics who taught me and helped me in various ways.

I wish to thank all my lab mates and colleagues for the constant support and encouragement they provided throughout my course. I wish to thank all my seniors who helped me in the early stages of my course and juniors in the latter stages.

A special thanks goes to V. S. Ashoka, G. V. Sudhakar Rao, S. Venugopal Rao, **Prem,** Naga Srinivas, Manoj, Srinath, Anitha, **Palas,** Sastri, Phani, **Soma** and Jyotsna. I also thank Abraham in the office of School of Physics.

Contents

NOTE

In this thesis we have used some abbreviations. Though we have mentioned their usage at respective places we list all the abbreviations used in this thesis here.

BS	Beam Splitter
HWP	Half Wave Plate
LA	Linear Analyzer
LP	Linear Polarizer
NLOE	Nonlinear Optical Element (medium)
OAM	Optically Active Medium
OE	Optical Element
POI	Plane of Interferometer
QWP	Quarter Wave Plate
SI	Sagnac Interferometer

eq.	Equation
eqs.	Equations
fig.	Figure
figs.	Figures
ref.	Reference
refs.	References

We have followed certain notations in the thesis, which we mention here. A number in a square bracket like '[1.15]' gives a reference number. A number in '(..)' at the end of equation/equations gives the number of that equation/equations.

We have shown the figures of each chapter at the end of the chapter.

There is some conflict regarding the spelling of **'GOUY'**. In which way it should be spelt **GOUY** or **GUOY.** In literature both the names are being used. In the book "LASERS' by A. E. Siegman the spelling **'GUOY'** is used and in the book "Principles of Optics" by M. Born and E. Wolf the spelling **"GOUY"** is used. **We use the spelling "GOUY" in this thesis.** Also the initials of Gouy are given differently by different authors. Therefore we choose not to give the initials for Gouy. Though we do not refer to the paper by Gouy we give the reference to complete the list.

ABSTRACT

*Study of different configurations of Sagnac interferometer has been done by placing variety of optical elements inside the interferometer and with different states of polarization of the input beam. Of the configurations studied, some configurations show the nonlinear behaviour of Pancharatnam 's phase in a simple fashion. These have been chosen to develop three new applications. We have developed and demonstrated experimentally an interferometric switch and a double beam polarimeter to determine the optical activity of a medium. We have studied theoretically an N-bit signal generator with slowly relaxing nonlinear medium using Sagnac interferometer and nonlinear behaviour of **Pancharatnam's** phase. Finally we have studied the effect of a lens in a Sagnac interferometer and demonstrate the effect of the difference in the Gouy phase accumulated by the counter propagating beams. This confirms the addition of Gouy phase accumulated in different sections of an optical system. Our Sagnac interferometer setup interestingly compares the addition of Gouy phase before and after a lens along two sequences of optical elements keeping the total path length constant. The question, which arises by looking at Collins chart, viz., "Is there a Gouy phase contribution due to movement on Collins chart by a thin lens transformation?" is also examined experimentally and answered in the thesis. Finally the solution of the propagation of Gaussian beam through a quadratic index medium is obtained by using a quantum mechanical disentangling procedure and Gouy phase from this solution is briefly discussed.*

Introduction

Pancharatnam [1.01,1.02], in 1956, had shown that a polarization state of a light beam allowed to traverse a closed circuit on Poincare sphere (briefly described in appendix A) representing different states of polarization, acquires an additional phase. He found that this phase is equal to half the solid angle subtended by the area enclosed in the closed circuit at the center of the Poincare sphere. This phase is now known as Pancharatnam's phase.

In 1984, Berry [1.03] showed that the wavefunction of a quantum system undergoes a phase shift when the system is adiabatically transported around a circuit in parametric space and the phase is known as geometric phase. Aharonov and Anandan [1.04] gave a formulation of geometric phase in which they showed that the condition of adiabatic evolution is not necessary. Ramaseshan and Nityananda [1.05]; and Berry [1.06] showed that Pancharatnam's phase is a classical analogue of Berry's geometric phase. The results of Pancharatnam's work [1.01,1.02] have been extended to give a more general formulation of geometric phase [1.07]. New approach to geometric phase based on kinematic ideas has been developed by Mukunda and Simon [1.08].

Berry's discovery of geometric phase led to a new field of research in physics. In optics, there is a renewed interest in 1) Pancharatnam's phase in polarization optics, 2) new experiments to reveal the geometry related to the phase of k-space, where k is the wave vector, 3) attempts to show Gouy's phase as a phase related to hyperbolic geometry [1.09] and as a phase related to the geometry of focusing sphere [1.10].

Chiao and Wu [1.11] discussed about Berry's geometric phase in optics and proposed an experiment, later reported by Tomito and Chiao [1.12]. Tomito and Chiao allowed a linearly polarized beam to pass through a helically wound fiber, so

that the direction of propagation makes a closed circuit on the sphere representing directions of propagation (k-space) and comes back to its original direction of propagation. The state of polarization doesn't come back to its original state, but gets rotated by an angle equal to solid angle subtended by the closed circuit at the center of the k-sphere. Chiao et al. [1.13] reported an experiment with nonplanar Mach-Zehnder interferometer where such a geometric phase is observed as a fringe shift. Lipson [1.14] gave a simple derivation of Berry's phase, for an electromagnetic wave propagating around a closed circuit in k-space, by solving Maxwell's equations in a rotating frame of reference. The works in refs. 1.11-14 discuss the phase acquired by a light wave when the direction of propagation is allowed to make a circuit in the k-space.

Several authors reported works on **Pancharatnam's** phase. Experiments for observing and measuring Pancharatnam's phase were reported in refs. 1.15-19. Bhandari and Samuel [1.15] performed an experiment where they measure the phase change in one of the beams in a Mach-Zehnder interferometer, when it traverses along a closed circuit on the Poincare sphere. This experiment involves both unitary and nonunitary transformations on the polarization state of the beam for which the phase change is observed. Chyba et al. [1.16] measured the Pancharatnam's phase using a Michelson interferometer involving only unitary transformations on the polarization state of one of the beams. Unitary transformations in refs. 1.15 and 1.16 are because of waveplates and the nonunitary transformation is due to a polarizer. Hariharan et al. [1.17] used a Sagnac interferometer with linear analyzers and circular analyzer to show Pancharatnam's phase as a geometric phase. Hariharan and Roy [1.18] observed Pancharatnam's phase in optical rotation, using a Sagnac interferometer and an optically active medium. Hariharan and Rao [1.19] performed a simple experiment with white light using Sagnac interferometer to observe Pancharatnam's phase.

Hariharan, Larkin and Roy [1.20] showed that the effects due to the introduction of a variable geometric (Pancharatnam's) phase are different from those due to changes in optical path difference. Earlier in the paper by Simon et al. [1.21], the authors had shown that an evolving geometric phase induces a frequency shift. They also reported an experiment implementing this effect to offset the frequency of a laser

beam. The unbounded nature of Pancharatnam's phase is demonstrated by Love [1.22]. Hariharan [1.23] discusses different possible optical interferometric configurations for the observation of geometric phase. Hariharan [1.24] showed how a Senarmont compensator makes use of the geometric phase in the measure of the phase retardation between two components of an elliptically polarized beam of light. Ernesto De Vito and Alberto Levrero [1.25] compared the classical theoretical analysis of Pancharatnam's phase with quantum mechanical analysis. Martinelli and Vavassori [1.26] report a novel control strategy in the control of the state of polarization and the phase shift using geometric phase concepts. Hariharan and Cidder [1.27] designed an achromatic phase shifter operating on the geometric phase. Hariharan and Roy [1.28] use an achromatic phase shifter operating on the geometric phase for surface profiling.

Works with Pancharatnam's phase took an interesting turn with the reporting of nonlinearity in Pancharatnam's phase [1.29-1.37]. Bhandari [1.29-1.34] discussed about the nonlinearity in the Pancharatnam's phase and about singularities connected with Pancharatnam's phase in detail. Schmitzer, Klein and Dultz [1.35] gave in detail the nonlinearity in Pancharatnam's phase achieved in a different manner. With the help of a simple Young's interference setup they showed optical switching. Tewari et al. [1.36] and Qu Li et al. [1.37] used the principle of Schmitzer et al. to demonstrate optical switching using Sagnac interferometer and Michelson interferometer respectively. The nonlinear character of Pancharatnam's phase in different experimental configuration makes it a versatile tool for applications in optical communications and measurements and hence requires to be investigated.

Though a lot of work has been done involving Pancharatnam's phase, its nonlinear behaviour is yet to be fully exploited. With an objective to improve understanding in this direction and to explore whether the nonlinearity in Pancharatnam's phase can be used for applications, a theoretical and experimental study of a Sagnac interferometer with different optical elements has been undertaken resulting in the thesis titled "New Applications of Geometric Phase in Optics using Sagnac Interferometer". (The works published prior to the discovery of Berry's phase and the

between Berry's phase and Pancharatnam's phase involving Sagnac interferometer which could (or not) be interpreted now in terms of geometric phase are not discussed here - as they take us away from the interest of the present work viz., the nonlinear behaviour of geometric phase).

The reason to choose Sagnac interferometer over other interferometers lies in its inherent advantages. Sagnac interferometer is stable to vibrations, has zero optical path difference under ideal conditions. If the polarization states of the beams are altered without changing the optical path difference as in the case of Sagnac interferometer, then the resultant changes in the interference fringe pattern are because of geometric phase differences only.

Before going into the actual problem of analyzing a Sagnac interferometer with different optical elements it would be better to introduce the method used to do the calculations and analysis in this thesis. A 4x4 matrix method developed using 2x2 Jones matrices [1.38] is used to perform the calculations. It may be remarked here that Spreeuw et. al.[l .39] reported a 4x4 matrix method for a ring cavity. Hariharan et. al [1.23] also used the same matrices in their work. The method presented in this thesis differs from that of in refs.1.23 and 1.39. Here scattering matrices are used instead of the transmission matrices used by others [1.23,1.39]. Scattering matrices are chosen as they give a clear picture of the action of the optical elements, one by one along the path of each beam inside the interferometer.

The reason to work with 4x4 matrices is simple. The interferometer with which this work is carried out is a four-port device with two input and two output ports. Each of the two input beams is made of two linearly independent orthogonal states of polarization. Hence there are four input states and four output states, which have to be related to each other through optical transformations. Using a 4x4 matrix method simplifies the calculations and analysis.

To demonstrate how the 4x4 matrices are constructed, consider a four-arm Sagnac interferometer as shown in fig.1.1 consisting of a beam splitter (BS), three

100% reflecting mirrors M_1, M_2, M_3 and a retardation plate (OE). A beam entering face-1 is divided into two at the beam splitting surface. The two beams emerge out from face-3 and face-4. The beam emerging from face-3 travels anti-clockwise along the path $M_1M_2M_3$ and reaches the face-4; and the beam emerging from face-4 reaches face-3 by travelling in the clockwise direction. These two beams merge at the beam splitting surface only to be split again into two beams, which emerge out from face-2 and face-1 as output beams. Similar analysis can be done if a beam enters the interferometer from face-2. Since each beam is made of two orthogonal states of polarization one has four linearly independent states entering the interferometer at face-1 and face-2 and four states emerging out from face-1 and face-2.

If $E_i = (E_\parallel^1, E_\perp^1, E_\parallel^2, E_\perp^2)^T$ is the 4x1 column vector representing the four input states on face-1 and face-2, where $\parallel$ and $\perp$ stand respectively for the components parallel and perpendicular to a plane of reference like the plane perpendicular to the plane of the interferometer (plane containing the axes of propagation of all beams in the Sagnac interferometer), then the output from Sagnac interferometer can be written as $E_o = S\ E_i$. Here S is the 4x4 matrix characteristic of Sagnac interferometer and E_o is the 4x1 column vector representing the output from the interferometer. To find what matrix S is, the Sagnac interferometer is divided into five parts. 1) The beam splitter as the input element of the interferometer, 2) the path from beam splitter till the optical element including the mirror effects, 3) the optical element (non-reflecting), 4) the path from optical element till the beam splitter including mirror reflections and 5) the beam splitter as output port element.

Let the matrix representing BS be S_1. The matrix representing the optical path from BS till the optical element with mirror reflections is obtained by multiplying the 2x2 Jones matrices for each of the two beams in the sequence in which they travel till the OE and then combining them to form a 4x4 matrix. Let $P_1 1$, P_{12}, P_{13}, P_14 and P_{15} be the 2x2 Jones matrices of the optical paths travelled by the beam emerging from face-3 and reaching face-4 in that order. Let P_{21}, P_{22}, P_{23}, P_{24} and P_{25} be the 2x2 Jones matrices of the optical paths travelled by the beam emerging from face-4 and reaching face-3 in that order. Let M_1, M_2 and M_3 be the 2x2 Jones matrices of the mir-

rors. Consider the beam from face-3 to face-4. It travels P_{11}, M_1 and P_{12} before OE and P_{13}, M_2, P_{14}, M_3 and P_{15} till BS. Therefore the matrix for this beam from BS to OE is given by $P_1 = P_{12} M_1 P_{11}$, and the matrix from OE to BS is given by $P_2' = P_{15} M_3$ P14 $M_2 P_{13}$. Similarly for the beam from face-4 to face-3 one has $P_2 = P_{23} M_2 P_{22}$ M3 P_{21} from BS to OE and $P_1' = P_{25} M_1 P_{24}$ from OE to BS. Now the matrix representing the path from BS to OE with mirror reflections for the two beams is given by S_2 and the matrix representing the path from OE to BS with mirror reflections for both beams is given by S3, where

$$S_2 = \begin{bmatrix} P_1 & O_2 \\ O_2 & P_2 \end{bmatrix}, \quad S_3 = \begin{bmatrix} P_2' & O_2 \\ O_2 & P_1' \end{bmatrix}, \quad P_{ij} = \begin{bmatrix} \exp(-i\Delta_{ij}) & 0 \\ 0 & \exp(-i\Delta_{ij}) \end{bmatrix} \quad \text{and}$$

$$M_k = \begin{bmatrix} 1 & 0 \\ 0 & -1 \end{bmatrix}$$

Δ_{ij} is the phase due to optical path travelled by the interfering **beams.** $i = 1,2; j = 1,5$ and $k = 1,2,3$ with O_2 being the 2x2 null matrix.

For a non-reflecting optical element the matrix is given by

$$S_4 = \begin{bmatrix} OE_1 & O_2 \\ O_2 & OE_2 \end{bmatrix}, \text{ where } OE_1 = \begin{bmatrix} oe_{11} & oe_{12} \\ oe_{13} & oe_{14} \end{bmatrix}, \quad OE_2 = \begin{bmatrix} oe_{21} & oe_{22} \\ oe_{23} & oe_{24} \end{bmatrix}.$$

Matrix representing the BS is given by

$$S_1 = \begin{bmatrix} r_\| & 0 & it_\| & 0 \\ 0 & r_\perp & 0 & it_\perp \\ it_\| & 0 & r_\| & 0 \\ 0 & it_\perp & 0 & r_\perp \end{bmatrix}$$

where, r's and t's are the reflection and transmission coefficients.

The total matrix is now given by S = S_1 S_3 S4 S_2 S_1. Thus one constructs the 4x4 matrices for any configuration of Sagnac interferometer and these matrices will be different for different configurations. The matrix described above is used in this thesis to do the theoretical calculations. In appendix B, the matrices relevant to different chapters of the thesis are given.

The thesis presents a detailed study of Sagnac interferometer with different optical elements and brings out three new applications with Pancharatnam's phase. All these applications use the nonlinearity in Pancharatnam's phase when an optical element, placed in one of the arms of the interferometer, is rotated. In appendix C a calculation to reveal the nonlinear variation of Pancharatnam's phase on Poincare sphere is given. An optical switch [1.36] is developed and experimentally demonstrated using a four-arm Sagnac interferometer with a quarter waveplate in one of the arms and a linear analyzer in the output arm. A double beam **polarimeter** resulted from the study of a three-arm Sagnac interferometer with an optically active element. Theoretical studies for the development of an ultrafast optical switch and an N-bit optical signal generation [1.40] overcoming the slow relaxation times of the nonlinear medium have been carried out following the work of K. Tajima [1.41]. A theoretical and experimental study of Gouy phase by placing a lens in a three-arm Sagnac interferometer is also presented.

The thesis is organized into following chapters.

1. Introduction
2. Sagnac Interferometer
3. Four-arm Sagnac Interferometric Switch
4. Double Beam Polarimeter
5. Ultrafast Optical Switch and N-bit Signal Generation using slowly relaxing Nonlinear medium
6. A study to show Gouy phase effects through Sagnac interferometer.

Chapter-wise discussion:

In chapter II different configurations of Sagnac interferometer with different optical elements inside and with different input beam polarizations are studied theoretically using the matrix method developed in the first chapter. Theoretical predictions are experimentally verified. Configurations studied include three-arm and four-arm Sagnac interferometers with 50:50 polarizing and non-polarizing beam splitters - with elements like retarder plates, polarizers and optically active media etc.

In chapter III an interferometric switch using a four-arm Sagnac interferometer and Quarter wave plate (QWP) is proposed. The setup consists of a four-arm Sagnac interferometer with a QWP in one of its arms. A linear analyzer is placed in the output arm of the interferometer such that its axis is orthogonal to the input linear polarization. Depending on the angle made by the QWP axes with input beam's polarization plane, switching action is observed when the linear analyzer placed in the output arm is rotated. Both theoretical and experimental studies are carried out.

In chapter IV entitled "Double Beam Polarimeter", the principle and development of a double beam polarimeter using a three-arm Sagnac interferometer is described. The setup consists of a three-arm Sagnac interferometer with 50:50 non-polarizing beam splitter, an optically active element, a quarter wave plate and a linear polarizer. The optically active element is placed in the central arm of the interferometer. A QWP is placed in the output arm of the interferometer followed by the polarizer. A beam, linearly polarized in the vertical direction, is allowed to pass through the interferometer. When the beam passes through the optically active element, its plane of polarization gets rotated and the two output beams will have different linear polarizations with their polarizations planes being separated by an angle equal to twice the optical activity. The QWP is so placed that these two beams will have elliptical polarizations on either side of and close to, the equator on Poincare sphere after passing through the QWP. If the polarizer is rotated movement of fringes is observed. Most of this movement of fringes takes place within an angle equal to twice the optical activity. Thus measuring this angle within which the major fringe shift occurs, op-

tical activity can be determined. Theoretical calculations have shown that the smaller the optical activity, sharper is the fringe shift. Hence this method may be more accurate in measuring smaller optical activity.

In chapter V, theoretical studies, for the generation of an N-bit signal overcoming the slowly relaxing nonlinear media are discussed. The proposed setup uses a three-arm Sagnac interferometer, consisting of a 50:50 non-polarizing beam splitter, two quarter-wave plates, two optical elements of nonlinear material (NLOE) and an analyzer. All the elements are arranged in such a way that no output is observed when a continuous wave (cw) probe beam, linearly polarized parallel to the plane of interferometer is passed through the interferometer when the NLOE are not excited. When the NLOEs are excited using strong pulses (pumps), they change the phase of the probe and an output signal is observed. For each excitation of an NLOE there are two output signals S_1 and $S_1^{/}$ (clockwise and anti-clockwise) of the probe beam. They are limited by the relaxation time τ_r and are separated by the optical path they travel in Sagnac interferometer. For sequential excitations of the two NLOE, there are two sets of two signals each (S_1, $S_1^{/}$, and S_2, $S2$) on the probe beam outside the interferometer. To overcome the limitation due to the relaxation times of the NLOE, the delay between the pumps is manipulated such that an output signal having pulses with widths shorter than the relaxation time are produced. The sequences of such pulses are allowed to overlap in a particular order to give rise to an N-bit optical signal.

In the case of retarder plates, analyzers and optically active medium as an optical element in Sagnac interferometer, polarization changes are involved and hence Pancharatnam's phase. When one uses a lens as an optical element in Sagnac interferometer another geometric phase is involved. This is an interesting case as this involves Gouy phase. Note that the effect of lens on the Gaussian beam is to change its beam waist resulting in changes to Gouy phase of the beam. How these changes affect the output from Sagnac interferometer, are studied in chapter VI. These studies become important keeping in view the possibility of nonlinear refractive index changes in high intensity laser experiments like the N-bit signal generation. If the changes in the refractive index have spatial distribution which is radial in nature then the system

will show lens effects too. This in turn will affect the beam phase properties. In order to analyze such effects one should know the effect of an ordinary lens. An experiment is performed to show the effect of a lens in Sagnac interferometer involving changes in Gouy phase. This setup consists of a three-arm Sagnac interferometer. The input beam is TEMoo Gaussian beam, and is passed through the interferometer such that its beam waist falls inside the interferometer. A lens is moved inside the interferometer and the resulting output is observed. One has three cases in this experiment.

1) The beam waists of the counter propagating beams fall short of each other i.e., in order to reach the waist of one beam from the beam waist of the second beam we have to travel in the forward direction.

2) Beam waists of both beams are coincident.

3) The beam waists of the two beams cross each other i.e., in order to reach the beam waist of one beam from the beam waist of the second beam one has travel in reverse direction.

In conclusion, results of this thesis are summarized.

References:

1.01   "*Generalized theory of interference and its applications*", S. Pancharatnam, Proc. Indian Acad. Sci. A 44 , 247 (1956)

1.02   "*Collected Works of S. Pancharatnam*", edited by G. W. Series (Oxford University Press, New York, 1975)

1.03 "*Quantal phase factors accompanying adiabatic changes*", M. V. Berry, Proc. R. Soc. London Ser. A **392,** 45 (1984)

1.04   "*Phase change during a cyclic quantum evolution*", Y. Aharnov and J. Anandan, Phys. Rev. Lett. 58, 1593 (1987)

1.05 *"The interference of polarized light as an early example of Berry's phase",* S. Ramaseshan and R. Nityananda, Curr. Sci. (India) 55, 1225 (1986)

1.06 *"The adiabatic phase and Pancharatnam's phase for polarized light",* M. V. Berry, J. Mod. Opt., 34, 1401 (1987)

1.07 *"General setting for Berry's phase",* J. Samuel and R. Bhandari, Phys. Rev. Lett. 60, 2339(1988)

1.08 *"Quantum kinematic approach to the geometric phase I. General formalism",* N. Mukunda and R. Simon , Annals of Physics 228, 205, 1993

1.09 *"Bargmann invariant and the geometry of Gu'oy effect",* R. Simon and N. Mukunda, Phys. Rev. Lett. 70, 880, 1993

1.10 *"Topological phase in Gaussian beam optics",* D. Subbarao, Opt. Lett. 20, 2162, 1995

1.11 *"Manifestations of Berry's topological phase for the photon",* R. Y. Chiao and Yong-Shi Wu, Phys. Rev. Lett. 57, 933 (1986)

1.12 *"Observation of Berry's topological phase by use of an optical fiber",* A. Tomita and R. Y. Chiao, Phys. Rev. Lett. 57, 937 (1986)

1.13 *"Observation of a topological phase by means of a nonplanar Mach-Zehnder interferometer",* R. Y. Chiao, A. Antaramian, K. M. Ganga, H. Jiao, S. R. Wilkinson and H. Nathel, Phys. Rev. Lett. 60, 1214 (1988)

1.14 *"Berry's phase in optical interferometry: a simple derivation",* S. G. Lipson, Optics Lett. 15, 154, 1990

1.15 *"Observation of topological phase by use of a laser interferometer",* R. Bhandari and J. Samuel, Phys. Rev. Lett., 60, 1211 (1988)

1.16 *"Measurement of the Pancharatnam phase for a light beam",* T. H. Chyba, L. J. Wang, L. Mandel and R. Simon, Opt. Lett., 13, 562, 1988

1.17 *"The Pancharatnam phase as a strictly geometric phase: a demonstration using pure projections",* P. Hariharan, Hema Ramachandran, K. A. Suresh and J. Samuel, J. Mod. Opt., 44, 707, 1997

1.18 *"The geometrical phase in optical rotation",* P. Hariharan and M. Roy, J. Mod. Opt., 40, 1687, 1993

1.19 *"A simple white-light interferometer operating on the Pancharatnam phase",* P. Hariharan and D. N. Rao, Curr. Sci., 65, 483, 1993

1.20   *"The geometric phase: interferometric observations with white light",* P. Hariharan, K. G. Larkin and M. Roy, J. Mod. Opt., 41, 663, 1994

1.21   *"Evolving geometric phase and its dynamical manifestation as a frequency shift: An optical experiment",* R. Simon, H. J. Kimble and E. C. G. Sudarshan, Phys. Rev. Lett. 61, 19 (1988)

1.22   *"The unbounded nature of geometrical and dynamical phases in polarization optics",* G. D. Love, Opt. Comm. **131,** 236 (1996)

1.23   *"Geometric phase interferometers Possible optical configurations"* P. Hariharan, J. Mod. Opt., 40, 985 (1993)

1.24   *"The Senarmont compensator: an early application of the geometric phase",* P. Hariharan, J. Mod. Opt. 40, 2061, 1993

1.25   *"Pancharatnam's phase for polarized light",* Ernesto De Vito and Alberto Levrero, J. Mod. Opt. 41, 2233, 1994

1.26   *"A geometric (Pancharatnam) phase approach to the polarization and phase control in the coherent optics circuits",* Mario Martinelli and Paolo Vavassori, Optics Comm. **80,** 166, 1990

1.27   *"An achromatic phase shifter operating on the geometric phase",* P. Hariharan and P. E. Cidder, Opt. Comm. **110,** 13, 1994

1.28   *"White-light phase-stepping interferometry for surface profiling",* P. Hariharan and Maitreyee Roy, J. Mod. Opt. 41, 2197, 1994

1.29   *"Evolution of light beams in polarization and direction",* R. Bhandari, Physica B **175,** 111(1991)

1.30   *"SU(2) phase jumps and geometric phases",* R. Bhandari, Phys. Lett. A 157, 221(1991)

1.31   *"Observation of Dirac singularities with light polarization. I ",* R. Bhandari, Phys. Lett. A **171,** 262 (1992)

1.32   *"Observation of Dirac singularities with light polarization. II ",* R. Bhandari, Phys. Lett. A **171,** 267 (1992)

1.33   *"Interferometry without beamsplitters - a sensitive technique for spinor phases",* R. Bhandari, Phys. Lett. A **180,** 21 (1993)

1.34   *"On geometric phase from pure projections",* R. Bhandari, J. Mod. Opt. 45, 2187(1998)

1.35   *"Nonlinearity of Pancharatnam's topological phase",* H. Schmitzer, S. Klein and W. Dultz, Phys. Rev. Lett., 71, 1530, 1993

1.36   "*A four-arm Sagnac interferometric switch",* S. P. Tewari, V. S. Ashoka and M. S. Ramana, Opt. Comm. **120,** 235, 1995

1.37   "*Experimental observation of the nonlinearity of the Pancharatnam phase with a Michelson interferometer",* Qu Li, L. Gong, Y. Gao and Y. Chen, Opt. Comm. **169,** 17 (1999)

1.38   "*Ellipsometry and Polarized Light",* R. M. A. Azzam and N. M. Bashara, North-Holland, 1977

1.39   "*Optical ring cavities as tailored four-level systems: An application of the group U(2, 2)",* R. J. C. Spreeuw, M. W. Beijersbergen and J. P. Woerdman, Phys. Rev. A 45, 1213, 1992

1.40   *"N-bit signal generation using a Sagnac interferometer and slowly relaxing nonlinear medium",* M. Sree Ramana and Surya P. Tewari , Proc. of National Laser Symposium -1999, Hyderabad (India), 441, 1999

1.41 "*All-optical switch with switch-off time unrestricted by carrier lifetime"* K. Tajima, Jpn. J. Appl. Phys., 32, L1746, 1993
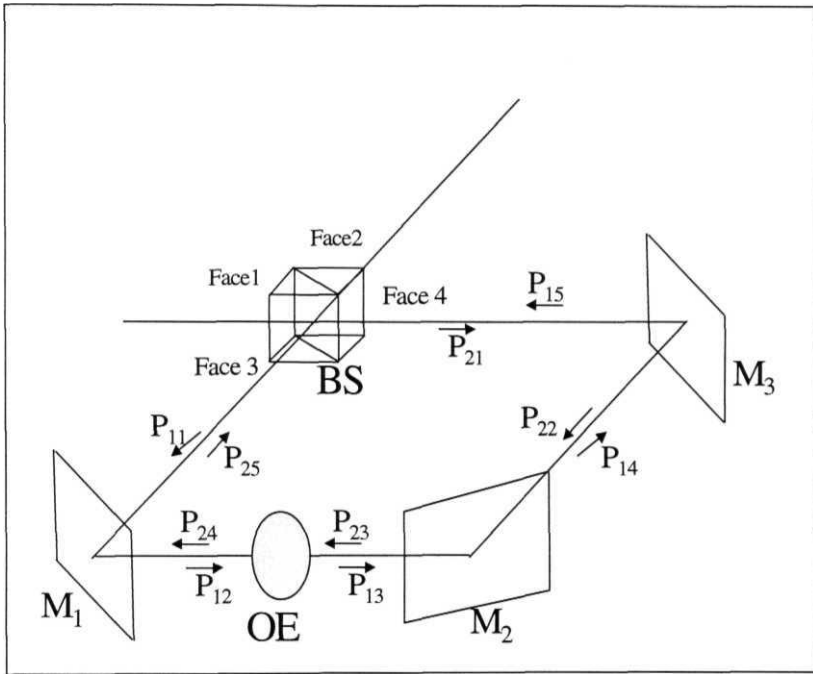
Fig.1.1: A four -arm Sagnac interferometer setup consisting of 50:50 non-polarizing beam splitter (BS), 100% reflecting mirrors (M_1, M_2 and M_3), optical element (OE)

Sagnac Interferometer

Changes in the states of polarization of two interfering beams affect the fringe pattern formed. Pancharatnam's phase is easily revealed as the phase associated with such changes. To study the effects of Pancharatnam's phase one is required to choose an interferometer. Sagnac Interferometer [2.1- 9] turns out to be the one made for this type of study. Here, the changes in the interference pattern can solely be attributed to changes in the state of polarization created by a polarization changing optical element placed inside the interferometer. Aim of this work is to study the effects of Pancharatnam's phase on the output of Sagnac interferometer and its nonlinear behaviour. To do that, it is necessary to look into how Sagnac interferometer works and what will be its output in its different configurations (The matrices giving the output for different configurations of Sagnac interferometer are given in appendix B). The best part of Sagnac interferometer is that the polarization states of the two counter-propagating beams can be altered by a single element. Both the beams are made to travel through the same optical element, which changes the polarization. Because of this, both the beams see the same propagation but different polarization effects. Sagnac interferometer is already known for its inherent stability towards vibrations and against any changes in optical path. All these factors make Sagnac interferometer suitable for this study.

The states of polarization of the two beams passing through the interferometer are altered by placing an optical element like a retarder, polarizer and an optically active medium in one of the arms of Sagnac interferometer. As a retarder or a polarizer is rotated, the polarization states change continuously and as a result the fringe pattern changes continuously. These modifications in the fringe pattern depend on the following factors. (i) Number of arms in the interferometer, (ii) type of the beam splitter (BS), (iii) state of polarization of the input beam (iv) nature of the optical element used to alter the polarization. Hence, as a part of the study different configurations of Sagnac interferometer are studied and are supported by experiments wherever possible. The configurations studied are:

I.   Four-arm Sagnac interferometer with non-polarizing 50:50 beam splitter.

II.   3-arm Sagnac interferometer with non-polarizing 50:50 beam splitter.

III.   Both the above configurations with polarizing beam splitter.

In each of the above cases, different optical elements are placed inside one of the arms and the output is observed for different states of polarization of the input beam. Though, some of these cases have been discussed in literature earlier, for the sake of completeness they have been included.

I. Four-arm Sagnac Interferometer.

Consider the four-arm Sagnac interferometer shown in fig 2.1 consisting of a 50:50 non-polarizing beam splitter (BS), three 100% reflecting mirrors (M_1, M_2 & M_3). The four elements of four-arm Sagnac interferometer, i.e., beam splitter and the three mirrors are arranged at the corners of a quadrilateral of suitable perimeter. One of the two faces marked 1 & 2 acts as an entrance for the input beam and the other acts as an exit for the output (though output beams emerge out of both the faces, the face other than the input face is considered keeping in view the experimental convenience).

Let a laser beam be incident on **face-1** of the beam splitter. This beam gets split into two at the beam splitting surface of the beam splitter. These beams marked B_1 and B_2 counter-propagate in the interferometer travelling the same path and meet again at the beam splitter. The beam travelling clockwise will take the path beam splitter - M_3 - M_2 - M_1 - beam splitter, while the counter-clockwise beam just takes the reverse path. Each of these beams is split into two at beam splitter once again, one exiting (not shown) from face-1 and other (shown by outgoing arrow) from face-2. Hence, the output consists portions of the two beams B_1 and B_2 traversing the interferometer. Plane of interferometer (**POI**) is defined as the plane containing the axes of propagation. It is useful now to define and associate with each beam a right handed Cartesian coordinate system. A beam travels along the z-axis of its coordinate system. The x-axis of the coordinate systems of different beams in **fig.2.1** are perpendicular to, and point out from the paper. Consequently the y-z plane in **fig.2.1** coincides with

POL It is readily seen that a polarization vector $E(e_x, e_y)$ at the input face-1 transforms at the output stage on face-2 as $E(e_x, -e_y)$ with respect to the coordinate system of the beams. This is due to the change in the sign of the component parallel to POI at each reflection. Thus a linearly polarized input coherent beam produces two coherent beams with similar polarization at the exit face-2.

Now consider the case when an optical element with an axis is placed in one of the arms of Sagnac interferometer as shown in fig.2.2. Let φ be the angle made by the axis of the optical element with x-axis. The counter-propagating beams see this optical element differently. One of the beams sees the optical element's axis making an angle $+\varphi$ (plus (p) with x-axis and the other beam sees the optical element to make an angle $-\varphi$ (minus φ). Hence, the polarization of the output beams will be different and will depend on the polarization of the input and the nature of the optical element.

The intensity pattern of the output of a four-arm Sagnac interferometer for an arbitrary input polarization and any non-reflecting optical element is given by

$$I_o = \left|E_o^x\right|^2 + \left|E_o^y\right|^2$$

$$E_o^x = [oe_{11} - oe_{21}e^{i\Delta}]E_i^x + [oe_{12} - oe_{22}e^{i\Delta}]E_i^y$$

$$E_o^y = -[oe_{13} - oe_{23}e^{i\Delta}]E_i^x - [oe_{14} - oe_{24}e^{i\Delta}]E_i^y$$

$$E_i^x = a$$

$$E_i^y = b\,e^{i\mu}$$

$$(2.1)$$

A is the phase difference due to optical path and the input is elliptically polarized with the component parallel to x-axis being 'a'$(=E_i^x)$ and the component parallel to y-axis is equal to 'b $\exp(i\mu)$' $(=E_i^y)$, μ being the phase advance of the y-component over the x-component. 'oe_{ij}' (i, j=1,2) are the elements of the transformation matrix of the optical element.

1) For retarder plates the transformation matrix elements are given by the following.

$oe_{11} = oe_{21} = \cos^2\varphi + e^{i\delta} \sin^2\varphi$; $oe_{14} = oe_{24} = \sin^2\varphi + e^{i\delta} \cos^2$ (p

$oe_{12} = oe_{13} = -oe_{22} = -oe_{23} = \cos\varphi \sin\varphi (1 - e')$

where, 8 is the retardation strength. 8 = TC/2 represents a quarter wave plate while 8 = TC represents a half wave plate and cp is the angle made by the fast axis of the wave plates with the x-axis.

2) For a linear polarizer the transformation matrix elements are

$oe_{11} = oe_{21} = \cos^2\varphi$ $oe_{14} = oe_{24} = \sin^2\varphi$

$oe_{12} = oe_{13} = -oe_{22} = -oe_{23} = \cos\varphi \sin\varphi$

where (p is the angle made by the axis of the polarizer with the x-axis.

3) For optically active medium the transformation matrix elements are

$oe_{11} = oe_{21} = oe_{14} = oe_{24} = \cos\varphi$; $oe_{12} = -oe_{13} = oe_{22} = -oe_{23} = \sin\varphi$

where φ is the angle by which the input polarization is rotated.

In the following work we consider a few representative cases of the above general expression given in eq.2.1.

A: Input beam is circularly polarized (a = b, μ=±π/2)

The intensity of the fringe pattern, when the incident beam is circularly polarized and when a half wave plate ($\delta=\pi$) is placed in one of the arms of four-arm Sagnac interferometer is given by

$$I_{hwp(\mu=\pm\pi/2)} = [1 - \cos(\Delta \mp 4\varphi)] / 2 \qquad (2.2)$$

Here '+' sign is for (X = -TC/2 (left circularly polarized) and '-' is for $\mu = \pi/2$ (right circularly polarized). In fig.2.3 the fringe pattern is plotted as a function of A (phase difference due to optical path difference between the two counter propagating beams) for different values of cp, where φ is the angle made by the fast axis of the half wave plate with x-axis. It is observed from the intensity expression and from fig.2.3 that, as the

half wave plate is rotated the fringes move across the observation plane i.e., along the A axis linearly. To see how Pancharatnam's phase evolves it is better to do the analysis using the Poincare sphere (fig.2.4). (For the details of the representation of polarization on Poincare sphere see Appendix A). Let the input polarization be right circularly polarized. Therefore the state of polarization of the counter-propagating beams is also circularly polarized just before passing through the half wave plate (the state of polarization of the beams before passing through the optical element of course depends on the arm in which the optical element is placed in Sagnac interferometer). Let the input right circular polarization be represented by the North Pole on the Poincare sphere for both the beams. As the two beams pass through the half wave plate the polarization changes from right circular to left circular. To define the trajectories on the Poincare sphere, along which these changes take place, one has to define an axis with respect to which all the calculations are done. The axis, which is chosen here, is the axis perpendicular to the plane of interferometer i.e., parallel to x-axis. The paths taken for the changes depend on the angle φ, which is the angle made by the fast axis of the half wave plate with the x-axis. When $\varphi = 0°$ the position of the axis of the half wave plate is taken to be lying on the equator at the point representing the linearly polarization along x-axis. Then the transformation occurs along the longitude passing through the linear polarization state, with azimuth -45° (with respect to x-axis), represented by the -90° point on the equator of the Poincare sphere. To know why the beams take the trajectories mentioned above, consider the half wave plate to be made up of two quarter wave plates. It is known that when a right circularly polarized light passes through a quarter wave plate, it gets converted into a linearly polarized light with its azimuth at -45° to the fast axis of the quarter wave plate. In this case, the first quarter wave plate will convert the right circularly polarized beam into a linearly polarized with azimuth at -45° (cutting the equator accordingly) and the second quarter wave plate will take it from equator to the left circular polarization state. Also, the trajectory to be taken by the beams should be along a circle, which is perpendicular to the axis joining the center of the Poincare sphere and the point representing the axis of half (or quarter) wave plate. In this case, as the input polarization is North Pole the circle along which the transformation takes place is a great circle i.e., a longitude.

When half wave plate is at $\varphi = 0°$ the trajectories take the paths mentioned above. As the half wave plate is rotated, φ changes and the paths taken for the transformation will be different for the two beams. This is because the beams see the axis of the half wave plate differently. One beam sees it at $-\varphi$ whereas the second sees it at $+\varphi$. Hence, for any arbitrary value of φ the transformation for one of the beams will be along the longitude passing through the point - 90° + 2(p on equator representing linear polarization state with azimuth φ - 45 , whereas for the other beam it will be along the longitude passing through the point - 90° - 2φ representing linear polarization (coming out of quarter wave plate) with azimuth $-\varphi$ - 45°. As the half wave plate is rotated, area covered by the two longitudes changes resulting in a change in the Pancharatnam's phase. Solid angle subtended by the area between the two longitudes at the center of the sphere is equal to 8φ. Pancharatnam's phase is half of this solid angle i.e., 4(p. It is clear that Pancharatnam's phase changes linearly with the change in (p. Therefore the intensity fringe movement is continuous and linear with the change in φ.

Experimental fringes for this case are shown in **fig.2.5** (print out of CCD images). In this figure we show the fringe pattern for (p = 0°, 45°, 90° 135° etc. The fringes move across the plane of observation towards right as in the theoretical fringe patterns.

When the half wave plate is replaced by a quarter wave plate $(\delta=\pi/2)$, it is observed in the experiments that the fringe pattern shows variation of the contrast of the fringes along with the movement of fringes. The fringe pattern is then governed by

$$I_{qwp(\mu=\pm\pi/2)} = [4 - 2\cos\Delta - 2\cos(\Delta \mp 4\varphi)]/4 \qquad \textbf{(2.3)}$$

with $\pm$ meaning the same as in the expression for the half wave plate. In this expression there are three terms. The first and third terms are similar to the terms in the intensity expression for the case of half wave plate. The second term creates a stationary fringe pattern in the field of view, which does not change with rotation of quarter

wave plate. The third term results in a moving fringe pattern with the rotation of cp. Thus, a fringe pattern moves over a stationary fringe pattern having same width and intensity of the fringes. This effect shows a variation in the contrast of the fringes along with the movement of fringes (fig.2.6). There are four positions where the fringe pattern disappears. At these points the states of polarization of the output beams are orthogonal to one another. This happens when cp = 45°, 135°, 225° and 315°. A similar variation of the contrast is observed when a linear polarizer is used instead of the quarter wave plate. The fringe pattern in this case has the same expression as for quarter wave plate except that the intensity gets reduced by 50%. To look at the role played by Pancharatnam's phase in both the quarter wave plate case and the linear polarizer case, Poincare sphere (fig.2.7) is used. Let the input beam be represented by the North Pole. In both cases, the trajectories of transformation end up on the equator but at different points. The trajectories followed for an arbitrary angle cp of quarter wave plate, are the longitudes which pass through the points - 90° + 2cp (P_2) and - 90° - 2cp (P_1) representing the linear polarization states with azimuths cp - 45° and -cp - 45° respectively. In the case of linear polarizer, the trajectories are longitudes passing through the points +2cp (P_3) and -2cp (P_4) representing the linear polarization states with azimuths +cp and -cp respectively.

Now consider the case where an optically active medium is placed as an optical element. The intensity expression for the fringe pattern is given by

$$I_{oam(\mu=\pm\pi/2)} = \frac{(a^2 + b^2)}{4}[1 - \cos(\Delta)]$$
 (2.4)

The above expression doesn't contain any term involving the optical rotation angle. Also the counter propagating beams see the optically active medium in the same way unlike in the earlier cases of wave plates. Because of this the output beams end with same polarization whatever be the angle of optical rotation. Therefore, there will not be any changes in the fringe pattern as one varies the optical rotation in a four-arm Sagnac interferometer.

B: Input beam is linearly polarized ($\mu = 0$)

Intensity of the fringe pattern when the input beam is linearly polarized parallel to x-axis (b=0) and a half wave plate is placed in one of the arms of a four-arm Sagnac interferometer, is given by the expression

$$I_{hwp(\mu=0)} = a^2 \left[2 - \cos(\Delta - 4\varphi) - \cos(\Delta + 4\varphi) \right] / 4 \qquad \textbf{(2.5)}$$

Where A is the phase due to optical path difference between the two beams and φ is the angle made by the fast axis of the half wave plate with the x-axis. On rotation of half wave plate the intensity of the fringes (fig.2.8) is observed to vary. This is in contrast to the movement of the fringes observed when input beam is circularly polarized, discussed earlier. Experimentally, in a full *2n* rotation of half wave plate, fringe pattern disappears eight times. This observation can be explained by the above expression. Here superposition of two fringe patterns moving in opposite directions takes place resulting in the variation in the intensity of the fringes. There is no difference with the change in the azimuth of the linear polarization of the input beam. From fig.2.8 it is observed that the intensity of the peaks start reducing as the half wave plate is rotated while the intensity of the minimum intensity points start increasing. At a point, (p = 22.5 , the intensities of the peaks and the minimum intensity points become equal resulting in the disappearance of the fringes. As the half wave plate is further rotated, the intensities of the earlier minimum points keep on increasing while the intensities of the earlier peaks keep on decreasing. As a result there is a swapping of the peaks with minima, after the disappearance of the fringe pattern. After reaching the maximum intensity point at $\varphi = 45$, the intensity of the new peaks start reducing and that of the new minimum points start increasing leading to another disappearance of the fringes and swapping of the peaks. This happens a total of eight time in a 2π rotation of the half wave plate and nowhere the total intensity becomes zero. In fig.2.9 experimental fringe pattern is shown for $\varphi = 0$, 22.5 , 45 , 67.5 , 90 etc. These patterns agree with the theoretical fringe patterns. Observe the swapping of the peak after the zero contrast patterns.

Replacing half wave plate with a quarter wave plate, it is observed that the fringe pattern when b=0 follows the expression given by

$$I_{qwp(\mu=0)} = \frac{(a^2)}{8}[4 - 2\cos(\Delta) - \cos(\Delta - 4\varphi) - \cos(\Delta + 4\varphi)] \tag{2.6}$$

Where A is the phase due to optical path difference and φ is the angle made by the fast axis of the quarter wave plate with the x-axis. As in the case with circularly polarized input beam, here also the stationary fringe pattern because of the first term (eq.2.6) masks the full effect of the remaining two terms. This causes fringe pattern to disappear four times within 2π rotation of quarter wave plate. The intensity fringe pattern is shown in fig.2.10. Experimental fringe patterns are shown in fig.2.11 for φ = 0°, 45°, 90 , 135 etc. In fig.2.12 a surface graph of the contrast function C=1-V(φ,δ) for linearly polarized incident beam is shown, where V(φ, 5) is the visibility function given by the eq.2.7 for the fringes around A = 0 . From this graph it is clear that all the wave plates with retardation strength $0<\delta\leq\pi/2$ and $3\pi/2\leq\delta\leq2\pi$ show poor visibility four times for a *2K* rotation of the wave plate. The transition from four to eight poor visibility positions occurs at $\delta=\pi/2$ and changes back to four poor visibility positions at $\delta=3\pi/2$. The poor contrast positions, for $\pi/2<\delta<3\pi/2$ are not equally placed on the φ-axis except for $\delta=\pi$ i.e., for half wave plate.)

$$V(\varphi,\delta) = \frac{I_{max} - I_{min}}{I_{max} + I_{min}} \tag{2.7}$$

When a linear polarizer is placed inside the Sagnac interferometer, it is observed that the intensity of the fringe pattern is not similar to the fringe pattern with a quarter wave plate, as in the case with circularly polarized input beam, where both with quarter wave plate and linear polarizer the intensity pattern remains similar. The intensity pattern in this case is given by

$$\begin{aligned} I_{lp(\mu=0)} = &[(a^2\cos^4(\varphi) + b^2\sin^4(\varphi) + (a^2+b^2)\cos^2(\varphi)\sin^2(\varphi)) \\ &- \cos(\Delta)(a^2\cos^4(\varphi) + b^2\sin^4(\varphi) + (a^2+b^2)\cos^2(\varphi)\sin^2(\varphi))]/4 \end{aligned} \tag{2.8}$$

Figure 2.13. shows the intensity pattern for different positions of φ for x and y polarization states of the input beam. It is observed that here also variation of intensity take place as the linear polarizer is rotated. The fringe pattern disappears four times and the total intensity goes to zero twice within a *2n* rotation of the linear polarizer. It is also found that the peak position swaps as in the case of half wave plate but instead of increase in intensity of the minimum position, the intensities of both the peaks and minimum intensity points start decreasing after they become equal. The decrease in the intensity is more compared to that of the minimum intensity points and this leads to the swapping of peak position. The intensities keep reducing until the total intensity becomes zero.

II. 3-arm Sagnac Interferometer with non-polarizing beam splitter.

A 3-arm Sagnac interferometer consists of a beam splitter and two mirrors as shown in fig.2.14. In this case beam splitter is 50:50 non-polarizing and mirrors are 100% reflecting. We can attach a right-handed Cartesian coordinate system to the beams travelling in the interferometer. If we do the polarization analysis for this interferometer one will find that the polarization states of the output beams will be same as that of the input when there is no element placed inside the interferometer. If any element like a wave retarder or a polarizer is placed then also the output beams will have same states of polarization but not same as the input. As a result, there will be no change in the intensity pattern if one rotates the optical element, which will be clear from the analysis given below. The output intensity pattern for an arbitrarily polarized input beam and a non-reflecting optical element is given by

$$I_o = \left| E_o^x \right|^2 + \left| E_o^y \right|^2$$

$$E_o^x = [oe_{11} - oe_{21}e^{i\Delta}]E_i^x + [oe_{12} + oe_{22}e^{i\Delta}]E_i^y$$

$$E_o^y = [oe_{13} + oe_{23}e^{i\Delta}]E_i^x + [oe_{14} - oe_{24}e^{i\Delta}]E_i^y$$

$$E_i^x = a$$

$$E_i^y = b\,e^{i\mu}$$

(2.9)

All the variables and constants carry the same meaning as in eq.2.1.

When a wave retarder is placed inside the three-arm Sagnac interferometer the fringe pattern is given by the following expression.

$$I_o = \frac{(a^2 + b^2)}{2}[1 - \cos(\Delta)] \tag{2.10}$$

It is obvious from this expression that there will not be any variation in the fringe pattern with the rotation of the retarder for any polarization state of the input beam. Similarly when a linear polarizer is placed in one of the arms of three-arm Sagnac interferometer, no change in the fringe pattern is observed. In both these cases the output beams have same polarization state.

Consider the case of an optically active medium placed in one of the arms of Sagnac interferometer. In the four-arm Sagnac interferometer with an optically active medium, it is found that there will not be any change in the fringe pattern. Here, in the three-arm case, the fringe pattern is given by the following expression when the input is linearly polarized.

$$I_{oam} = \frac{(a^2 + b^2)}{4}[2 - \cos(\Delta - 2\varphi) - \cos(\Delta + 2\varphi)] \tag{2.11}$$

This expression is similar to that of half wave plate in four-arm Sagnac interferometer with linearly polarized input. This changes the intensity level only but will not shift the fringe pattern. Pancharatnam's phase doesn't come into picture, as the trajectories do not enclose a surface between them as they lie on the same circle, which will be parallel to equator of the Poincare sphere (fig.2.15). If P represents the input state of polarization then P_1 and P_2 represent the two output polarization states. P_1 and P_2 are separated by an angle 2φ if φ is the amount by which the optically active medium rotates the input polarization states. As the optically active medium only rotates the plane of polarization it doesn't change the ellipticity of the input polarization. Therefore, states of polarization of the output beams will also have the same ellipticity and

hence will lie on a circle parallel to the equator if input arbitrarily polarized. If input is linearly polarized then that circle will be equator itself.

III. Three and four-arm Sagnac interferometers with polarizing beam splitters

Till now the interferometers discussed have a non-polarizing beam splitter. Now the three and four-arm Sagnac interferometer configurations will be studied with a polarizing beam splitter. The intensity fringe pattern is found to be same for both three and four-arm configurations. The fringe patterns for different cases of optical elements are given by the following expressions.

$$
\begin{aligned}
I_{hwp} &= (a^2 + b^2) \cos^2 2\varphi \\
I_{qwp} &= (a^2 + b^2)(\cos^4 2\varphi + \sin^2 2\varphi) \\
I_{lp} &= (a^2 \cos^4 2\varphi + b^2 \sin^4 2\varphi) \\
I_{oam} &= (a^2 + b^2)\cos^2 \theta
\end{aligned}
\qquad (2.12)
$$

I_{hwp}, I_{qwp}, I_{lp} and I_{oam} are the the intensity patterns for half wave plate, quarter wave plate, linear polarizer and an optically active medium as optical elements inside the three and four-arm configurations. φ is the angle which the axes of half wave plate, quarter wave plate and the linear polarizer make with the x-axis. Whereas 0 is the angle of optical rotation of the optically active medium. It is clear from the above expressions (note the absence of A) that one will not have any fringe pattern. There will be change only in the intensity.

We have recorded in this chapter various kinds of variations and changes in the fringe pattern as a result of optical elements placed in a Sagnac interferometer. These changes in the fringe pattern can be used as signals in devices and applications. Also note some of these configurations like a wave plate or polarizer in four-arm configurations with linearly polarized input can show nonlinear behaviour of Pancharatnam's phase. In the next chapter, we study one such device, using this nonlinear behavior of Pancharatnam's phase, called an interferometric switch.

References:

2.01   *"The Pancharatnam phase as a strictly geometric phase: a demonstration using pure projections",* P. Hariharan, Hema Ramachandran, K. A. Suresh and J. Samuel, J. Mod. Opt., 44, 707, 1997

2.02   *"The geometrical phase in optical rotation",* P. Hariharan and M. Roy, J. Mod. Opt., 40, 1687, 1993

2.03   "A *simple white-light interferometer operating on the Pancharatnam phase",* P. Hariharan and D. N. Rao, Curr. Sci., **65**, 483, 1993

2.04   *"The geometric phase: interferometric observations with white light",* P. Hariharan, K. G. Larkin and M. Roy, J. Mod. Opt., 41, 663, 1994

2.05   *"Geometric phase interferometers Possible optical configurations"* P. Hariharan, J. Mod. Opt., 40, 985 (1993)

2.06   *"An achromatic phase shifter operating on the geometric phase",* P. Hariharan and P. E. Cidder, Opt. Comm. **110,** 13, 1994

2.07   *"White-light phase-stepping interferometry for surface profiling",* P. Hariharan and Maitreyee Roy, J. Mod. Opt. 41, 2197, 1994

2.08   "*A four-arm Sagnac interferometric switch",* S. P. Tewari, V. S. Ashoka and M. S. Ramana, Opt. Comm. **120,** 235, **1995**

2.09   *"N-bit signal generation using a Sagnac interferometer and slowly relaxing nonlinear medium",* M. Sree Ramana and Surya P. Tewari , Proc. of National Laser Symposium -1999, Hyderabad (India), 441, 1999
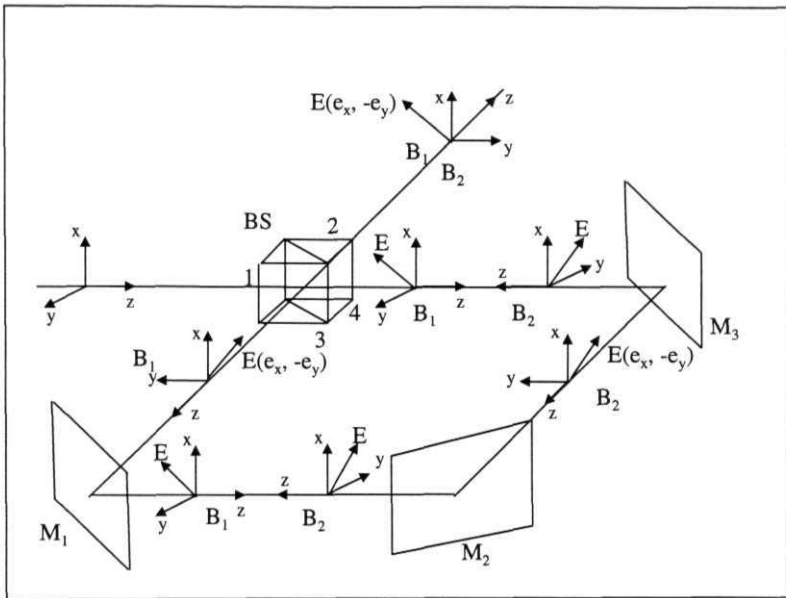
Fig.2.1: This figure shows the setup of a four-arm Sagnac interferometer. It consists of a 50:50 nonpolarizing beam splitter BS, three 100% reflecting mirrors M_1, M_2 and M3. A right handed cartesian coordinate system is attached to the beam in all all the arms. Observe the change in the vector E after each reflection. It changes sign along the y-axis. The output vector is not parallel to the input vector. Both the beams have parallel E-vector. The faces 1, 2, 3 and 4 of the beam splitter are shown by the numbers 1, 2, 3 and 4. B_1 and B_2 are the two counter propagating beams.
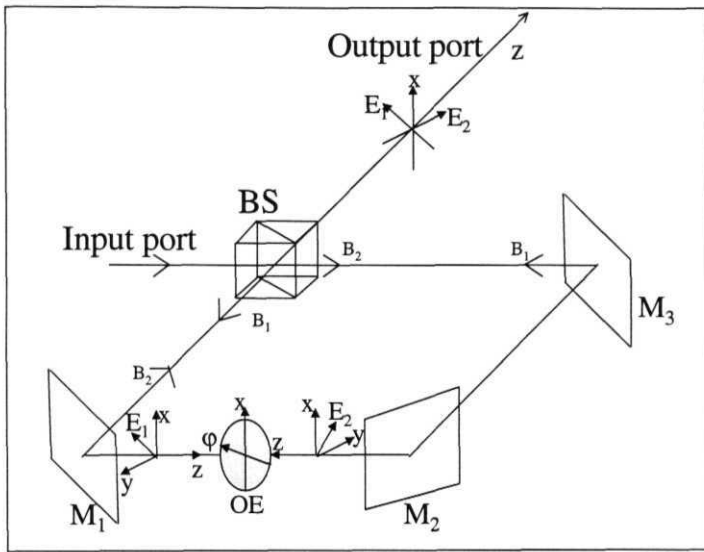
Fig.2.2: Same as fig.2.1 with an optical element and with coordinate frames shown in one arm only. OE is the optical element with its axis making an angle, φ with the x-axis of the coordinate frames of the counter propagating beams. Observe that the axis of the OE will be at an angle φ for the beam 1 (BO and for the beam 2 (B_2) it will be at an angle -(p. As a result the output beams will have their vectors at an angle to each other. This angle will be equal to 4(p when input beam is linearly polarized along the x-axis.
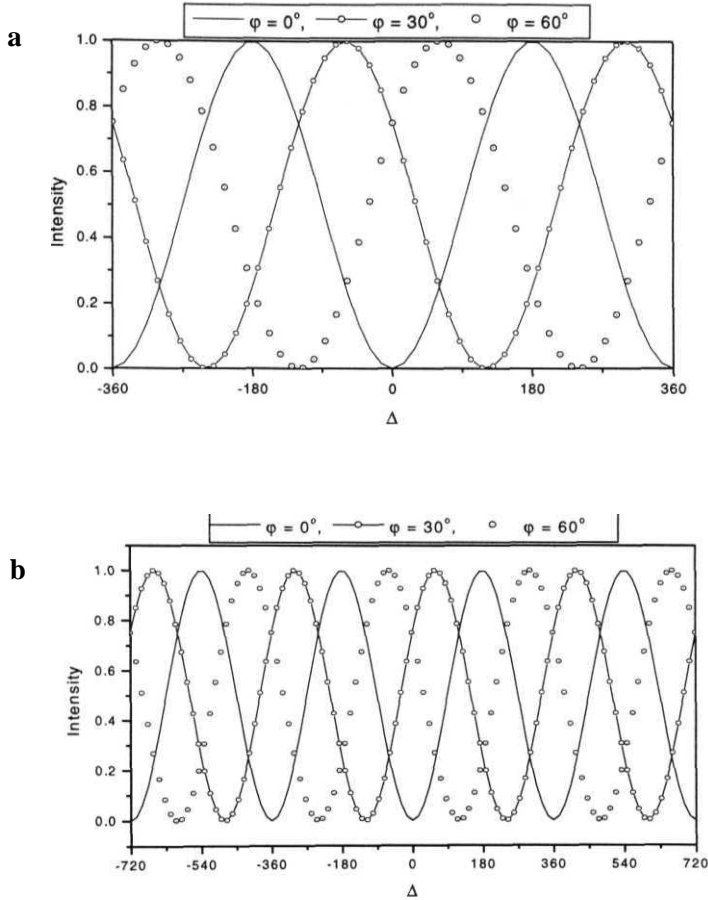
Fig 2.3a and b: Shown is the fringe pattern (eq. 2.2) for circularly polarized input light and **HWP** inside 4-arm Sagnac interferometer. It is clear that as **HWP** is rotated (φ is changed) the fringe pattern moves linearly and the direction of movement (along A-axis) depends on the input polarization as well as the sense of rotation of HWP. a) Input is right circularly polarized and rotation of HWP is anti-clockwise. b) Input is left circularly polarized and rotation of HWP is anti-clockwise.

a

b
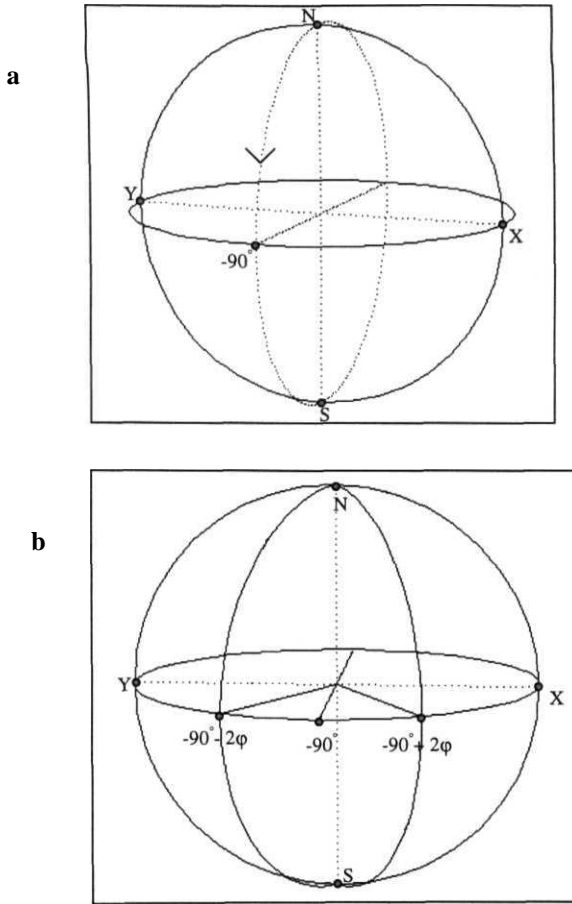
Fig.2.4a and b: Poincare sphere representation of the changes in the polarization states is shown in these figures. The point 'X' represents the linear polarization parallel to x-axis and the point 'Y' represents the linear polarization parallel to y-axis. North Pole represents the right circular polarization while South Pole represents the left circular polarization.

a) In this figure we show the case when the fast axis of the half wave plate is parallel to the x-axis. Observe that both the beams move along the same trajectory $N(-90^{\circ})S$.

b) In this figure we show the case when the fast axis of the half wave plate is an angle φ with the x-axis. Observe the trajectories taken by the two beams in this case. In the earlier case the area enclosed is zero. But here it is not equal to zero. The solid angle subtended by the area enclosed is equal to the 8(p.
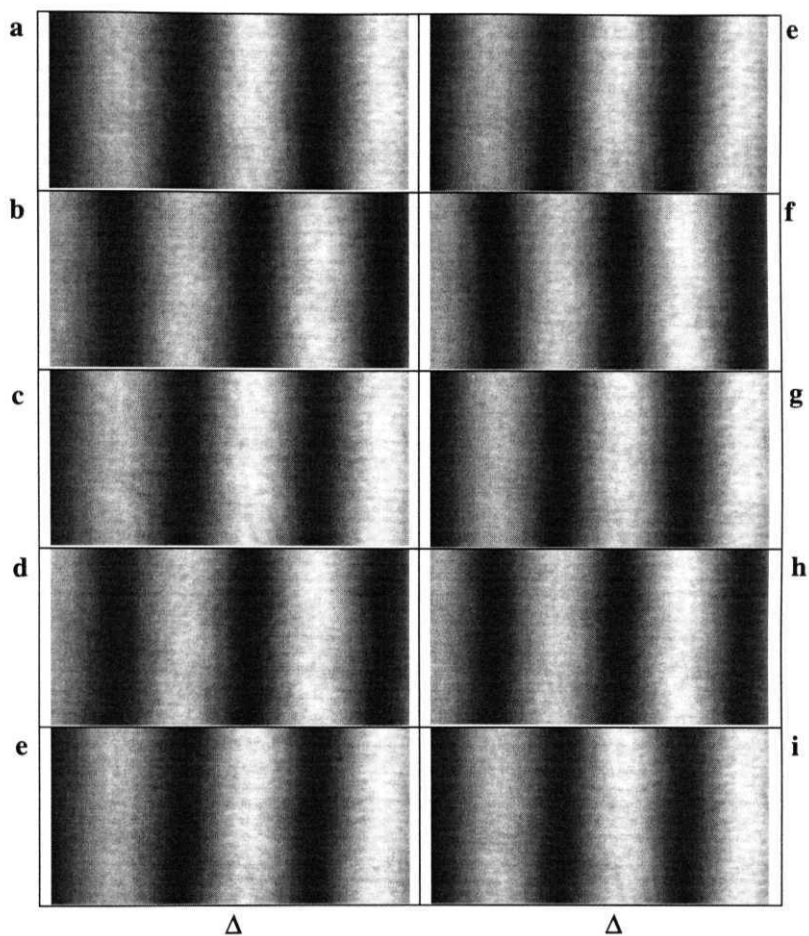
Fig.2.5 : Experimental fringes recorded using a CCD camera, for the case when a half wave plate is placed inside a four-arm Sagnac interferometer and input is circularly polarized, are shown in this figure. Fringe patterns for different angles of half wave plate are shown as the half wave plate is rotated. a) The half wave plate angle is $\varphi = 0°$, b) $\varphi = 45°$, c) $\varphi = 90°$, d) $\varphi = 135°$, e) $\varphi = 180°$, f) $\varphi = 225°$, g) $\varphi = 270°$, h) $\varphi = 315°$ and i) $\varphi = 360°$. Observe the shift in the fringes along the A-axis as the half wave plate is rotated. Though fringe patterns for intermediate angles are not shown it is obvious that the movement is linear along the A-axis with the rotation of half wave plate angle (p.
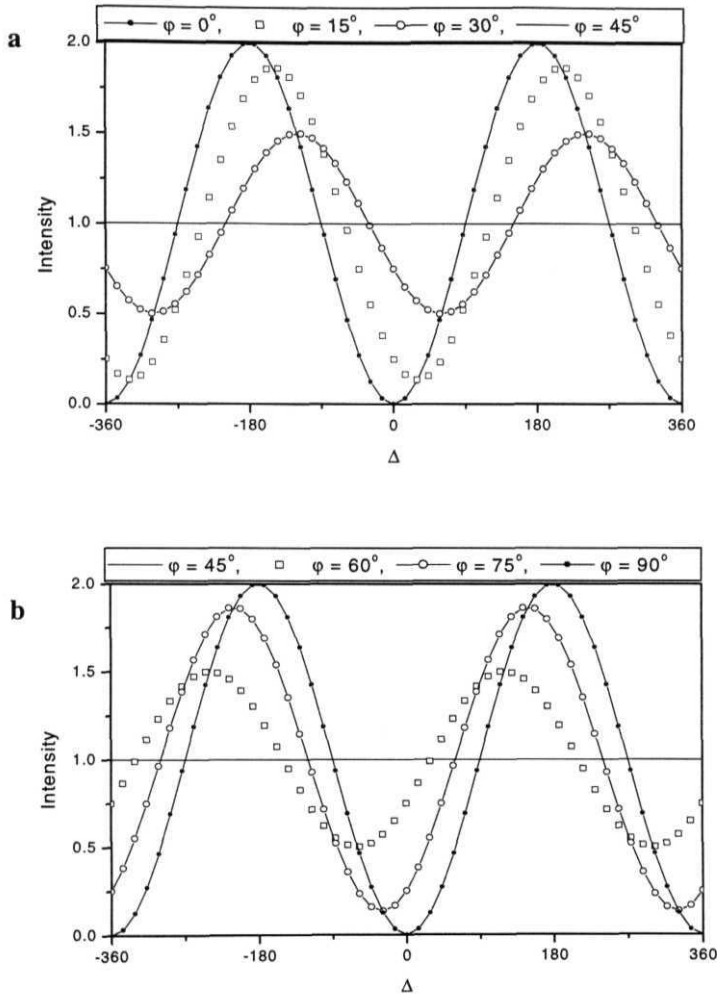
Fie.2.6a and **b:** Fringe pattern for circularly polarized input light and QWP inside the 4-arm Sagnac interferometer. In this case the fringes move and there is change in the visibility (eq.2.7) of fringes as the quarter wave plate is rotated (φ changes). φ is given different values for different curves. Fringes disappear at φ = 45° + nπ (n=0,l,2,..) when the fringe visibility becomes zero (i.e., intensity = constant for all values of A)
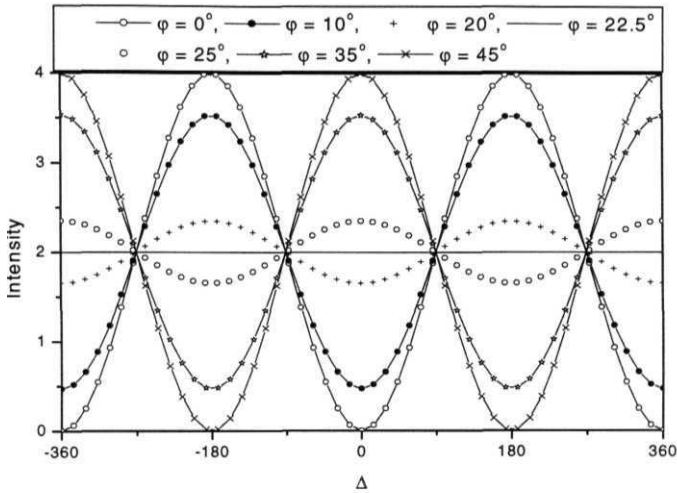
Fi g. 2.7: In this figure we show the Poincare sphere representation of the trajectories taken by the counter propagating beams when a quarter wave plate is placed in a four-arm Sagnac interferometer. If North Pole represents the input polarization then one beam moves along the longitude NP_1 while the other beam take the path along the longitude NP_2. P_1 will be at a point which is -90° - 2(p away from the x-axis and P_2 is at a point -90° + 2(p away from x-axis where φ is the angle made by the fast axis of the quarter wave plate with the x-axis.
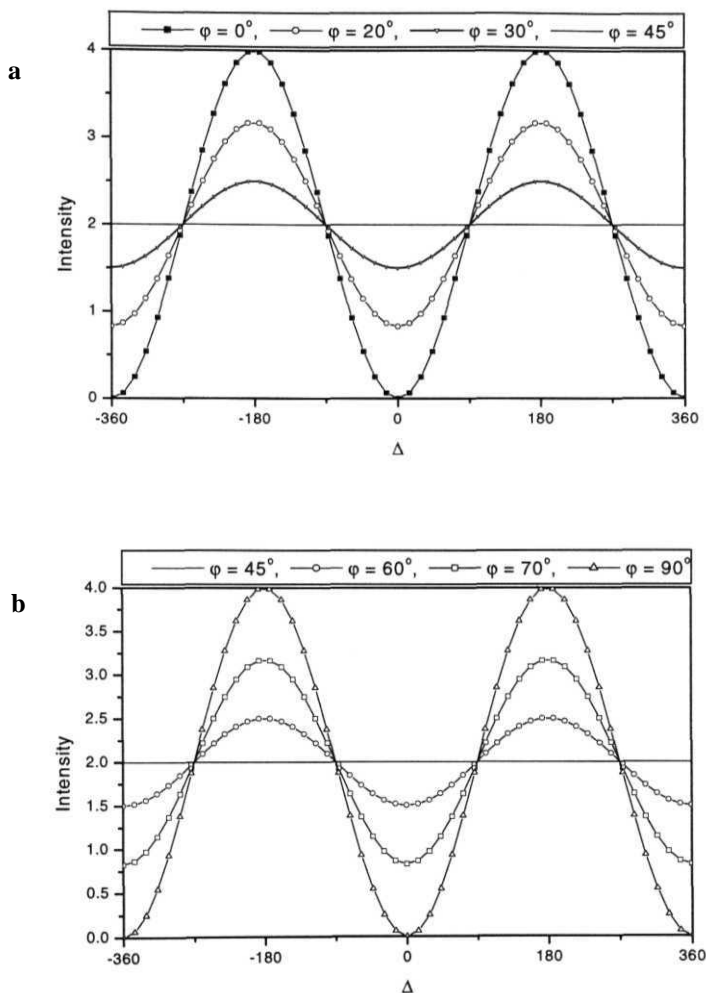
Fig. 2.8: Intensity fringe pattern for the case of half wave plate in a four-arm Sagnac interferometer with input light linearly polarized. Observe the variation in intensity for different values of (p. The fringes disappear at (p = 22.5°. After this disappearance of fringes the peak position swaps with the minimum intensity position.
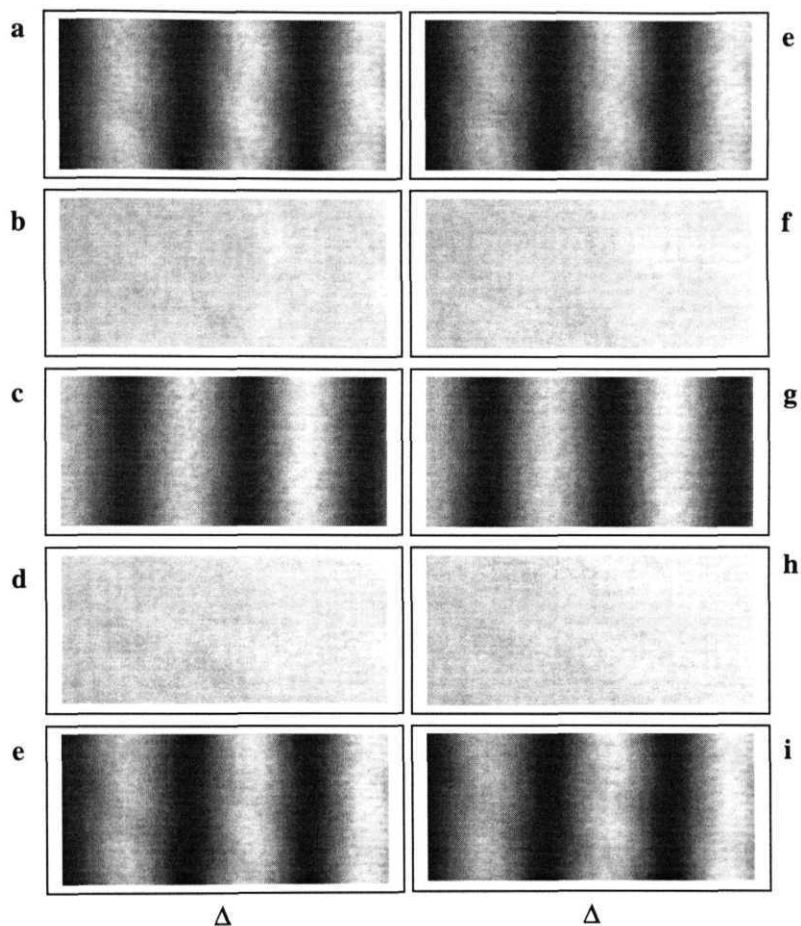
Fig.2.9: In this figure we show the fringe pattern for different angles of half wave plate placed inside a four-arm Sagnac interferometer when the input beam is linearly polarized parallel to x-axis. Observe the zero contrast positions at $\varphi = 22.5°$, $67.5°$, etc. This takes place for every $45°$ and occurs eight times in full $2n$ rotation of the half wave plate. a) (p = 0°, b) <p = 22.5°, c) q> = 45°, d) (p = 67.5°, e) $\varphi = 90°$, f) (p = $112.5°$, g) (p = 135°, h) $\varphi = 157.5°$ and i) $\varphi = 180°$. Observe the swapping of the peak after every zero contrast position.

Fig; 2.10a and b: Intensity fringe pattern for a quarter wave plate placed in a four-arm Sagnac interferometer with input light linearly polarized, parallel to x-axis. Observe that the intensity of the fringes vary as φ is varied. Fringe pattern disappears once in a 90° rotation of quarter wave plate. Note there is no swapping of peaks with minimum intensity points as in the case of half wave plate.
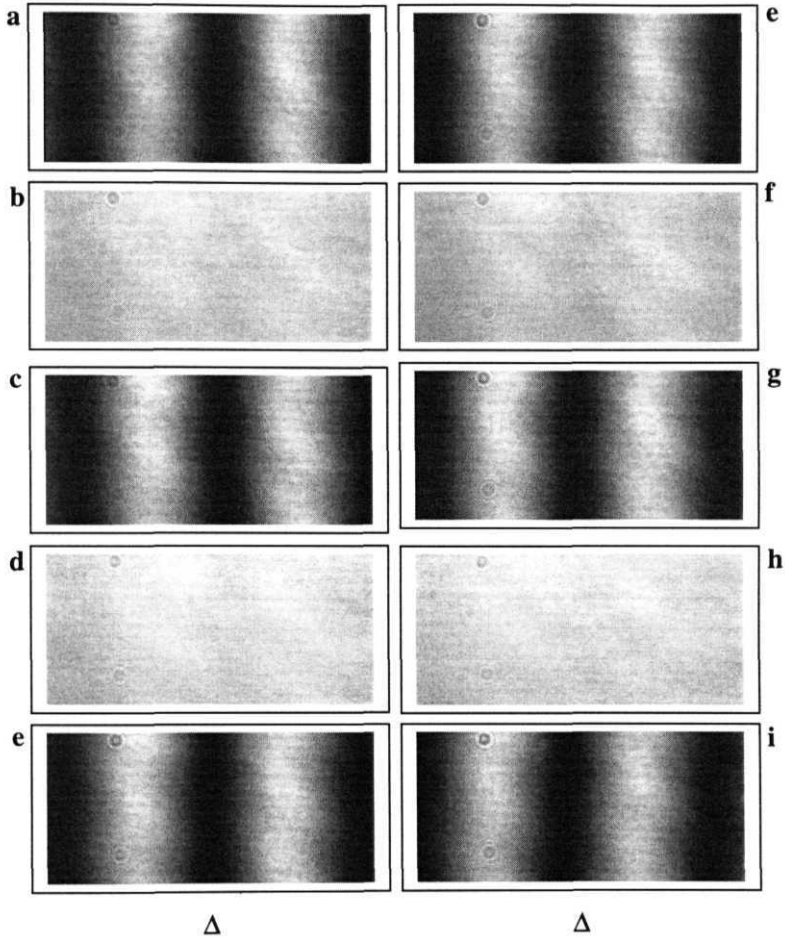
Fig.2.11: In this figure we show the experimental fringe pattern, recorded using a CCD camera, when a quarter wave plate is placed inside a four -arm Sagnac interferometer and input beam is linearly polarized along x-axis. Fringe patterns for different angles (φ) of the quarter wave plate are shown. a) $\varphi = 0$, b) $\varphi = 45$, c) (p = 90°, d) $\varphi = 135°$, e) $\varphi = 180°$, f) (p = 225°, g) $\varphi = 270°$, h) $\varphi = 315°$ and i) $\varphi = 360°$. Observe the disappearance of the fringes for $\varphi = 45$, 135 , 225 and 315 . There is no fringe movement observed here in this case. Only intensity variations take place.
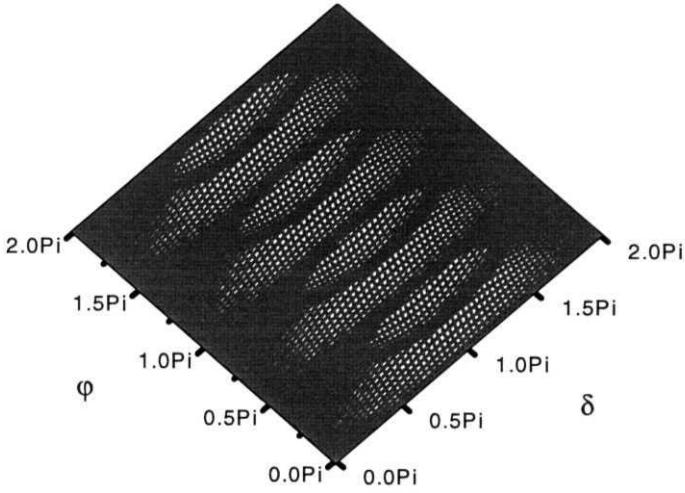
Fig. 2.12: In this figure we show the surface plot of the contrast function defined as C(8, (p) = 1 - v(5, (p), where V is the visibility function around A = 0 point. φ is the angle made by the fast axis of the retarder with x-axis. Here z-axis is not shown but the height at a point on the graph gives the contrast at that point. Observe that the number of contrast positions when 8 = π/2 are four. For δ = ‰ there are eight place where contrast goes to one within a *2K* rotation of the retarder.
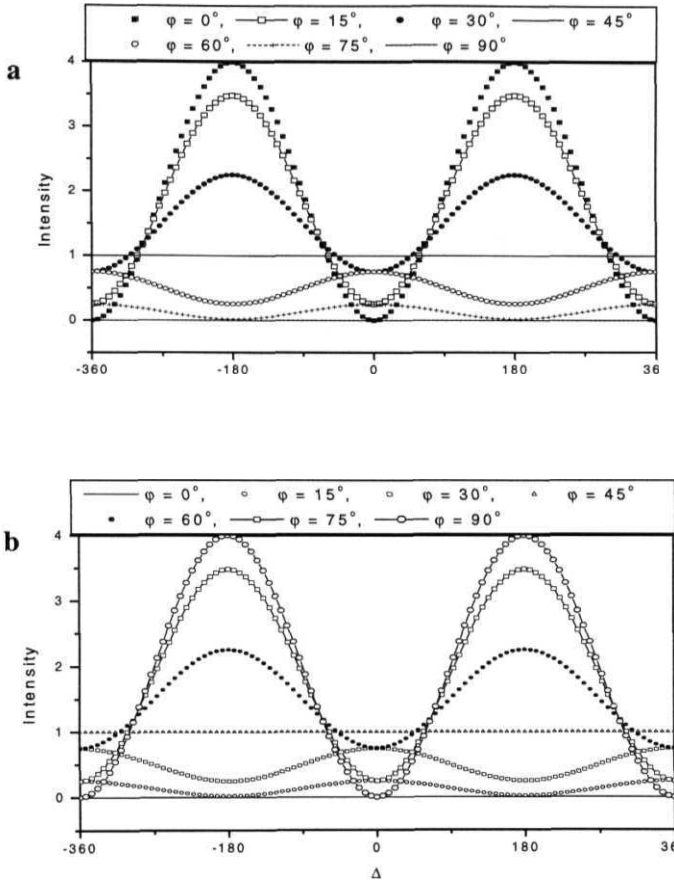
Fig. 2.13: Intensity fringe pattern when a linearly polarizer is placed in a four-arm Sagnac interferometer with input light linearly polarized. Here the intensity varies as ϕ is varied and fringe pattern disappears once within a 90 rotation of the polarizer.

a) Input polarization is parallel to x-axis. Total intensity becomes zero at $\phi = 90$.

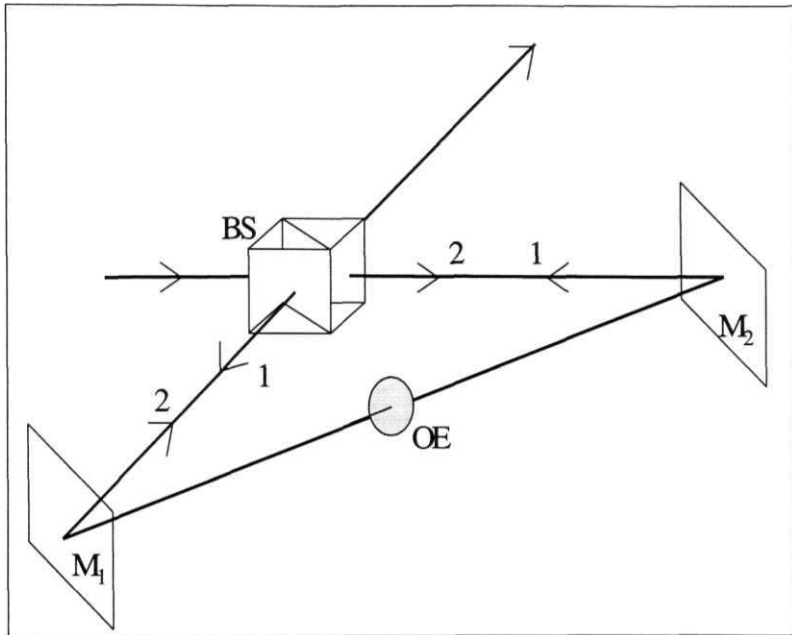b) Input polarization is perpendicular to x-axis (parallel to y-axis). Total intensity becomes zero at $\phi = 0$.

Fig. 2.14: This figure shows a three-arm Sagnac interferometer. An optical element is placed in one of the arms of the interferometer. One can attach a right handed cartesian coordinate system to the beams here also. The two beams emerge out with same polarization as the input if no optical element is placed inside the interferometer. If any optical element like a wave retarder is placed then the two beams have same polarization outside but not same as the input.
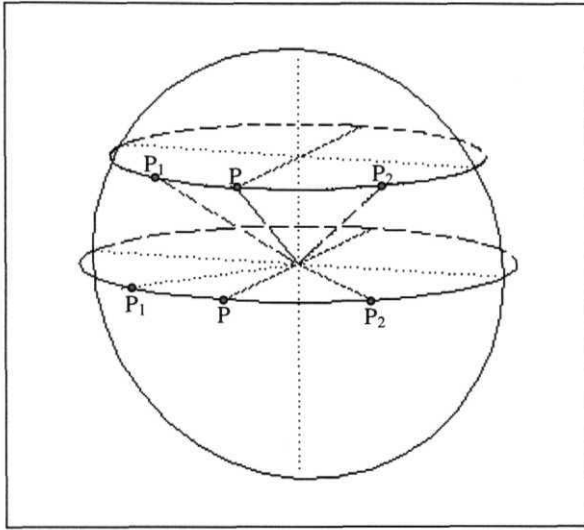
Fig. 2.15: This figure shows the output states of polarization of the counter propagating beams in a three-arm Sagnac interferometer. If P represents the input state of polarization then P_1 and P_2 represent the two output polarization states. P_1 and P_2 are separated by an angle 2⦅p if φ is the amount by which the optically active medium rotates the input polarization states. As the optically active medium only rotates the plane of polarization it doesn't change the ellipticity of the input polarization. Therefore states of polarization of the output beams will also have the same ellipticity and hence will lie on a circle parallel to the equator if the input is arbitrarily polarized. If input is linearly polarized then that circle will be equator itself.

Four-arm Sagnac Interferometric Switch

As briefly mentioned in the introduction, nonlinearity in Pancharatnam's phase has potential for use in optical switching. Schmitzer et. al. [3.1] have demonstrated switching action in Young's interference setup using nonlinear behaviour of Pancharatnam's phase. Also, R. Bhandari [3.2-7] brought out works involving nonlinear behaviour of Pancharatnam's phase. In all these works, principle behind the nonlinear behaviour is same. To see this behaviour, R. Bhandari has projected an elliptically polarized input light onto an analyzer and obtained the phase of the output by interfering it with a reference beam, whose polarization state is same as that of the input. Or modified the states of polarization of two beams and allowed them to interfere after passing them through an analyzer. Schmitzer et. al. projected the two beams which are polarized differently onto a single state of polarization and observed the phase difference in terms of a shift in fringe pattern by rotating the analyzer. From these works, it is clear that to observe the nonlinearity in Pancharatnam's phase one needs to have beams with different elliptical polarizations and project them onto a state of polarization using a suitable analyzer.

In chapter II it is shown that different configurations of Sagnac interferometer give out beams, which are polarized differently. Consider the case where a quarter wave plate is placed inside a four-arm Sagnac interferometer. This configuration gives two beams elliptically polarized such that they are placed on either side of the equator on the Poincare sphere when input beam is linearly polarized either in x or y directions. This configuration can be used for optical switching [3.8] using the nonlinearity in Pancharatnam's phase.

To show the switching, an analyzer is placed in the output arm of the four-arm Sagnac interferometer with a quarter wave plate in one of its arms as shown in fig.3.1. Let the input linear polarization be parallel to x-axis. The quarter wave plate is placed with its fast axis making a small angle with the linear polarization state of the input

beam i.e., x-axis. The analyzer is rotated and the shift in the fringe pattern is moni-
tored using a CCD camera. The intensity of this fringe pattern is governed by the fol-
lowing expression obtained by using the 4x4 matrices as explained in introduction.

$$I_o = [\cos \eta \ (\cos^2 \varphi + i \sin^2 \varphi) \ (1 - e^{i\Delta})]$$

$$-[\sin \eta \cos \varphi \sin \varphi \ (1-i)(1+e^{i\Delta})] \qquad (3.1)$$

Here cp is the angle, which the fast axis of quarter wave plate makes with the input
linear polarization, η is the angle made by the axis of the analyzer with the input po-
larization i.e., x-axis and A is the phase difference between the two interfering beams
due to optical path difference, in the plane of observation. Observations are made for
fixed values of cp = 5°, 10° and 45° and rotating the analyzer (η). Fig 3.2a-f shows
fringe pattern recorded in the experiment for different positions of the analyzer i.e.,
for different values of η for the above values of cp. The pixel number on the abscissa
represents the variation along A-axis. It is observed that the peak height and peak po-
sitions are different along A-axis for different values of η. Corresponding theoretical
curves are shown in figs.3.3a-f. The experimental variations in the peak position as *r*
is varied for different values of cp are plotted in fig.3.4a. Apart from some scatter due
to the imperfections in the optics, the sudden shift in the peak position is observed.
Theoretical curves for the same values of cp and η are shown in fig.3.4b. From both
experimental and theoretical curves it is clear that the sudden shift is steeper for
smaller angles of cp and is linear for cp = ± 45°.

This can be understood from the analysis using Poincaré sphere. Figure 3.5
shows the Poincare sphere with P_1 and P_2 being the states of polarization of the two
beams coming out of Sagnac interferometer and before passing through the analyzer.
A point, say, A on the equator of the Poincare sphere represents the analyzer and as
the analyzer is rotated this point A moves on the equator with twice the angle with
which the analyzer is rotated. Let the point I represent the state of polarization of the
input beam. Pancharatnam's phase is half the solid angle subtended by the area en-
closed by the spherical triangle P_1P_2A. The arcs P_1P_2, P_1A and P_2A joining the points

P_1 and P_2, P_1 and A and P_2 and A respectively lie on the great circles passing through them with the center at the center of the **Poincaré** sphere. The great circle joining the points P_1, P_2 is fixed for all values of A as it depends only on the output from the Sagnac interferometer and it passes through the point I on the equator. When the point A, on the equator lies, on the arc P_1P_2 i.e., at the point I representing the input polarization, all the three great circles coincide with the great circle $IP_1I'P_2I$. The area enclosed is zero as one has only a line instead of a triangle. As the analyzer is rotated the point A moves away from the point I and hence the spherical triangle P_1P_2A encloses an area. As A moves away in anti-clockwise direction on the equator away from the point I the area enclosed by it increases because of which the phase difference between the two interfering beams changes resulting in the movement of fringes. The great circles joining the points P_1 and A and P_2 and A make an angle (P_1AP_2) at the point A. This angle becomes smaller as the point A moves along the equator until it reaches a point at 90 from the point I, while the area increases continuously but slowly. Both the angle P_1AP_2 and area increase slowly as the point A moves away from this point until it reaches the point M closer to the point I' representing the orthogonal polarization state to that of the input polarization state. From this point onwards the increase in the angle P_1AP_2 and the area is rather fast and the angle P_1AP_2 becomes π when the point reaches the point I'. Again the three great circles coincide with the great circle $IP_1I'P_2I$. These changes continue to be fast and nonlinear till the point A reaches a point N on the other side of I'. After that the changes slow down and become zero when the point returns to the point I. The nonlinear changes in the area can be attributed to the region in which the great circles fly past the North and South poles of the Poincare sphere. As noticed above the region of nonlinear change in area depends on the separation of P_1 and P_2 from the equator. When P_1 and P_2 are far apart and coincide with the North and South poles of the Poincare sphere the area covered by the spherical triangle P_1AP_2 changes linearly with movement of point A on the equator. This is the case when $\varphi = 45$. But when P_1 and P_2 are close to the equator the area increases nonlinearly. So we see that smaller the value of φ steeper is the nonlinear shift of the peak position, as seen in fig.3.4. To get a clear picture of the nonlinear change in the area of the spherical triangle P_1AP_2 refer appendix C.

Clearly it is shown that Pancharatnam's phase can be used for switching using a four-arm Sagnac interferometer. This type of switching can also be obtained in some of the other configurations of four-arm Sagnac interferometer. Consider the case where a half wave plate is placed inside the Sagnac interferometer with input beam linearly polarized. In this case a quarter wave plate is placed in the output arm of the Sagnac interferometer just before the linear analyzer. The quarter wave plate is placed with its axis parallel to the input linear polarization. The analyzer is rotated as in the earlier case to observe the sudden shift in the fringes for smaller angles of φ_H. Where, φ_H is the angle made by the axis of half wave plate with the input polarization.

In this chapter the principle of switching action of a Sagnac interferometer has been shown. Such switching action can be created mechanically, electrically, acoustically or using intense radiation. We shall discuss the development of a double beam polarimeter using the principle of switching in the next chapter.

References:

3.1 *"Nonlinearity of Pancharatnam's topological phase",* H. Schmitzer, S. Klein and W. Dultz, Phys. Rev. Lett., **71,** 1530, 1993

3.2 *"Evolution of light beams in polarization and direction",* R. Bhandari, Phys. Lett. A **175,** 111, 1991

3.3 *"SU(2) phase jumps and geometric phases",* R. Bhandari, Phys. Lett. A **157,** 221,1991

3.4 *"Observation of Dirac singularities with light polarization. I ",* R. Bhandari, Phys. Lett. A **171,** 262, 1992

3.5 *"Observation of Dirac singularities with light polarization. II ",* R. Bhandari, Phys. Lett. A **171,** 267, 1992

3.6 *"Interferometry without beamsplitters - a sensitive technique for spinor phases'",* R. Bhandari, Phys. Lett. A **180,** 21, 1993

3.7 *"On geometric phase from pure projections",* R. Bhandari, J. Mod. Opt. 45, 2187, 1998

3.8   "*A four-arm Sagnac interferometric switch",* S. P. Tewari, V. S. Ashoka and M. S. Ramana, Opt. Comm. **120,** 235, 1995
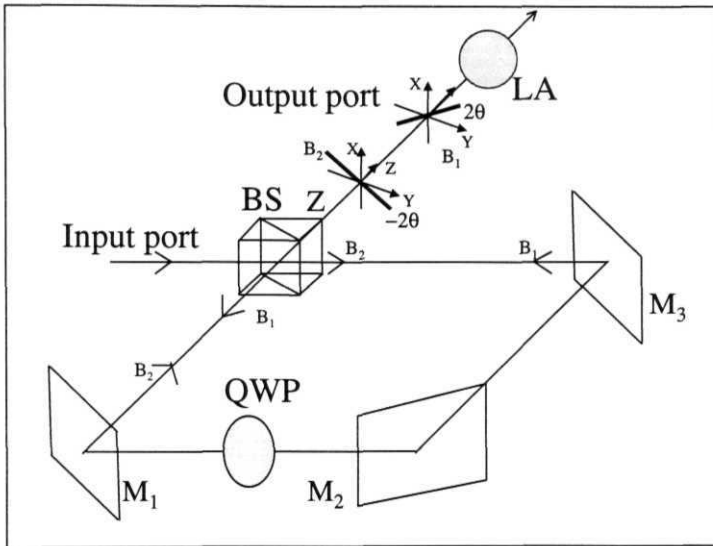
Fig3.1: This figure shows the setup for the interferometric switch. It consists of a four-arm Sagnac interferometer, 50:50 non-polarizing beam splitter BS, three 100% reflecting mirrors M_1, M_2 and M3, a half wave plate HWP, a quarter wave plate QWP in one of the arms of the interferometer and a linear analyzer LA in the output arm.
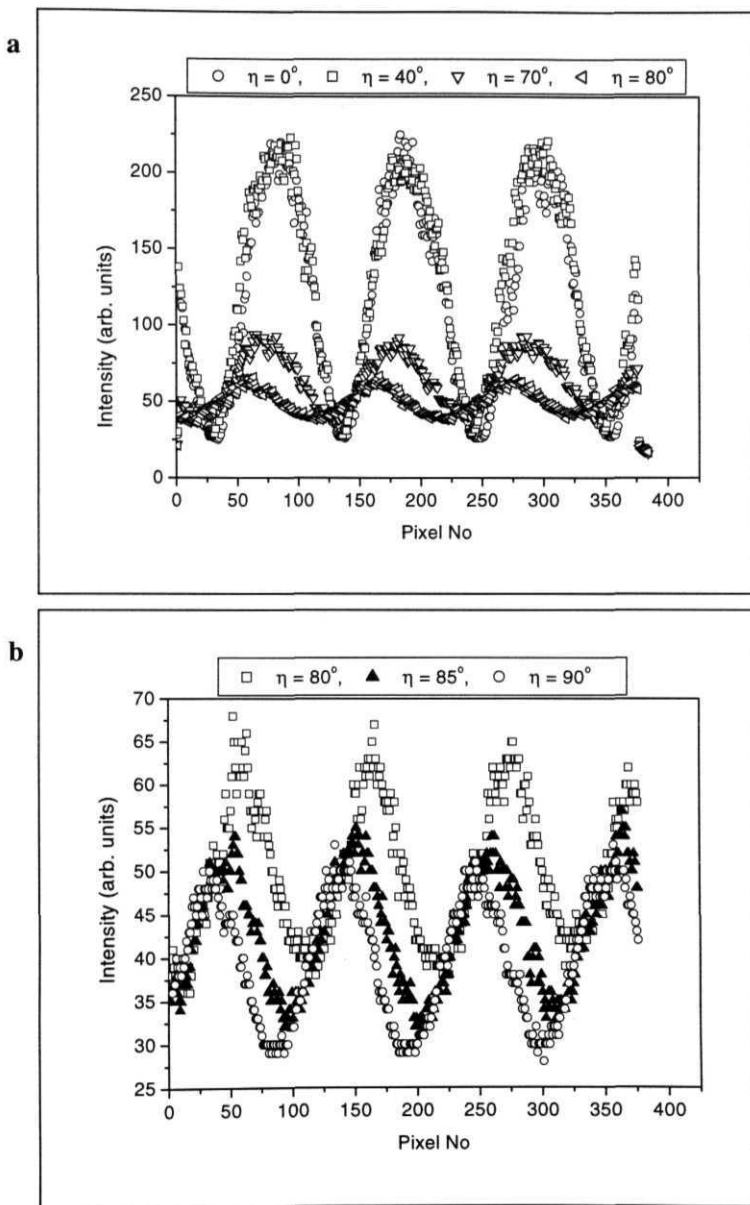
Fig.3.2
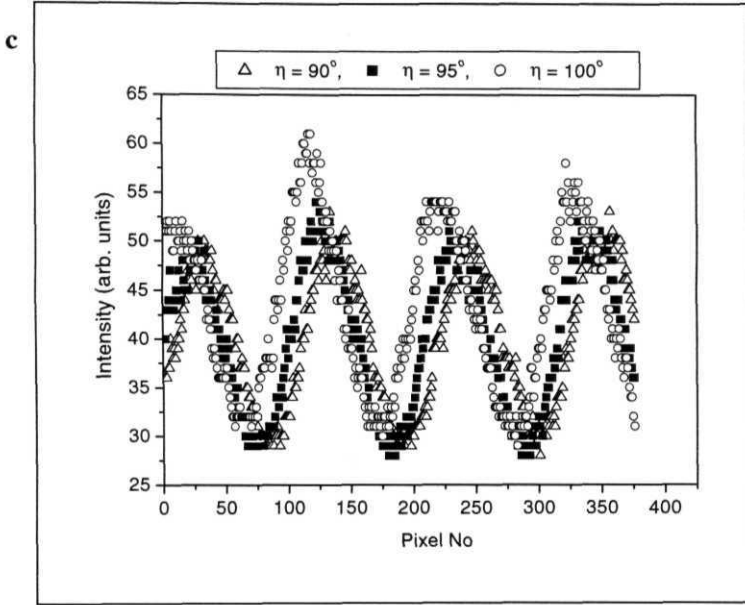
Fig.3.2a-c: Interference fringes recorded in the experiment. a, b and c show the intensity fringes for $\varphi = -5°$ and d, e and f show the fringes for $\varphi = -10$ (shown in the next two pages). A CCD camera (Samsung model no. SHC 410PF) having a sensor of dimensions 4.89mm X 3.64mm along with a frame grabber card giving 384 x 287 pixel image is used to record the images.

Fringes are shown in a) for $\eta = 0°$, 40°, 70° and 80°; in b) for $\eta = 80°$, 85° and 90°; and in c) for $\eta = 90°$, 95° and 100°. Observe the movement of fringes to the left and the variation in the intensity. Also note in 'b' the sudden shift taking place between $\eta = 80°$ and $\eta = 90°$.
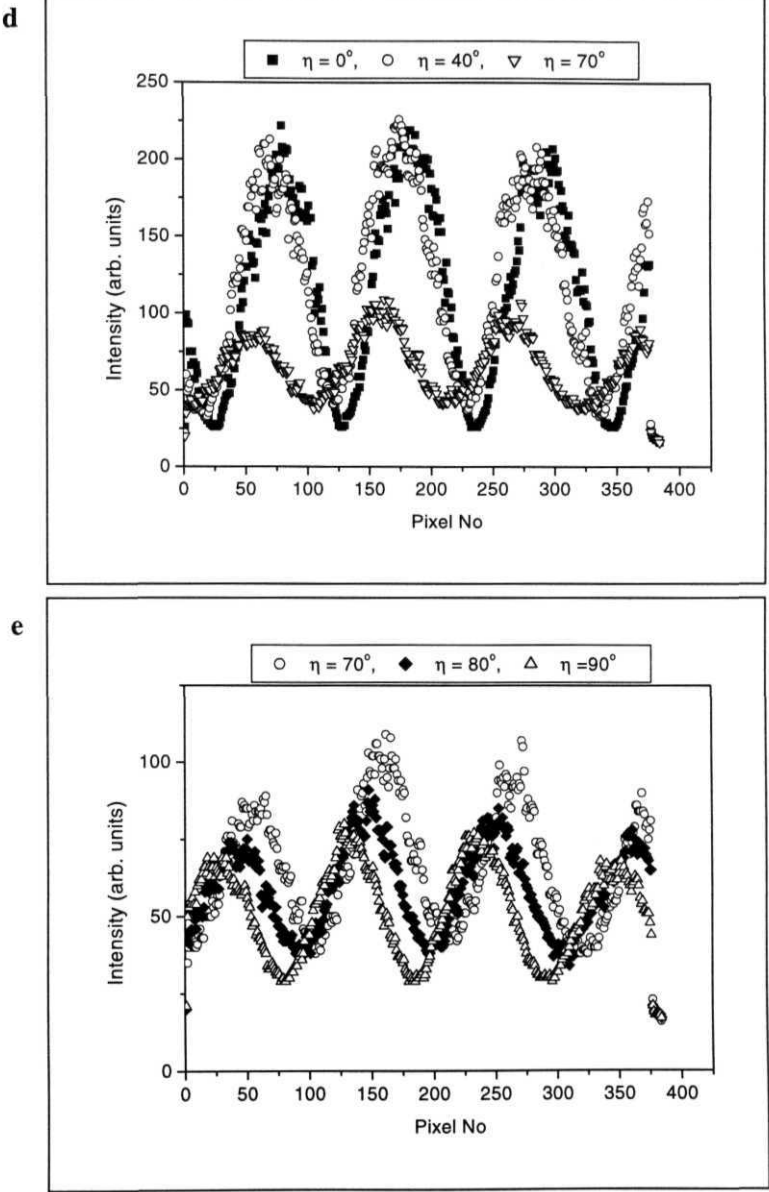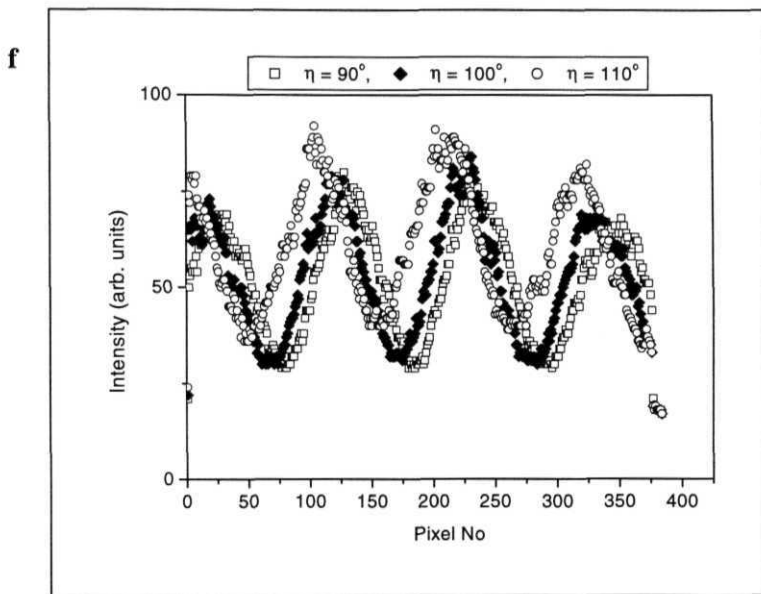
d

e

Fig.3.2

For figure caption see next page

Fig.3.2d-f: Interference fringe pattern recorded in the experiment for different values of η with φ = -10°. A CCD camera (Samsung model no. SHC 410PF) having a sensor of dimensions 4.89mm X 3.64mm along with a frame grabber card giving 384 x 287 pixel image is used to record the images.

Fringes are shown in d) for η = 0°, 40° and 70°; in e) for η = 70°, 80° and 90°; and in f) for η = 90°, 100° and 110°. Observe the movement of fringes to the left and the variation in the intensity. Also note in 'b' the sudden shift taking place between η = 70° and η = 90°. Note the difference in the interval in which the sudden shift is taking place in the two cases φ = -5 and φ = -10 .
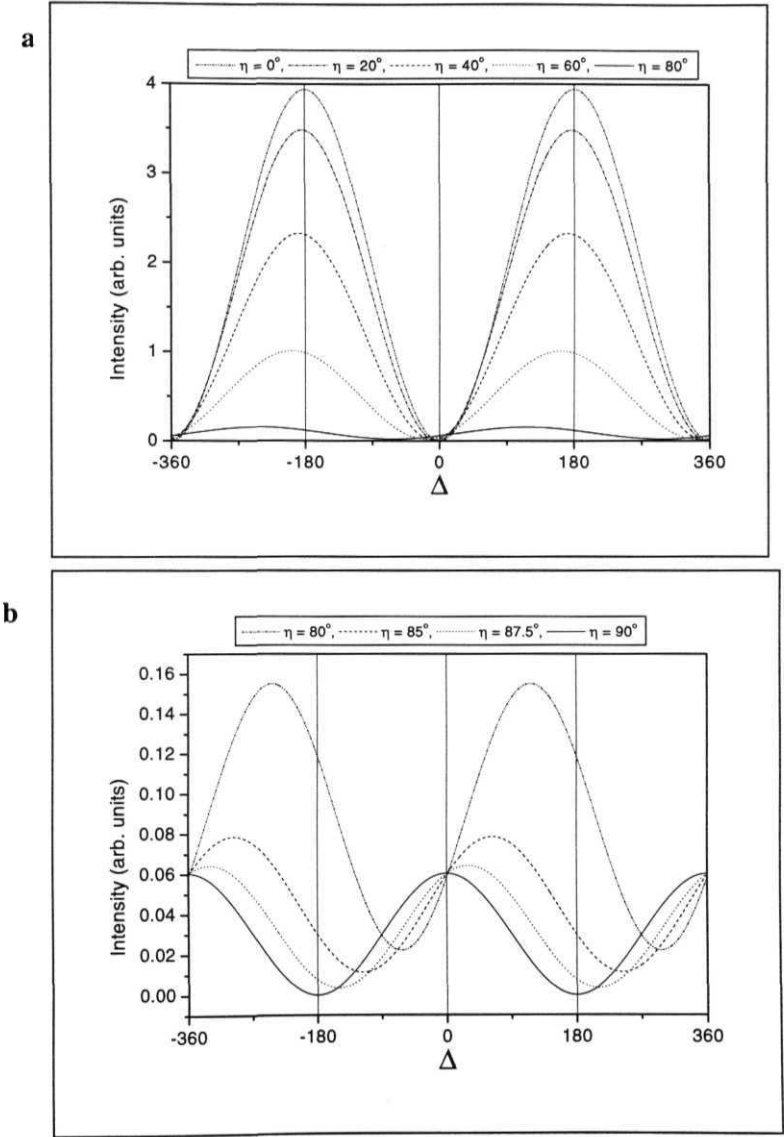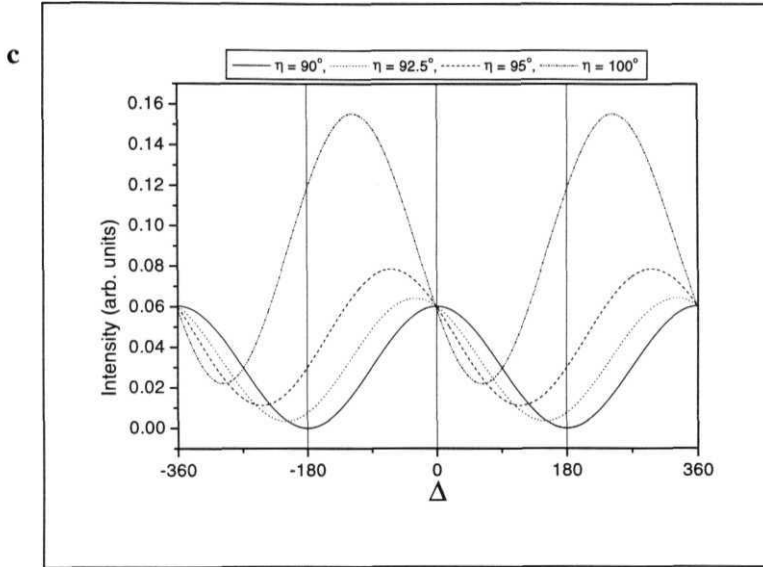
Fig.3.3

For figure caption see next page

c

Fig.3.3a-C: Theoretically generated interference fringe pattern for different values of η with (p = -5°. a) Fringe pattern when r| = 0°, 20°, 40°, 60° and 80° is shown. b) Fringe pattern when η = 80°, 85°, 87.5° and 90° is shown. c) Fringe pattern when r| = 90°, 92.5°, 95° and 100° is shown. Observe that the fringe pattern moves to the left on the A-axis. Also, note the variation in the intensity as the fringes move.
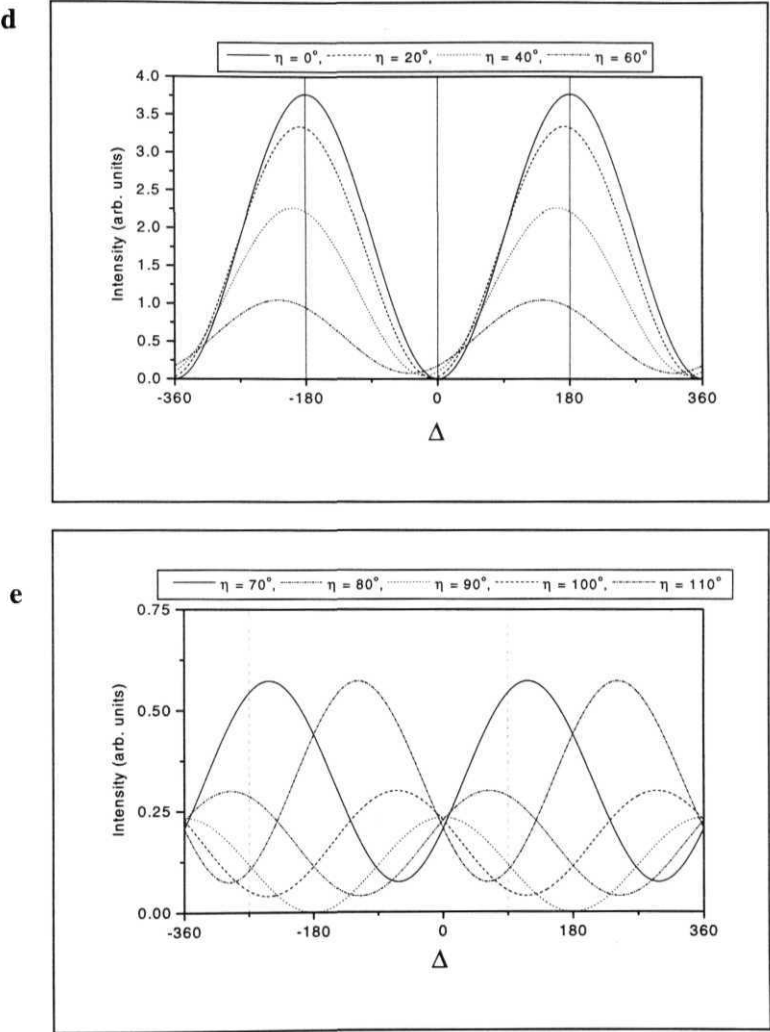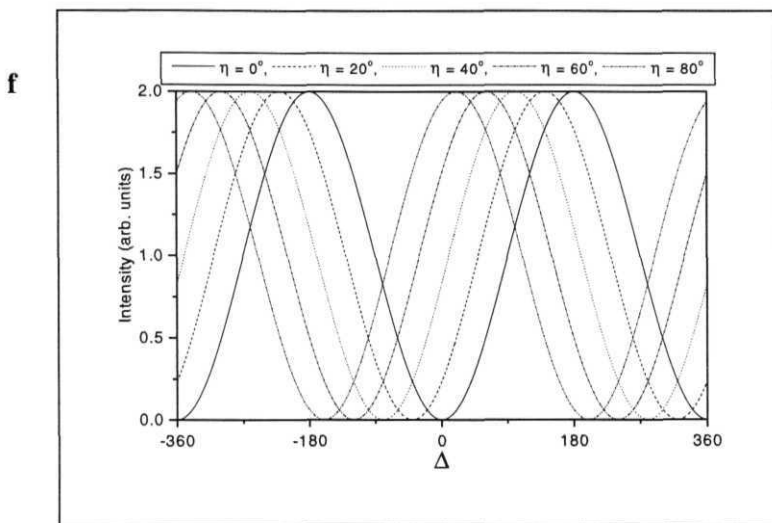
Fig.3.3

f

Fig.3.3d-f: Theoretically generated interference fringe pattern for different values of η with φ = -10° and <p = -45°. d) Here fringe pattern when η = 0°, 20 , 40 and 60 is shown for φ = -10°. e) Here fringe pattern when r| = 70°, 80°, 90°, 100° and 110° for φ = -10° is shown. Observe that the fringe pattern moves to the left on the A-axis and the variation in the intensity as the fringes move. Also note the sudden shift taking place between η = 70° and η = 110°. f) Here fringe pattern when η = 0°, 20°, 40°, 60° and 80° is shown for φ = -45°. Note the linear movement of fringe pattern as η is varied.
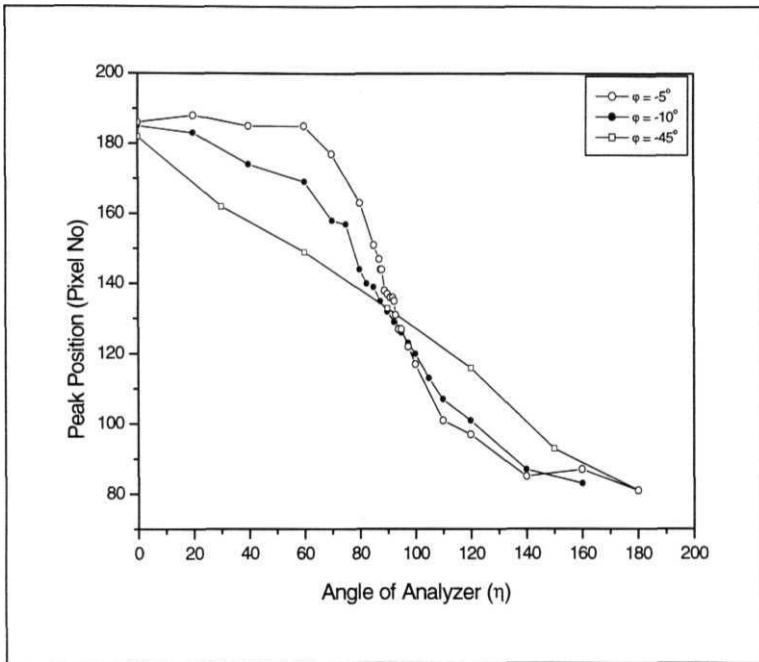
Fig.3.4a; In this figure we have shown the change (experimental) in the peak position for different values of (p. Observe the sudden shift for smaller values of φ despite some scatter. Also note the linear movement of fringes for (p = -45°. Peak positions are measured in terms of pixel no as in fig.3.2.

Fig. 3.4b: Here change in the peak position (theoretical) on the A-axis is shown for the cases same as in fig.3.4a. Observe the steepness in the shift of the peak position for smaller values of (p. Also note the linear change for the case (p = -45°.

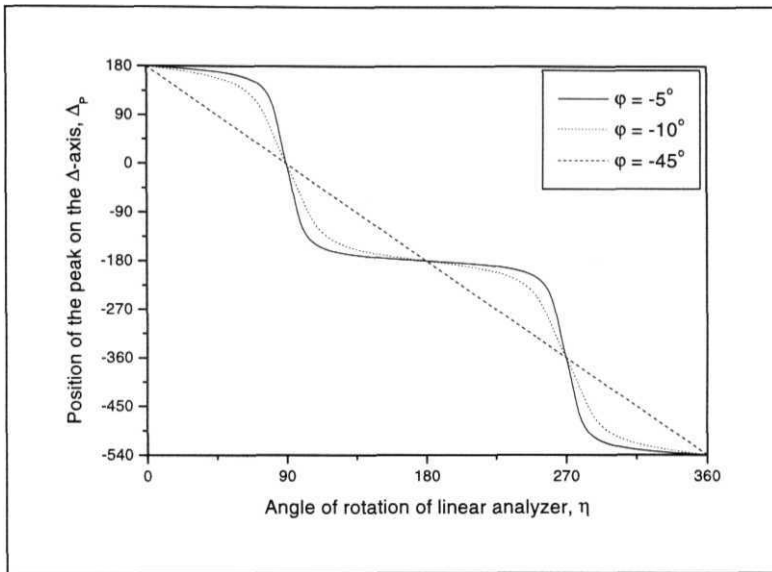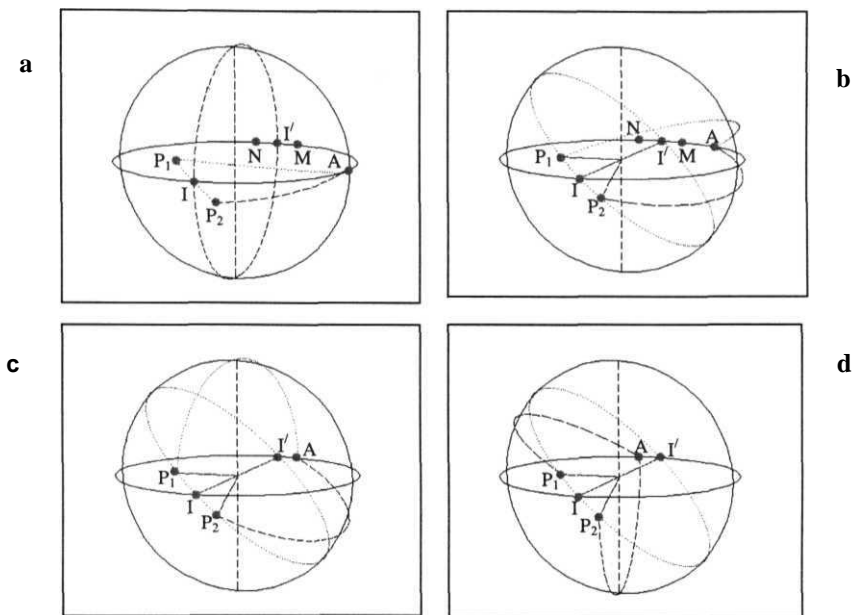**Fig.3.5a - d:** Poincare sphere representation of the polarization changes taking place in the experiment mentioned in this chapter. Point I represents the input state of polarization parallel to x-axis. Quarter wave plate position for the two counter-propagating beams is at $\pm 2\varphi$ on either side of the point I. P_1 and P_2 are the states of polarization of the output beams from the Sagnac interferometer in the said experiment. I represents the input polarization and I' represents the orthogonal polarization to the input. Point A represents the angle made by the axis of the analyzer with the input polarization. a) When the point A is at 90 to the point I. b) The point A is at 135° away from the point I and is closer to the point M. c) The point A is at 170° (point M) away from the point I. d) The point A is at 190 (point N) away from the point I. Observe the sudden flip taking place as the point A move from M to N. Also, the change in area as the point A moves from M to N is more compared to the change in the area as the point moves from I to M.

Chapter IV

Double Beam Polarimeter

In this chapter, a new technique [4.1] to measure the optical activity of a medium is demonstrated. It uses nonlinearity of Pancharatnam's phase and a Sagnac interferometer. The setup consists of a three-arm Sagnac interferometer with the medium, whose optical activity has to be determined, placed in one of the arms of the Sagnac interferometer as shown in fig.4.1. A laser beam, linearly polarized perpendicular (vertical) to the plane of interferometer i.e., parallel to the x-axis, is allowed to pass through the Sagnac interferometer. The laser beam splits into two beams at the beam splitter (BS) and these two beams propagate through Sagnac interferometer in opposite directions. The optically active medium rotates the planes of polarization of these two counter-propagating beams by an angle say, 9. The two counter propagating beams emerge out of SI into the output port as shown in fig.4.1. The two beams remain linearly polarized but with their azimuths at ±9 to the input polarization i.e., to the x-axis. After that the two beams are passed through a quarter wave plate (QWP) and a linear analyzer as shown in fig.4.1. This setup is called "Double Beam Polarimeter". The output intensity in the fringe pattern is governed by the following equation.

$$I_o = [(2 + 2\cos A)\, 2\cos^2(9) + 2\cos^2(2\varphi + 9) + 2\cos^2(2\varphi - 9)$$
$$+ 4\cos(A)\cos(2\varphi + 9)\cos(2(p - 9) - 4\sin(A)\sin(2(p)\sin(29)]\cos^2\eta$$
$$+ [(2 - 2\cos\Delta)\, 2\sin^2(\theta) + 2\sin^2(2\varphi + \theta) + 2\sin^2(2\varphi - \theta)$$
$$+ 4\cos(A)\sin(2\varphi + 9)\sin(2\varphi - 9) - 4\sin(A)\sin(2\varphi)\sin(29)]\sin^2\eta$$
$$+ [4\sin(4\varphi)\cos(29) + 4\cos(A)\sin(4\varphi) - 8\sin(A)\cos(2\varphi)\sin(29)]\cos(r|)\sin(\eta)$$

(4.1)

Where φ (quarter wave plate angle) and T| (analyzer angle) are the angles made by the axes of the quarter wave plate and the linear analyzer with the input polarization i.e., x-axis. To determine the angle 9 one has two options. One can keep the linear analyzer fixed while rotating the quarter wave plate or fix the quarter wave plate and rotate the linear analyzer. Both these cases are discussed below.

   Consider the case in which the axis of the linear analyzer is kept fixed at $\eta =$ 90 to the input polarization. The two beams, which have different planes of polarization, pass through the quarter wave plate evolving into elliptically polarized light. These beams then pass through the linear analyzer and the resulting interference pattern is observed as the quarter wave plate is rotated. Figure 4.2 shows the intensity fringe patterns along A-axis for different values of the quarter wave plate angle (p. From these graphs, it can be seen that there is movement in the fringe pattern along with change in the intensity level. The movement of fringes is nonlinear in nature. This nonlinear behavior is due to the nonlinearity in Pancharatnam's phase. The nonlinear behavior of fringe movement is more explicit in fig.4.3 where shift in the peak position along the ordinate is plotted as the quarter wave plate is rotated for different values of θ using the following equation.

$$\Delta_p = \tan^{-1}\left[\frac{\sin(2\theta)\sin(2\varphi)}{\sin^2\theta - \sin(2\varphi - \theta)\sin(2\varphi + \theta)}\right]_{\eta = \pi/2} \tag{4.2}$$

This equation gives the peak position as a function of quarter wave plate angle (p. As (p varies the peak position also varies. This can be seen from the curves in fig.4.3 where we plot Δ_p as a function of φ for different values of fixed 9. The amount of shift in the peak position i.e., the total change in the value of Δ_p, along the A-axis is equal to $360°$ - 4θ which occurs in between $\varphi=45°$ and $\varphi=135$. As the value of θ increases, the amount of this shift decreases. By finding the amount of the peak shift between $\varphi = 45°$ and $\varphi = 135°$ position of quarter wave plate, it is possible to obtain the value of 0.

   From the fig.4.3 one can find that there is no movement in fringes for major part of quarter wave plate rotation when 0 is small. Maximum peak shift occurs within an angle of 40. This major shift in the peak position is called the sudden shift in the peak position. The sudden shift occurs four times within 2π rotation of quarter wave plate when $\varphi = 0°$, $90°$, $180°$ and $270°$. In order to show this effect, the rate of

change in the peak position, given by the following equation, is plotted as a function of φ for different values of 0.

$$\frac{\partial \Delta_p}{\partial \phi} = \frac{1}{1 + \left(\dfrac{\sin(2\theta)\sin(2\phi)}{\sin^2\theta - \sin(2\phi-\theta)\sin(2\phi+\theta)} \right)^2} \left[\frac{2\sin(2\theta)\cos(2\phi)}{\sin^2\theta - \sin(2\phi-\theta)\sin(2\phi+\theta)} \right.$$

$$\left. + \frac{2\sin(2\theta)\sin(2\phi)\sin(4\phi)}{\left(\sin^2\theta - \sin(2\phi-\theta)\sin(2\phi+\theta) \right)^2} \right]_{\eta=\pi/2} \qquad (4.3)$$

The rate of change in the peak position is shown in fig.4.4. There is a pair of peaks each at $\phi = 0°$, $180°$ and $360°$ and a pair of valleys (inverted peaks) each at $\phi = 90$ and $270°$. These correspond to the sudden shift in the peak positions shown in fig.4.3. The separation between these peaks or valleys of each pair in fig.4.4 is related to 0. From this separation, the angle of optical rotation can be obtained. The highest point of the peaks and the lowest point of the inverted peaks represent the fastest change in the peak position (fig.4.3) of the fringes (fig.4.2).

All the above observations are the manifestation of nonlinearity in Pancharatnam's phase. This can be explained using the analysis on the Poincaré sphere. Consider fig.4.5 showing the equatorial plane of the Poincare sphere. Let A and B be the positions of the polarization of the two output beams just before the quarter wave plate. O and O′ represent the input linear polarization and linear polarization orthogonal to the input. Linear analyzer angle is made parallel to O′ i.e., T| = 90 . A point Q on the equator represents the quarter wave plate with its fast axis making an angle φ with x-axis. As the quarter wave plate is rotated Q moves along the equator AOBCO DA. There are two regions of concern 1) AB and CD and 2) BC and DA.

When the quarter wave plate (angle) position is in between AB or CD the two beams see the quarter wave plate in opposite sense and evolve as elliptically polarized light with helicities differing in sign. Therefore, they lie on either side of the equator on the Poincare sphere. Now, these polarizations are projected onto the 90 position of

the linear analyzer. Change in the Pancharatnam's phase (area of the spherical triangle P_1P_2O' in fig.4.5) is more when the quarter wave plate is between A and B (C and D). Pancharatnam's phase increases as the quarter wave plate approaches A (C) and will decrease by a small amount when the quarter wave plate reaches the middle of AB (CD). This is because the mid-point (O) of AB is away from both A and B. Pancharatnam's phase increases again as we move away from O (O') towards B (D). As a result of the above decrease and increase in the Pancharatnam's phase, the slope of peak shift curve decreases and increases in magnitude, whenever φ crosses O or O'. φ crosses O when $\varphi = 0°$ and $180°$ and crosses O' when $\varphi = 90°$ and 270°.

Now consider the regions BC and DA. In these regions, the quarter wave plate sees the two output beams from the interferometer in the same sense and hence, the resulting elliptically polarized beams lie on the same side of the equator. Consequently for small θ, the two beams lie close to each other on the Poincare sphere. Therefore, when quarter wave plate is rotated, there is negligible change in the Pancharatnam's phase. As a result the shift in the peak position is negligible in these regions and the major shifts occur in the regions AB and CD. For large values of 6 and Q in the region BC or DA, the two beams lie on the same side of the equator. They are well separated form each other, resulting in considerable shift of the fringe pattern in the regions BC and DA. This explains the case when the quarter wave plate is rotated keeping the linear analyzer fixed.

Now consider the case in which the quarter wave plate is fixed and the linear analyzer is rotated. Here φ is fixed and is equal to zero i.e., the fast axis of quarter wave plate is parallel to the input polarization. The resultant fringe pattern is observed through a detector placed after the linear analyzer. To determine the angle 6 linear analyzer is rotated i.e., η is varied. As the linear analyzer is rotated the fringe pattern shifts, the direction of shift depending on the direction of rotation of linear analyzer. Figure 4.6 shows the fringe pattern for 9 = 5°. From this figure we observe that there is a sudden shift in the fringe pattern between $\eta = 80°$ and $100°$.

To understand what is happening here once again analysis is done on the Poincare sphere (fig.4.7). Let O be the input polarization and O' be the polarization orthogonal to O. Quarter wave plate is fixed at an angle $\varphi = 0^o$. At this angle the quarter wave plate is represented by the point O on the Poincare sphere. Let the point A represent the position of the linear analyzer. This point will be at angle 2r| from O where, η is the angle made by the axis of the linear analyzer with x-axis. As the linear analyzer is rotated, η varies and the point A moves along the equator, $OO'O$. The polarization states of the output beams, just before the quarter wave plate, are represented by the points I_1 and I_2. These points lie on either side of O on the equator. When the beams pass through the quarter wave plate one beam gets transformed into an elliptically polarized light (P_1) in the upper hemisphere while the other gets transformed into an elliptically polarized light (P_2) in the lower hemisphere. This is because the quarter wave plate sees one beam at angle $+\theta$ (plus 0) and the second beam at an angle -0 (minus 0) with respect to its axis. Let the two new polarization states be P_1 and P_2. Both these points lie on the same longitude. Pancharatnam's phase is the solid angle subtended by the spherical triangle P_1P_2A at the center of the Poincare sphere. As η is varied, point A moves along the equator changing the solid angle subtended by the triangle P_1P_2A. Therefore Pancharatnam's phase also changes resulting in the corresponding changes in the interference fringe pattern shown in fig.4.6. As η approaches the value of 90°, point A approaches the point O' on the Poincare sphere. When 0 is small, the points P_1 and P_2 lie close to the equator and the change in Pancharatnam's phase is large as the point A approaches O'. Maximum shift in the peak occurs within an angle of ± 20 to O'. Change in the Pancharatnam's phase away from O' is small when 0 is small. For large 0 the two points P_1 and P_2 lie away from the equator and hence there is considerable change in the Pancharatnam's phase even when A is away from O'.

The peak shift and the rate at which the peak shifts are governed by the equations 4.4 and 4.5 respectively.

$$\Delta_p = \tan^{-1}\left[-\frac{\sin(2\theta)\sin(2\eta)}{\cos(2\eta)+\cos(2\theta)}\right]_{\varphi=0^\circ} \tag{4.4}$$

$$\frac{\partial \Delta_p}{\partial \eta} = \frac{1}{1+\left(\dfrac{\sin(2\theta)\sin(2\eta)}{\cos(2\eta)+\cos(2\theta)}\right)^2}\left[\frac{2\sin(2\theta)\cos(2\eta)}{\cos(2\eta)+\cos(2\theta)}+\frac{2\sin(2\theta)\sin^2(2\eta)}{(\cos(2\eta)+\cos(2\theta))^2}\right]_{\varphi=0^\circ}$$

$$\tag{4.5}$$

For small values of 0 we approximate the expression in eq.4.5 by the following Lorentzian function.

$$\tag{4.6}$$

where p = η - $\pi/2$. The width of this Lorentzian function is 20. The peak position (Δ_p in eq.4.4) of the fringes is plotted against the angle η in fig.4.8. Rate of change in the peak positions (eq.4.5) is plotted in fig.4.9. From the fig.4.9 it is found that the full width at half maximum of the inverted peaks is related to the angle 20. This can be approximated to 20 for small values of 0 as given in eq.4.6.

We check these results experimentally in another setup, which mimics the double beam polarimeter. This setup is a four-arm Sagnac interferometer with a half wave plate placed in one of the arms. A quarter wave plate and a linear analyzer are placed in the output arm. The setup is shown in fig.4.10. The intensity fringe pattern in this case is given by the following equation.

$$
\begin{aligned}
I_0 = &[(2+2\cos\Delta)\,2\cos^2(2\theta)+2\cos^2(20+2\theta)+2\cos^2(20-20) \\
&+4\cos(A)\cos(20+20)\cos(20-20)-4\sin(A)\sin(20)\sin(40)]\cos^2\eta \\
&+[(2-2\cos A)\,2\sin^2(20)+2\sin^2(20+20)+2\sin^2(20-20) \\
&+4\cos(A)\sin(20+20)\sin(20-20)-4\sin(A)\sin(20)\sin(40)]\sin^2\eta \\
&+[4\sin(40)\cos(40)+4\cos(A)\sin(40)-8\sin(A)\cos(20)\sin(40)]\cos(\eta)\sin(\eta)
\end{aligned}
$$

$$\tag{4.7}$$

where ϕ, θ and η are the angles made by the quarter wave plate, half wave plate and the linear analyzer with the input polarization. Comparing eq.4.1 with eq.4.6, one finds that θ in former is replaced by 2θ in the latter. Therefore the effect of a half wave plate in a four-arm Sagnac interferometer is similar to an optically active medium in a three-arm Sagnac interferometer for a linearly polarized input. The experiment is done for the second case where the quarter wave plate is fixed and the linear analyzer is rotated. Figure 4.11 shows the peak position of the fringe patterns as the linear analyzer is rotated i.e., η is varied, for two different angles of half wave plate. These curves are plotted by finding the peak positions (Δ_p) of the fringe patterns, recorded using a CCD camera for different values of η. Instead of finding the angle θ the difference between the angles corresponding to the two positions of the half wave plate is determined. This difference between the two angles is clearly reflected in the results obtained. The difference in θ for the two positions of the half wave plate is 0.5, which is measured in multiples of 0.017° where 0.017 is the least count of the vernier scale used to rotate the half wave plate. The minimum angle with which the analyzer is rotated using a stepper motor is 0.023. Therefore the maximum possible error on measuring the change in θ is ± 0.04. The rate at which the peak position (Δ_p) changes is plotted in fig.4.12 for the two positions of the half wave plate. These curves are then fitted with a Lorentzian function. The difference between the angles obtained from the widths of the Lorentzians fitted to the curves in fig.4.12 is 0.514. This is within the expected error limit of $\pm 0.04^\circ$ involved in the rotation of half wave plate.

Thus a new method to find the amount of optical rotation by an optically active medium using a Sagnac interferometer has been described and demonstrated. Hariharan and Singh [4.2] worked with a similar setup as in fig.4.1, to show that ordinary, unpolarized light is made up of random plane polarized components.

References:

1. "*Double beam polarimeter*", M. Sree Ramana and Surya P. Tewari, Proc. of National Laser Symposium-2000, New Delhi (INDIA), 405

2. *"Random, Plane-polarized Components in Ordinary, Unpolarized light",* P. Hariharan and R. G. Singh, JOSA 51, 1148, 1961
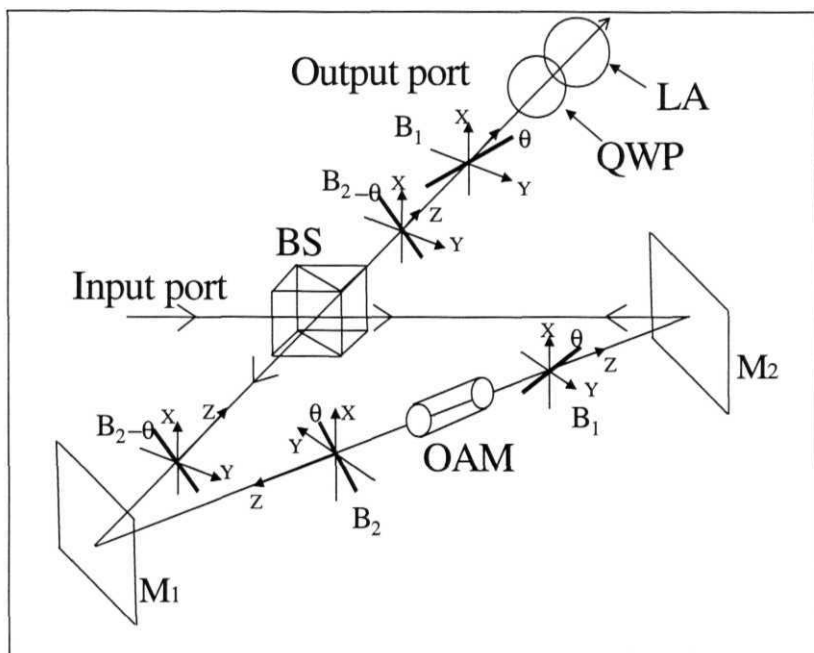
Fig.4.1. Double beam polarimeter setup: Three-arm Sagnac interferometer consisting a beam splitter and two mirrors M_1 and M_2, optically active medium (OAM), quarter wave plate (QWP) and linear analyzer (LA). B_1 and B_2 represent the anti-clockwise and clockwise beams respectively. θ is the angle by the optically active medium rotates the plane of polarization.

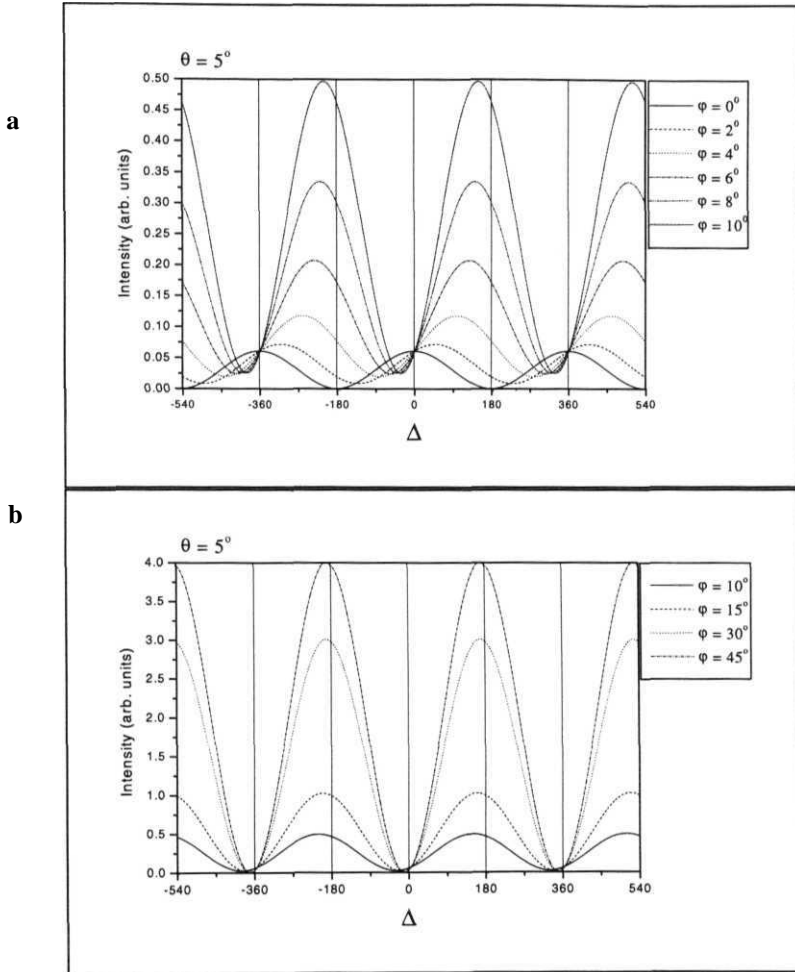**Fig.4.2a and b:** Intensity fringe pattern (eq.4.1) for different values of quarter wave plate angle φ and for different values of θ. Case of 9 = 5° is shown in this page and 9 = 10° is show in next page.

a) and b) 9 = 5°. Observe the shift in the peak position. The peak position shifts towards right on the A-axis. Also note that the shift is more, and sudden between the angles (p = 0° and φ = 10 .

Fig.4.2c and d: Intensity fringe pattern (eq.4.1) for different values of quarter wave plate angle φ and for different values of 0.

c) and d) $0 = 10^\circ$. Observe the shift in the peak position. The peak position shifts towards right on the A-axis. Also note that the shift is more and sudden between the angles $\varphi = 0^\circ$ and $(p = 20$.

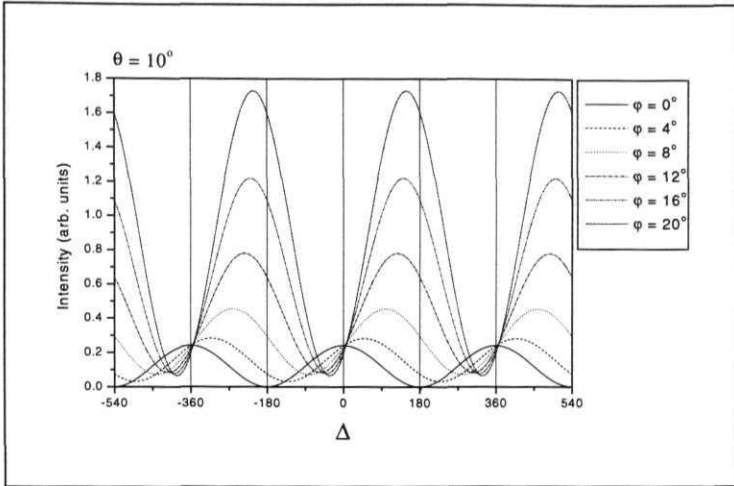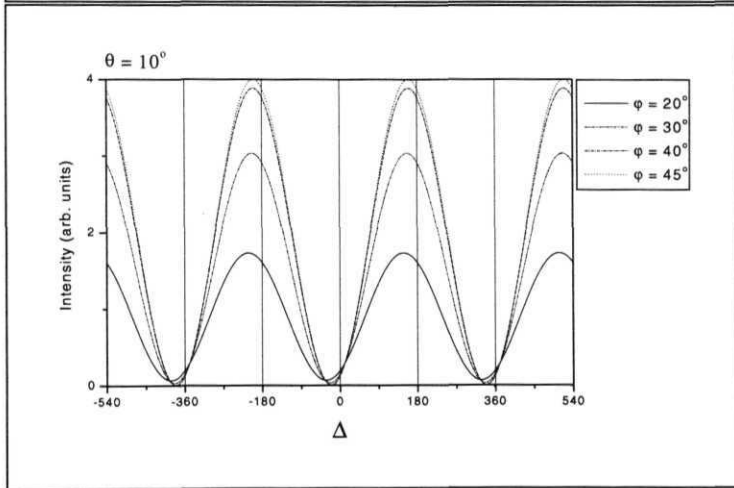In this figure (a-d) intensity fringes are shown till $\varphi = 45^\circ$ only. Beyond $\varphi = 45^\circ$ the fringe pattern starts moving back towards left symmetrically.

a
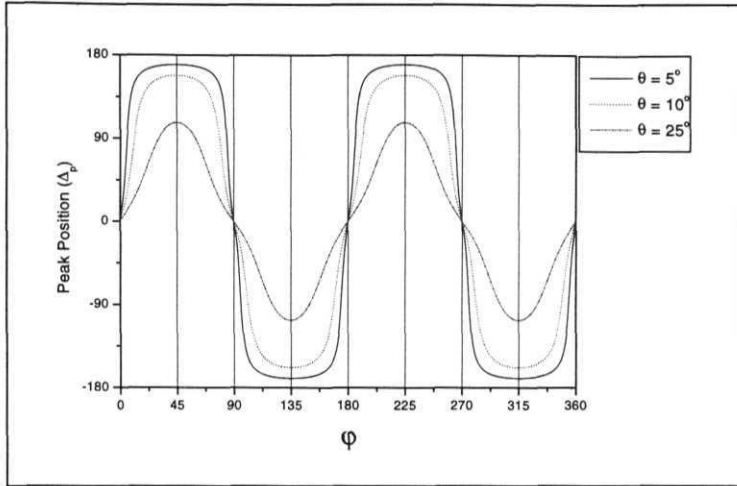
b
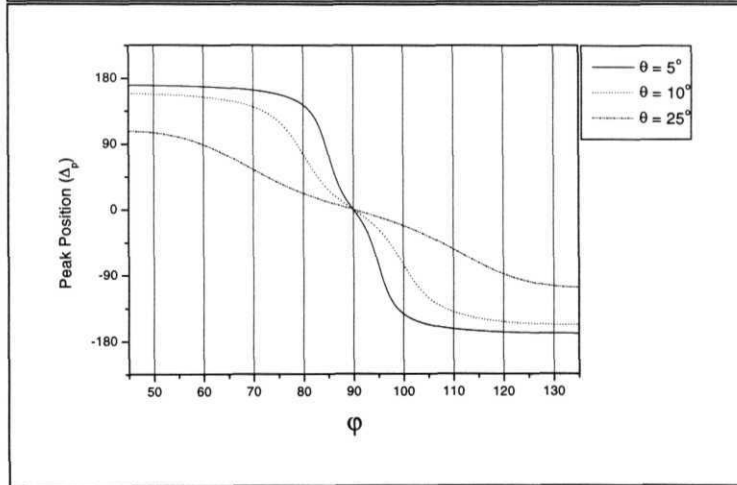
Fig.4.3a and b: Peak position (eq.4.2) is plotted against the quarter wave plate angle φ for different values of optical activity angle θ. Observe the shift in the peak position as the angle φ is varied. a) Shift in peak position from $\varphi = 0°$ to $<p = 360°$ is shown. For smaller values of 9 a sudden shift occurs in a narrow range around ($p = 0°$, $90°$, $180°$, $270°$ and $360°$. Also observe that the amount of total shift in the peak position along the ordinate is equal to $360° - 4\theta$ occurring between $\varphi = 45°$ and $135°$; $135°$ and $225°$; $225°$ and $315°$. b) Shift in peak position from $\varphi = 45°$ to $\varphi = 135°$ is shown. The sudden shift (major portion of the shift) takes place within an angle $A(p = 4\theta$.
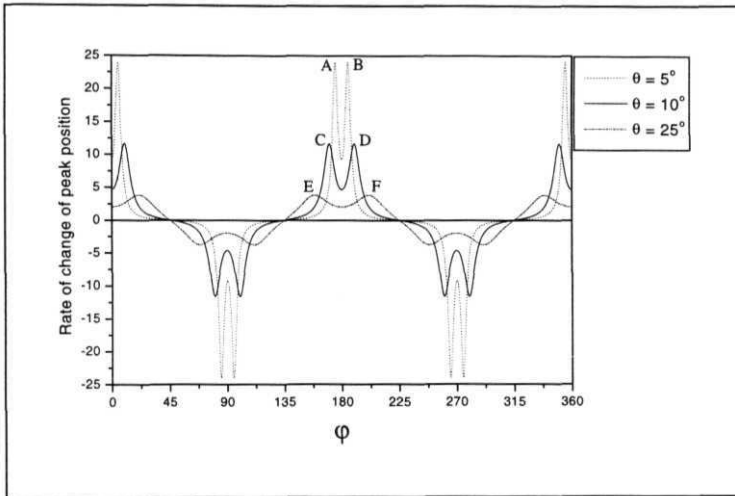
Fig.4.4: Rate of change in the peak position (eq.4.3) along the A-axis is plotted as φ is varied for different values of 9. Observe that the magnitude of the rate of change in peak position decreases within each pair of peaks situated at (p = 0 , 180 and 360 and increases within the pair of inverted peaks situated at cp = 90 and 270 . The separations AB, CD and EF along the (p-axis within which these changes occur are related to 9.
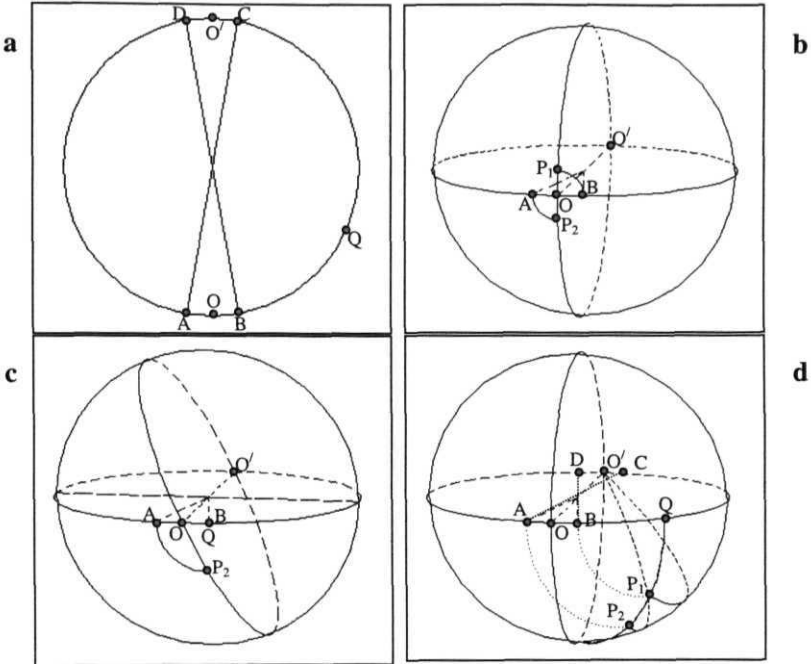
Fig.4.5: a) This figure shows only the equatorial plane of the Poincare sphere. Points A and B represent the polarization states of the two output beams from the Sagnac interferometer. C and D represent the orthogonal states of A and B respectively. O and O' represent the input polarization state and polarization state orthogonal to it.

b) Here we show Poincare sphere for the case when the quarter wave plate is between A and B. The point Q coincides with the point O. Therefore the points A and B get converted to points P_2 and P_1 respectively.

c) In this figure, the fast axis of the quarter wave plate is parallel to the state of polarization of the output beam represented by the point B. Here the point Q coincides with the point B. Therefore only the point A gets converted to point P_2.

d) In this figure we show the case when the quarter wave plate (Q) is between B and C. Therefore the points A and B get converted to points P_2 and P_1 respectively.

Observe the change in the area enclosed by the spherical triangle P_1P_2O' in all the cases mentioned above. In the case b the area enclosed is the maximum and in d it is the minimum. Therefore when the quarter wave plate is between the points B and C or D and A, the rate at which the area changes will be slow. In contrast, observe the large change in the area in the cases b and c.
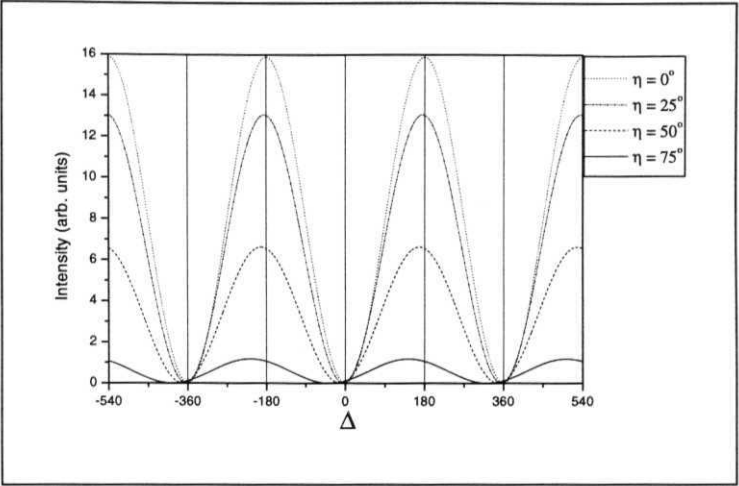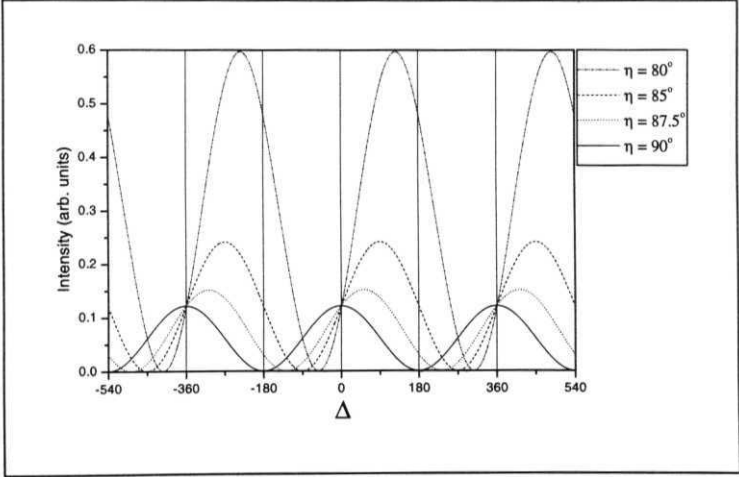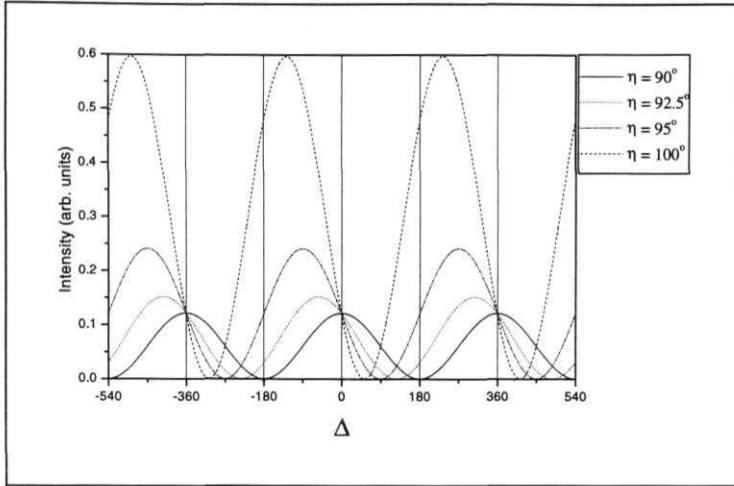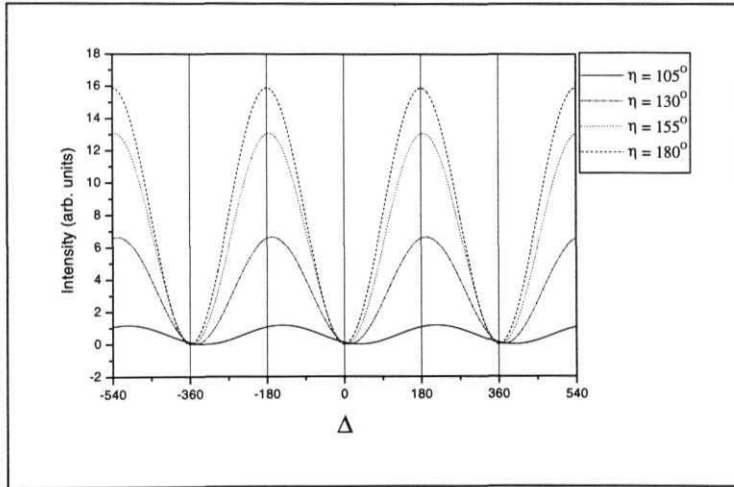
Fig.4.6

Fig.4.6a - d: Intensity fringe pattern (eq.4.1) for different values of linear analyzer angle η and $0 = 5$.

a) $0° < \eta < 80°$. b) $80° < \eta < 90°$. c) $90° < \eta < 100°$. d) $100° < \eta < 180°$

Observe the shift in the peak position. The peak position shifts towards left on the A-axis. The major shift takes place between $\eta = 80°$ and $100°$.
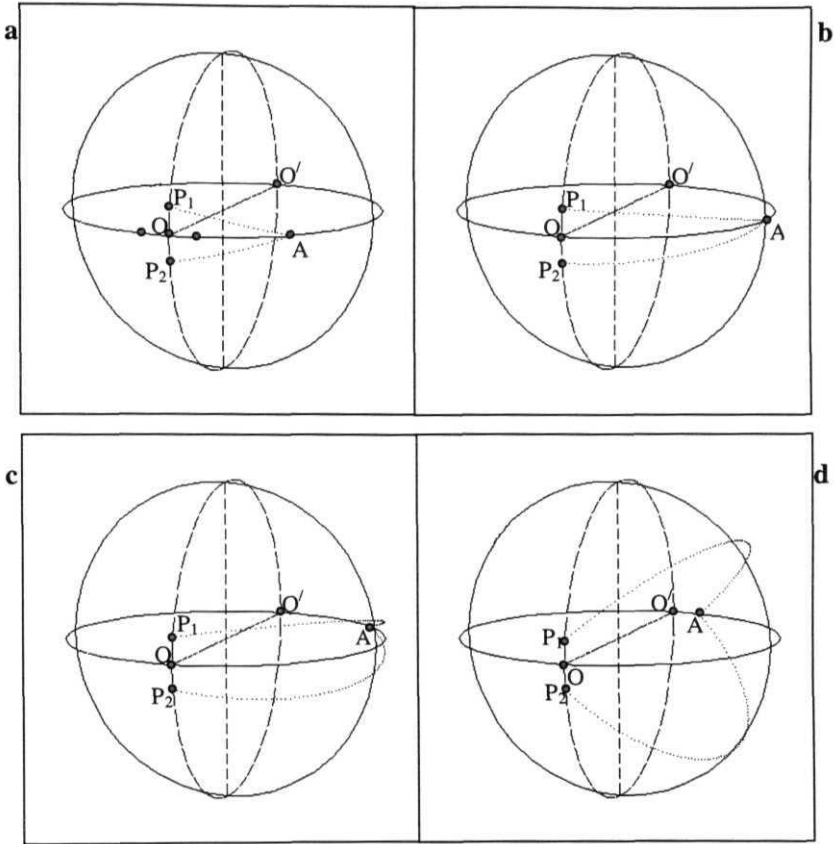
Fig.4.7a-d: In this figure the Poincare sphere representation of the polarimeter experiment is shown. P_1 and P_2 are the points representing the polarization states of the two output beams of the Sagnac interferometer and just before the analyzer. The position of the analyzer is shown by the point A. O and O' represent the input linear polarization and polarization orthogonal to the input polarization. P_1 and P_2 are separated by an angle of 20°. a) The angle made by the axis of the analyzer with the input linear polarization is $\eta = 22.5°$. This is represented by point A and A is away from point O by an angle of 45°. b) $\eta = 45$ and A is at a point 90° away from the point O. c) $\eta = 67.5°$ and A is at a point $135°$ away from the point O. d) $\eta = 80$ and A is at a point $160°$ away from the point O.

4.8
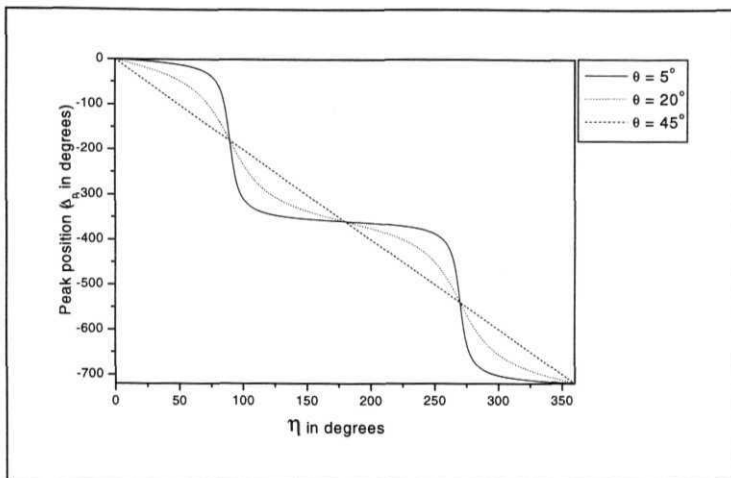
4.9
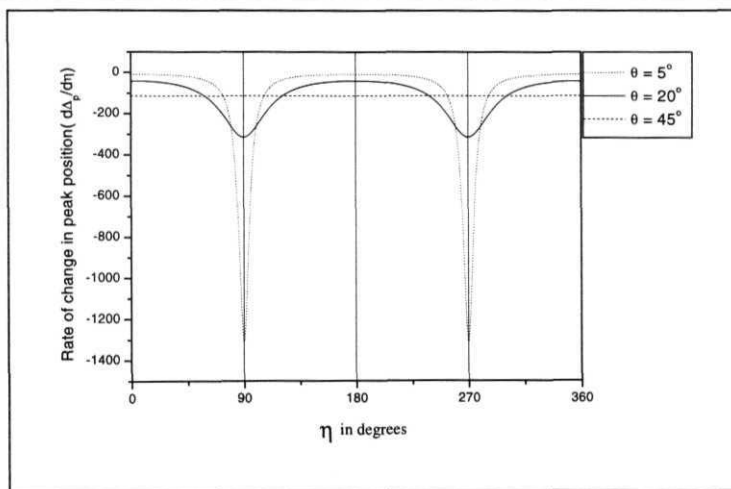
Fig.4.8; Peak position is plotted against the angle η for different values of θ. Observe the continuous shift in the peak position as η is varied. For smaller values of 9 a sudden shift occurs in a narrow range around $\eta = 90°$ and 270. The shift in the peak position is linear for $\theta = 45$.

Fig.4.9: Rate of change in peak position as η is varied is plotted for different values of 9. The width of the valleys is related to θ and it is found that the full width at half minimum is equal to 20.
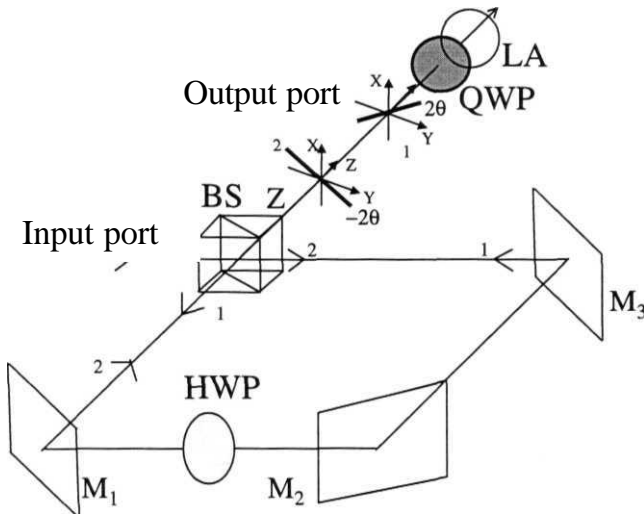
Fig4.10: This figure shows the setup for the experiment mimicking the double beam polarimeter. It consists of a four-arm Sagnac interferometer, 50:50 non-polarizing beam splitter BS, three 100% reflecting mirrors M_1, M_2 and M_3, a half wave plate HWP in one of the arms of the interferometer and a quarter wave plate QWP and linear analyzer LA in the output arm.

4.11

Peak position (Δ_p in pixel no.) vs Angle of Rotation of Linear Analyzer

Position 2 of HWP

Position 1 of HWP

4.12

$d\Delta_p/d\eta$ vs Angle of rotation of linear analyzer (η)

Position 2 of HWP

Position 1 of HWP
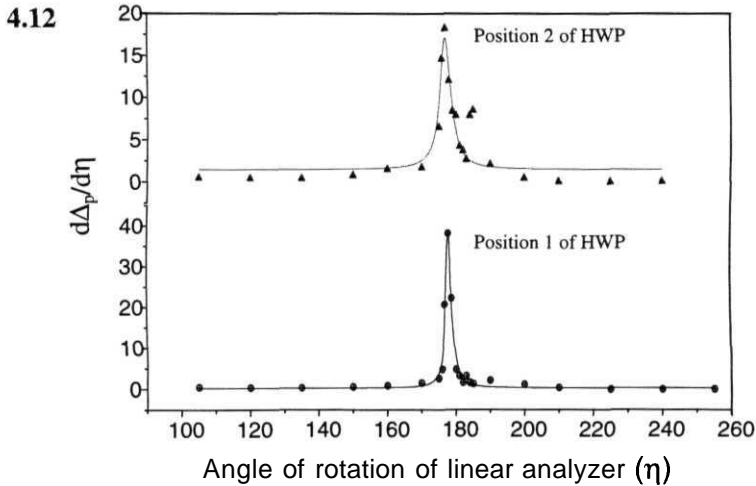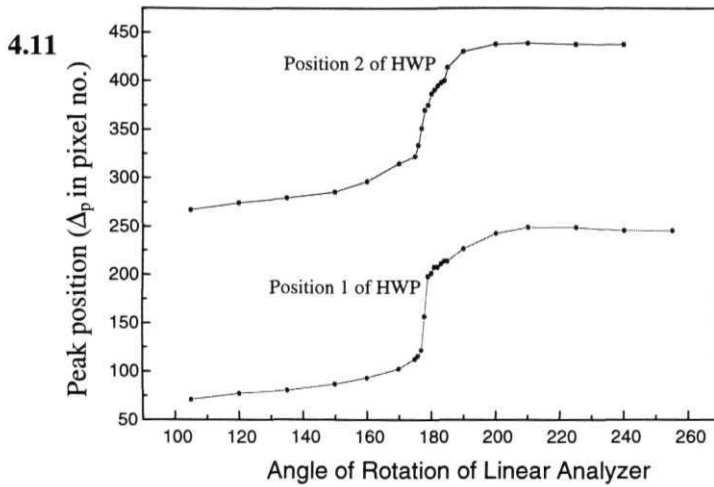
Fig.4.11: In this figure we show the shift in the peak position, for the mimic experiment in which a half wave plate is placed inside the Sagnac interferometer, and the linear analyzer in rotated. Observe the sudden shift in the peak for the two cases. Peak position is in pixel no. Details of the CCD camera used are same as given in fig.3.2 except that here a 640 X 480 pixel image is obtained.

Fig.4.12: This figure shows the slope of the curves shown in fig.4.11 giving the rate of change in the peak position. The data in this figure is fitted to Lorentzian functions. The full width at half maximum is equal to 2θ as in eq.4.6.

An ultrafast optical switch and N-bit signal generation using slowly relaxing nonlinear medium

In the last two chapters we have studied nonlinear effects of **Pancharatnam's** phase with respect to the rotation of an optical element inside a Sagnac interferometer. In this chapter we propose a method to generate an N-bit signal using nonlinear effects of Pancharatnam's phase with respect to time and optical kerr effect. The optical kerr effect is an induced anisotropy in a nonlinear material, due to change in the refractive index, excited by an intense linearly polarized beam. The refractive index change (8n) is different along the directions parallel $(\delta n_{\parallel})$ and perpendicular (6nx) to the linear polarization of the intense beam. This effect is time dependent when a pulse is used to excite the nonlinear medium. As a result of this induced anisotropy, the phase of a linearly polarized probe beam passing through the medium gets retarded. The phase retardation [5.1] after passing through the excited nonlinear medium is given in eq.(5.1).

$$\delta n_{\parallel} - \delta n_{\perp} = \left(\frac{n_2}{2\tau_r} \right) \int_{-\infty}^{t} \exp(\frac{t'-t}{\tau_r}) E_2^2(t') dt',$$

$$\delta\varphi = \left(\frac{2\pi l}{\lambda} \right) (\delta n_{\parallel} - \delta n_{\perp}),$$

$$\delta\varphi = \left(\frac{2\pi l}{\lambda} \right) \left(\frac{n_2}{2\tau_r} \right) \int_{-\infty}^{t} \exp(\frac{t'-t}{\tau_r}) E_2^2(t') dt'. \tag{5.1}$$

Here, τ_r is the relaxation time of the nonlinear medium, n_2 is its nonlinear ken-coefficient, E_2 is the amplitude of the pump, λ is the wavelength of the probe and 1 is the length of the nonlinear medium. This retardation takes place until the nonlinear medium relaxes.

Optical switches made using nonlinear medium are in general limited by the relaxation times of the nonlinear material in use. As it is difficult to get nonlinear material with ultrafast relaxation time, such switches are slow. **Tajima** [5.2] had shown a technique to overcome this slow relaxation to achieve short pulses in a Mach-Zehnder interferometer circuit. They used a symmetric Mach-Zehnder containing two nonlinear semiconductors one each in the two arms. The two nonlinear media are excited using two control pulses with some delay. When the first control pulse is absorbed by the nonlinear medium, refractive index change is induced and signal light is switched from one port to the other port. The action of the second nonlinear medium, which absorbs the second control pulse after a certain time delay, is to switch off the output signal. This happens as the refractive index changes in the second nonlinear medium were so induced to cancel the effect of the first medium. Therefore the on time depends on the time delay between the two control pulses. Rick Trebino and Carl C. Hayden [5.3] show a similar effect in a Sagnac interferometer using a single nonlinear element. They use a three-arm Sagnac interferometer in which a nonlinear element is placed. An external pump pulse excites this element. The two counter propagating probe pulses pass through the nonlinear element. The resultant output intensity is given by

$$I_{out} = \left| E_{cwp} - E_{ccwp} \right|^2$$

where, E_{cwp} and E_{ccwp} are the clockwise propagating (cwp) and counterclockwise propagating (ccwp) complex field amplitudes after the pulses traverse the interferometer and the output arm of the interferometer.

Following the techniques mentioned above, a method is proposed to overcome the limitation of the slow relaxation times of the nonlinear material to produce fast optical switching action and to generate an N-bit signal. First, fast switching overcoming the relaxation time of a nonlinear medium is discussed and then an experiment [5.4] to generate an N-bit signal is proposed using a Sagnac interferometer.

The setup to produce the fast switching action and N-bit signal generation is shown in fig.5.1. The setup is a three-arm Sagnac interferometer consisting of a 50:50 non-polarizing beam splitter, two Quarter Wave Plates, two Nonlinear Optical Elements (NLOEs), two mirrors and a linear analyzer. A cw laser beam, linearly polarized parallel to x-axis i.e., perpendicular to the plane of the interferometer (as defined in earlier chapters), is passed through the interferometer and this beam acts as the probe beam for the two NLOEs. Let us recall the working of a three-arm Sagnac interferometer similar to the setup shown in fig.5.1 but without the quarter wave plates and the NLOEs inside the interferometer. If a beam polarized along x-axis is sent through the interferometer, it is already shown in chapter II that the output beams emerge out from the interferometer with their polarization states same as the input polarization. A linear analyzer is kept with its pass axis perpendicular to the input polarization. Therefore no output is seen. Now consider the case in which a retarder plate is kept inside a three-arm Sagnac interferometer. From chapter II we know that this will not have any effect on the output fringe pattern. In order to have the effect of a retarder [5.4] in a three-arm Sagnac interferometer we introduce two quarter wave plates, placed orthogonally, one each on either side of the retarder inside the Sagnac interferometer. The two quarter wave plates are so arranged that their fast axes, for a beam travelling through them in the same direction, are orthogonal to each other. The two quarter wave plates are placed such that their fast axes are at ±45° to the x-axis. Consider the propagation of the anti-clockwise beam. The beam after passing through the first quarter wave plate gets converted into left circularly polarized beam. This beam, after passing through the retarder gets converted to an elliptically polarized beam, which in turn will be converted into another state of elliptic polarization by the second quarter wave plate. Similarly the clockwise beam also goes through the quarter wave plate - retarder - quarter wave plate combination and gets converted into an elliptically polarized beam with the transformation at the retarder being opposite to that occurring to the anti-clockwise beam. As a result, the two output beams from the interferometer (before the analyzer) lie on either side of the equator, on the Poincaré sphere. The components perpendicular to the input polarization will therefore be out of phase with each other and cancel while passing through the analyzer.

Now consider the case where only one NLOE is present between the two quarter wave plates. When this NLOE is not excited it is assumed to be isotropic and does not make any changes to the beams, except for an additional optical path, which will be same for the counter propagating beams traveling through the Sagnac interferometer. Hence, no output is observed. The NLOE is excited using an intense laser pulse (pump, not shown in fig. 5.1), which is linearly polarized parallel to the fast axis of one of the quarter wave plates. The excited NLOE acts like a retarder with its fast axis parallel to the pump polarization and hence parallel to the fast axis of one of the quarter wave plates. The anisotropic behaviour of the NLOE varies with time. The change lasts until the NLOE relaxes. Phase of a probe passing through an excited nonlinear medium changes according to (eq.5.1). Because of this transient retardation the counter propagating beams emerging out of the interferometer are elliptically polarized. As a result each beam has a component parallel to the pass axis of the analyzer, which are out of phase. This is because the two beams are on opposite side of the equator after passing through the three element combination quarter wave plate - NLOE - quarter wave plate. The output signal is given by

$$I_1 = 4 - 2\cos\delta_1 - 2\cos\delta_2 + 2\cos A + 2\cos(A + \delta_2 - \delta_1) - 2\cos(\Delta - \delta_1) - 2\cos(\Delta + \delta_2)$$
$$(5.2)$$

where, A is the total optical path difference between the two pulses, δ_i (i=1,2) is the phase retardation in the counter propagating beams as measured at the observation point. A constant factor is omitted for convenience.

The output will consist of two pulses resulting from the time dependent phase retardation of the counter propagating beams. The width of these pulses is equal to the relaxation time of the NLOE, assuming there to be no dispersion anywhere in the circuit. Let S_1 and $S_1^{/}$ be the output pulses respectively, resulting from the clockwise and anti-clockwise probe beams in the interferometer. These two output pulses S_1 and $S_1^{/}$ are separated from each other or overlap, depending on the optical path, they travel inside the interferometer, after the phase retardation at the NLOE. Let Z_1 and Z_2 be the distance traversed by these counter-propagating beams after NLOE. Figure 5.2a

show one of the output pulses, say S_1, on time axis. Both output pulses are limited by the relaxation time of the NLOE. As the polarization components, of the two output beams, parallel to the axis of the analyzer have opposite sign, when they overlap the two pulses cancel each other in the region of overlap to give a single shorter pulse. The width of the resultant pulse is shorter than the relaxation time of the NLOE. Figs.5.2b-d show different cases of this overlap. Here the overlap is shown for different Z_1 with fixed Z_2. More the overlap shorter will be the pulse. Thus it is shown that the relaxation times of nonlinear medium can be overcome to produce fast switching action. So, adjusting the distance travelled by the counter propagating beams after the NLOE one can get a single output pulse having pulse width smaller than the relaxation time of the NLOE.

The principle explained above is now used to generate an N-bit signal. The setup for the proposed N-bit signal generation is shown in fig.5.1. (three-arm Sagnac interferometer with two NLOEs placed symmetrically in the interferometer). As mentioned earlier the two NLOEs do not make any changes to the beams when not excited resulting in zero output. The two NLOEs are excited using two intense laser pulses (pumps). One of the pump pulses is linearly polarized parallel to the fast axis of one of the quarter wave plates and will excite the NLOE adjacent to that quarter wave plate. The other pump pulse is linearly polarized parallel to the fast axis of the second quarter wave plate and will excite the NLOE adjacent to the second quarter wave plate. When the two NLOEs are excited by respective pumps (not shown in Fig.5.1), their anisotropy changes and the phase of the counter propagating beams passing through them gets retarded and the fast axis of the two NLOEs will be parallel to the fast axis of the quarter wave plate adjacent to them. (Recall that the two quarter wave plates are arranged so that their fast axes are orthogonal). The intensity of the output after the analyzer is given by

$$I = 4 - 2\cos(\delta\varphi_{12} - \delta\varphi_{11}) - 2\cos(\delta\varphi_{22} - \delta\varphi_{21}) + 2\cos(\Delta + \delta\varphi_{22} - \delta\varphi_{12})$$
$$+ 2\cos(\Delta + \delta\varphi_{21} - \delta\varphi_{11}) - 2\cos(\Delta + \delta\varphi_{21} - \delta\varphi_{12}) - 2\cos(\Delta + \delta\varphi_{22} - \delta\varphi_{11})$$

$$\text{(5.3)}$$

where, $\delta\varphi_{ij}$ (i, j =1,2) are the phase retardations, given by Eq.5.4, due to the two NLOEs as seen from the observation points and A is the optical path difference between the beams coming out of the Sagnac interferometer. The above intensity has a constant multiplicative factor, which is omitted for convenience.

$$\delta\varphi_{ii} = \left(\frac{2\pi l}{\lambda}\right)\left(\frac{n_2}{2\tau_r}\right)\int_{-\infty}^{t} \exp(\frac{t'-t}{\tau_r}) \ E_2^2(t'-z_k/v) \ dt'$$

$$\delta\varphi_{ij(i\neq j)} = \left(\frac{2\pi l}{\lambda}\right)\left(\frac{n_2}{2\tau_r}\right)\int_{-\infty}^{t} \exp(\frac{t'-t}{\tau_r}) \ E_2^2(t'-\tau-z_k/v) \ dt' \qquad \textbf{(5.4)}$$

where, k=1,2 and all other parameter are same as defined earlier.

One excited NLOE resulted in two (S_1 and $S_1^{/}$) output pulses and when both NLOEs are excited we get two more output pulses S_2 (clockwise) and $S_2^{/}$ (anti-clockwise). These are also limited by the relaxation time. Among the four output pulses, any pulse can overlap with any other pulse or they can be separated arbitrarily from one another. All this depends on factors like the delay between the pumps used to excite the two NLOEs, the total length of the interferometer, the distance between the two NLOEs and their distances from the observation point.

In fig.5.3 the output intensity for different delay times between the two pumps is shown. Here, the delay between the two pumps is so adjusted and the NLOEs are so placed that the output pulses, $S\backslash$ and $S_1^{/}$ overlap followed by the overlap of S_2 and $S_2^{/}$ (figs 5.3a,b). This will result in two short pulses. The two pumps are so delayed, that the two output pulses are well separated. When the delay between the two pump pulses is reduced then these two output pulses merge to give one single pulse (figs. 5.3c,d). In fig. 5.3c the two pulses are adjacent to each other to give a single pulse of larger width intensity equal to the intensity of the two individual pulses. In fig 5.3d the delay is still reduced resulting in a single pulse whose intensity is larger than that of the two individual pulses. From these calculations it is clear that in the example

considered when the two output pulses overlap each other exactly they will add up to give the bit, say '1' and when they partially (half) overlap it will result in the bit, say '0'. In order to get a signal containing such 0's and 1's as bits, it is necessary to have a series of pulses produced in the desired manner. This is achieved here by optical control over the bits generated. When the two NLOEs are excited by a series of pump pulses we get a series of output pulses, say, S_1, S_1', S_2, S_2', ... S_i, S_i',... and so on. Adjusting the delay between the pump pulses and the distance between the two NLOE's one can control these output pulses. The output pulses are controlled in such a way that the pulse S_1' overlaps with S_2 followed by the overlap of pulses S_2' and S_3 and so on. Depending on the extent of overlap the bits 0's and 1's are generated. As an example a 3-bit signal is theoretically generated. For generating a 3-bit signal four pairs of pump pulses are required. Fig. 5.4 shows 3-bit signals for different delay conditions of pump pulses resulting in signals '111', '110', '101'...and so on. Here we have used one nanosecond pulses as pump pulses and the relaxation time for the two NLOEs is taken to be one microsecond. The kerr coefficient is assumed to be 10^{-15}. All the signals have an initiator pulse and ending pulse. These pulses will have the same intensity as that of the '0' bits but with different width. These two pulses will have smaller width when compared to the width of '0' bits. So if one wants to read a signal the first and last pulses of the each pulse train has to be neglected and these pulses can be used to find where the signal starts and ends. To generate a 3-bit signal four pairs of pump pulses are required and to generate a N-bit signal $N+1$ pump pulse pairs are required.

The signal generation is optically controlled and this effect may be useful in optical communications and optical computations or related fields. In this chapter we have shown with the Sagnac interferometer, a method to generate an N-bit signal using slowly relaxing medium. Since high intense laser pulses have to be used to excite the NLOEs, there is a possibility that the transient refractive index has a spatial profile for example, like a quadratic index medium. In this chapter such effects are assumed to be absent, we may however ask the question what effects a lens has in a Sagnac interferometer. In the next chapter we study the effect of a lens in Sagnac interferometer.

REFERENCES:

5.1 *"An ultrafast gate"*, M.A.Duguay and J.W.Hansen, Appl. Phys. Lett, 15, 192 (1969)

5.2 "*All-optical switch with switch-off time unrestricted by carrier lifetime*", Kazu-hito Tajima, Jpn. J. Appl. Phys., 32, L 1746 (1993)

5.3 *"Antiresonant-ring transient spectroscopy"*, Rick Trebino and Carl C. Hayden, Opt. Lett. **16**, 493, 1991

5.4 "*N-bit signal generation using a Sagnac interferometer and slowly relaxing non-linear medium"*, M. Sree Ramana and Surya P. Tewari, Proc. of National Laser Symposium-1999, Hyderabad (INDIA), 441

5.5 "*A geometric phase interferometer"*, P. Hariharan and M. Roy, J. Mod. Opt., 39, 1811,1992
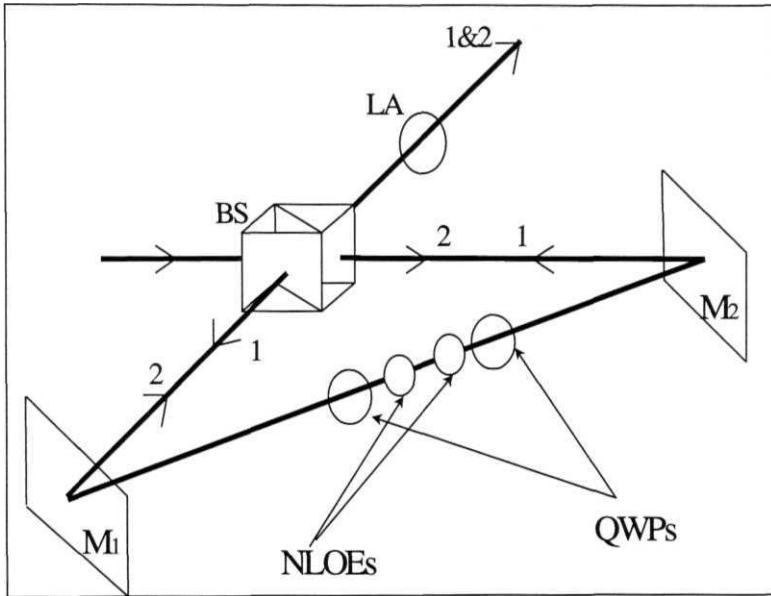
Fig.5.1: A three-arm Sagnac interferometer with 50:50 non-polarizing beam splitter(BS), 100% reflecting mirrors(M_1, M_2), two quarter wave plates(QWPs) and two Nonlinear optical elements(NLOEs).
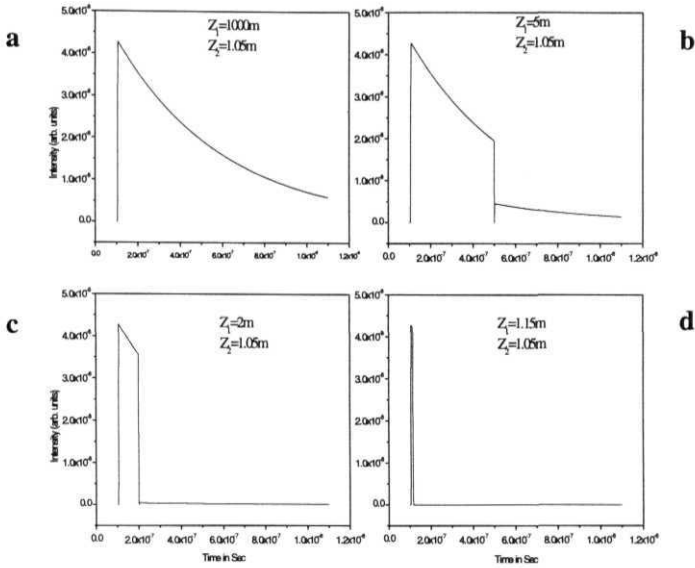
Fig. 5.2a: This shows one single output pulse whose width is limited by the relaxation time of the NLOE. This is the theoretical output when only one NLOE is placed in the setup shown in fig.5.1.

Fig. 5.2b-d: These figures show the output signals (theoretical) from the setup shown in fig.5.1 but with only one NLOE. The two pulses, which emerge out from the interferometer overlap to give these signals. Here the signals for different overlap conditions controlled by the distances Z_1 and Z_2 (see text), are shown on the same scale.
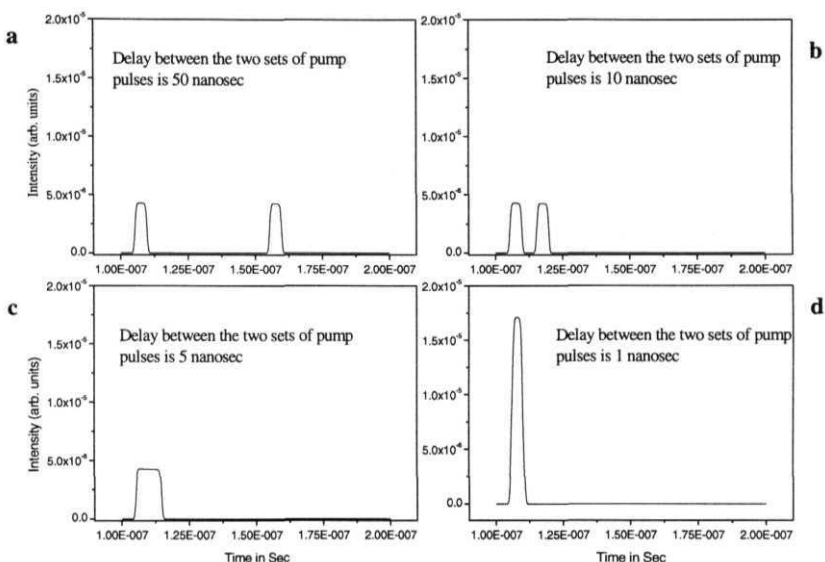
Fig 5.3: In this figure output signals (theoretical) from the setup shown in fig.5.1 with the two NLOEs present are shown for different delay times of the two pumps used to excite the NLOEs. The distances between the two NLOEs and the detector are kept fixed in all cases shown in this figure.
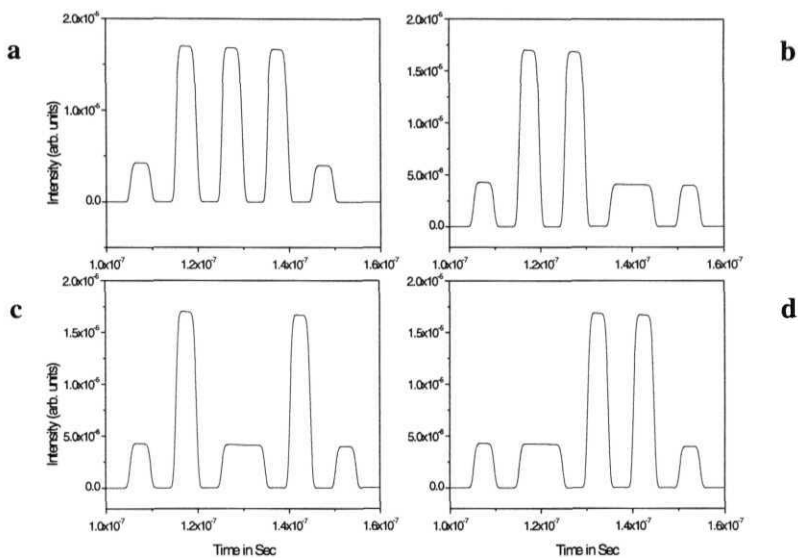
Fig.5.4: 3-bit signals generated theoretically for the setup shown in fig.5.1. These signals are generated using one-nanosecond pulses as the pumps to excite the NLOEs with one-microsecond relaxation times. The kerr coefficient is assumed to be 10^{-15}. The figures show signals for different delay times between each set of pump pulse pairs. a) Shows the signal '111'. b) Shows the signal '110'. c) Shows the signal '101'. d) Show the signal '011'.

A Study to Show Gouy Phase Effects Through Sagnac Interferometer

In the earlier chapters we studied the effects of wave plates and optically active elements on Pancharatnam's phase in a Sagnac Interferometer. In this chapter we study the effect of a lens on Gouy phase in a three-arm Sagnac interferometer. The setup (fig.6.1) consists of a three-arm Sagnac interferometer and a lens L as an optical element placed in one of the arms of the interferometer. The output intensity fringe pattern is observed as the lens L is moved inside the interferometer. A linearly polarized He-Ne cw laser beam (TEM_{00}) is passed through the interferometer. The beam splits into two at the beam splitter. These two beams counter-propagate inside the Sagnac interferometer and in the process pass through the lens L. The lens L inside the interferometer transforms these beams into two new beams, which emerge out of the interferometer and interfere. This interference will depend on the relative phase of the two output beams. Before going into the details of this experiment we will first look at the action of a lens on a Gaussian beam. The amplitude of the TEMoo Gaussian beam is given by [6.1]

$$E_1(x, y, z) = E_o \left(\frac{\omega_o}{\omega(z)} \right) \exp\left[-i[kz - \eta(z)] - i\frac{kr^2}{2q(z)} \right] \tag{6.1a}$$

$$\frac{1}{q(z)} = \frac{1}{R(z)} - \frac{i\lambda}{\pi\omega^2(z)} \tag{6.1b}$$

$$\omega_{io} = \omega(z = 0) \tag{6.1c}$$

$$z_o = \frac{\pi\omega_{io}^2}{\lambda} \tag{6.1d}$$

where, z is the propagation direction, x and y are the transverse directions, ω_{io} is the beam waist of the beam, $r=[x^2 + y^2]^{1/2}$ and $2 z_o$ is called the Rayleigh range. R(z) and $\omega(z)$ are respectively the radius of curvature of the wavefront and the beam spot size at a distance z from the beam waist ($\omega(z=0) = \omega(0) = \omega_{io}$) and $\eta(z) = \tan^{-1}(z/z_o)$. The

action of a lens placed at z = 1 on this beam is to add a phase of $\exp[-ikr^2/(2f)]$, where f is the focal length of the lens, given by the transformation $1/q' = (1/q\,(1)) - (1/R\,(1))$. The amplitude of the new beam with its beam waist at a distance z_n from z = 0 is given by

$$E_1(x, y, z') = E_o\left(\frac{\omega_o'}{\omega'(z')}\right)\exp\left[-i[kz' - \eta'(z')] - i\frac{kr^2}{2q'(z')}\right] \tag{6.2a}$$

$$z' = z - z_n \tag{6.2b}$$

$$\frac{1}{q'(z')} = \frac{1}{R'(z')} - \frac{i\lambda}{\pi\omega'^2(z')} \tag{6.2c}$$

$$\omega_o' = \omega'(z' = 0); \quad z_o' = \frac{\pi\omega_o'^2}{\lambda} \tag{6.2d}$$

Here $z' = 0$ at the new beam waist position z_n. All primed terms have the same definition as in [6.1] with z replaced by z'.

Now few questions arise. What happens to the $\eta(z)$ function after lens transformation? Should this term be added to the phase of the new beam or should it be left out? Does the lens introduce any other phase difference apart from the said change? Our experiment tries to provide answers to these questions. It's a well-known fact that the function r|(z) is related to the Gouy phase [6.2]. Gouy phase is an additional phase shift of π which any focused electromagnetic beam undergoes as it evolves though the focus. This phase shift was first discovered by Gouy [6.3] in 1890. $\eta(z)$ is the Gouy phase of the Gaussian beam from the beam waist. Therefore total Gouy phase shift for a Gaussian beam of TEMoo mode is *n* [6.2] when the beam travels from -infinity to + infinity. We may observe that by studying the effects of a lens inside a Sagnac interferometer we will be studying the relative effects of Gouy phase shifts of the two counter propagating beams.

For elaborating the above observation and to understand the effect of a lens we use a popular representation of Gaussian beams on Collins chart [6.2]. Collins chart (fig.6.2a) represents the complex $1/q$ plane with real axis being $\lambda/\pi\omega^2$ and imaginary axis being $1/R$, where ω and R are the spot size and radius of curvature of the beam. 'GO' being always greater than zero restricts one to positive real axis i.e., to the first and fourth quadrants of the plane. Each point in this half plane represents a Gaussian state hence we can trace a Gaussian beam, as it propagates, in this plane. A Gaussian beam which has a waist ω_o is represented by a circle of radius $1/2Z_R$ with its center at $(1/2Z_R, 0)$, where $Z_R = (\pi\omega_o^2)/\lambda$ is the Rayleigh range. As the beam propagates from -infinity to +infinity it moves on this circle from the origin in the anti-clockwise direction. The beam waist position is on the real axis as $1/R$ is zero at this point and is given by $x=1/Z_R$. The points representing the minimum radii of curvature lie on the line parallel to y-axis passing through the center of the circle as shown in fig.6.2a. The phase term r| is defined as $\tan^{-1}(y/x)$ and the Gouy phase at a point z with respect to the origin may be given by the angle subtended at the origin by the arc of the circle or half the angle subtended at the center of the circle. So, for a full circle, one has a phase shift of *n.* For a part of the circle, this shift will be equal to the angle subtended by that arc of the circle at the origin or half the angle subtended at the center. This provides a simple way of representing and understanding Gouy phase. Different circles, with centers lying on the x-axis and origin as a common point to all the circles, represent different beams. Circle with infinite radius describes the beam with point focus and the point circle represents the beam with infinite beam waist. A lens transformation is represented, in fig.6.2b, by a vertical line parallel to y-axis. The length of this line is equal to $1/f$, where f is focal length of the lens. If (x, y) is the point before transformation, then (x, y - $1/f$) is the point after the transformation. This means that the beam gets transformed into a new beam after the lens and will be described by a new circle. What will be the phase difference along these vertical lines representing the lens transformations? What will be the total Gouy phase difference for a combination of beams undergoing a lens transformation and completing, in the **anti-clockwise** direction, a closed circuit $OP_{11}P_{12}O$ or $OP_{21}P_{22}O$ on the Collins chart as shown in fig.6.2b. Will the Gouy phase be equal to *n* or more or less than π? What happens if

the full circle is not completed? In interference experiments should one consider the $\eta(z)$ as the Gouy phase or should one consider the phase for the part of the circles the beams travel? Our experiment examines answers to these questions. It would be proper if we discuss, before presenting our experiment, some of the earlier works on Gouy phase.

From the time of discovery of Gouy phase several authors have given the physical explanation for this phase. In the recent time couple of authors described it as a Berry's geometric phase [6.4-5]. Fatih Erden and Ozaktas [6.6] provided a solution theoretically to the questions raised in the above paragraph. First we discuss about the works describing Gouy phase as a geometric phase.

Mukunda and Simon [6.4] showed the connection between Berry's geometric phase and Bargmann gauge invariant to demonstrate that the geometric phase associated with a Gaussian beam is the Gouy phase. In this paper the authors consider the complex plane associated with a Gaussian beam characterized by complex number $\xi = z - iZ_R$, where z is the propagation distance plotted on the real axis and Z_R is the parameter related to the beam waist and is plotted along the imaginary axis. All the gaussian states are represented by different points of the -ve half plane of ξ plane, as Z_R is always +ve. As the beam propagates in space, ξ evolves along a straight line parallel to the real axis, with Z_R on the -ve imaginary axis. The minimum beam spot size of the beam lies on the imaginary axis. To find the phase difference between two points on any straight line parallel to the real-axis, the authors connect the two points with the **geodesics** of the plane completing a geodesic quadrangle. In this case the **geodesics** are the circles with centers on the real-axis and straight lines normal to real-axis as this plane is a hyperbolic plane. The phase difference between the two points is related to the geometric phase associated with the area of the geodesic quadrangle connecting the two diagonally opposite points. The geometric phase for the geodesic quadrangle is equal to one fourth of the area enclosed by the quadrangle and is given by

$$\varphi_g = -(1/2) \left(\tan^{-1}(z_2/Z_R) - \tan^{-1}(z_1/Z_R) \right) \tag{6.3}$$

This phase is the Gouy phase shift for the Gaussian beam with one transverse coordinate. z_1, z_2 are the distances of the two points from the z=0 at beam waist. Will the phase difference between these two points still be given by eq.6.3, if one takes a different path, other than the straight line mentioned above, while traversing from one point to the other?

Subbarao [6.5] has discussed Gouy phase as a geometric phase in a different manner. Subbarao projected the complex $1/q$ plane onto a focusing sphere of unit diameter where, $1/q = -i\ [(\lambda/\pi\omega^2)+(i/R)]$ with ω being the gaussian beam spot size and R being the radius of curvature of the wavefront. Both co and R are functions of distance z from the beam waist. If the path traced by the beam on the complex $1/q$ plane is a circle C then the path traced on the surface of the sphere is also a circle (spherical circle), C_s. The geometric phase for such a path on the sphere is given by the solid angle subtended by C_s at the center of the sphere, which is given by

$$\varphi_g \quad = \quad -2 \quad \pi\rho^2/(\quad 1 \quad +p^2) \quad = \quad -\pi(\quad 1 \quad -\cos\theta_c) \quad (6.4)$$

where p and θ_c are the radius of the circle C and angular radius of the spherical circle C_s respectively. In the works mentioned above, the authors have shown Gouy phase as another manifestation of Berry's geometric phase. What happens in the case of a lens transformation as shown in fig.6.2b? Will the Gouy phase be still given by the angle subtended by the area enclosed within the closed circuit on the focusing sphere?

Gouy phase shift is an on axis phase. For a multiple optical element system it accumulates as calculated by Fatih Erden and Ozaktas [6.6]. They provided an expression for the accumulated Gouy phase in terms of the parameters of the optical system through which the beam propagates. The expression for the Gouy phase shift is given by

$$\tan \varphi_g = \frac{B}{\left(A+\dfrac{B}{\lambda R_{in}}\right)\pi\omega_{in}^2}$$

where A and B are the elements of transformation matrix $T = \begin{bmatrix} A & B \\ C & D \end{bmatrix}$ (det $T = 1$)

through which the beam propagates. This phase depends only on the elements of first row and is independent of the second row elements. According to this expression the thin lens transformation does not result in any Gouy phase shift as $B = 0$. They also showed that if a gaussian beam propagates through different optical elements then the total Gouy phase is equal to sum of the Gouy phase shifts of all the elements involved and that this can also be determined considering the entire system as one unit using a transformation matrix, which is the product of the transformation matrices of the optical elements involved. That is, if a beam propagates a distance of d_1 before a lens and a distance d_2 after the lens then the total Gouy phase shift is $\varphi = \varphi_1 + \varphi_2$, where φ_1 and φ_2 are the Gouy phase shifts for the first and second portions of the Gaussian beam. This means that parts of beams may not see the full Gouy phase shift of π associated with infinite extent of the full Gaussian beam.

This gives a theoretical answer to the questions raised in the very beginning of this chapter. Our experiment in this chapter provides an experimental proof to the questions raised. As our experiments are done with Sagnac interferometer and we observe the changes in the fringe pattern we will be obtaining the difference between the accumulated Gouy phases of the two interfering beams rather than the total Gouy phase accumulated by each beam.

The setup shown in **fig.6.1** consists of a three-arm Sagnac interferometer with a 50:50 non-polarizing beam splitter and two **Al** coated 100% reflecting mirrors. A lens L_1 of focal length f_1 is placed at a distance l_o from the beam waist of the input laser beam and the beam splitter is at a distance d_l away from the lens L_1. Beam waist of the input beam is ω_{io}. Depending on the focal length f_1, distances l_o and d_l and the total length (1) of the Sagnac interferometer, the beam waist of the beam after the lens L_1 lies before, inside or after the Sagnac interferometer. If it falls inside the Sagnac interferometer then there are two points at which one finds this beam waist; as the beam gets split into two beams inside the interferometer. These beam waist positions

for the two beams can be coincident at the center of the Sagnac interferometer, or can be separated from each other before/after the center of Sagnac interferometer. These beams are referred as the input counter-propagating beams. Another lens L_2 of focal length f_2 is placed inside the interferometer at a distance l_{11} from the BS in the direction of the clockwise beam. The two beams traversing the interferometer pass through this lens from opposite directions and get transformed into new beams with different beam waists. The difference in the beam waists of the transformed beams is because the lens is placed at different positions with respect to the beam waists of the two input counter-propagating beams. These transformed beams traverse the remaining part of the interferometer and emerge out from the output port of the interferometer to give an interference fringe pattern in the field of view. This is recorded using a CCD camera placed at a distance d_c from the beam splitter in the output arm.

We now explain our system using Collins chart in figs. 6.3a and b. Let ω_0 be the beam waist of the input beam after the lens L_1. Then the circle with a radius $\lambda/(2\pi\omega_0^2)$ defines our input circle C_0. Let the position of the lens L_1 on this circle be L_1 (not shown for clarity in the figures as it falls before the beam splitter position B_1). From this point onwards the output of lens L_1 starts traversing on the input circle. The beam encounters the beam splitter twice while traversing forward through the interferometer. We call the first encounter as first beam splitter and the second encounter as second beam splitter. The first beam splitter is at a distance of d_1 from the output of the first lens L_1 and is represented by a point B_1 on the input circle. This point is found using the simple relations for radius of curvature and spot size in terms of Z and Z_R. If there is no lens inside the interferometer both beams travel on the same circle C_0 from B_1 to the point B_2 representing the second beam splitter and continue till the point D (not shown in figures for clarity) representing the detector where the beams are recorded. Note that the propagation of both beams in the interferometer is shown in the same direction on the circle C_0 on Collin's chart. If the lens L_2 is placed inside the interferometer then the position of this lens will be different for the counter propagating beams in the Sagnac interferometer. Since the lens L_2 is at a distance of l_{11} from the first beam splitter along the clockwise direction then it will be at a distance of $l_{21} = l-l_{11}$ for the anti-clockwise beam where, l is the total length of the inter-

ferometer. Hence the points representing the lens L_2 will be different on this circle. These are represented by L_{11} and L_{21} on the circle C_o for clockwise and anti-clockwise beams respectively. The clockwise beam undergoes a lens transformation at L_{11} whereas the counter-clockwise beam undergoes the lens transformation at L_{21}. After these transformations the beams are represented by, different circles C_1 and C_2 depending on their new beam waists. If the $1/R$ is the y-coordinate before transformation, then $1/R - 1/f$ is the y-coordinate after the transformation. Hence the transformed beam will not trace full circle representing the transformed beam. They will trace a part of these circles starting from the points L_{12} and L_{22} on circles C_1 and C_2 respectively as shown in the fig.6.3. The position of the detector is found on these circles and obviously this will be at different points for the two beams (shown as D_1 and D_2 in the fig.6.3). Now the representation is complete. Let us look at the Gouy phase shifts at the detector from a common point on circle C_o. First the clockwise beam - this beam travels first the arc B_1L_{11}, then the vertical line $L_{11}L_{12}$ and finally the arc $L_{12}D_1$. Similarly the second beam travels the path $B_1L_{21}L_{22}D_2$. The Gouy phase for different portions, along the path of the clockwise beam, if it is assumed that no Gouy phase is added along the vertical line representing the lens transformation, is given by the sum of the angles subtended by the arcs B_1L_{11} ($\varphi_{11} = \eta_{11} - \eta_{b1}$) and $L_{12}D_1$ ($\varphi_{12} = \eta_{d1} - \eta_{12}$) at the origin. For the counter-clockwise beam it is equal to the sum of the angles subtended by the arcs B_1L_{21} ($\varphi_{21} = \eta_{21} - \eta_{b1}$) and $L_{22}D_2$ ($922 = \eta_{d2} - \eta_{22}$) at the origin. $\eta_{b1}, \eta_{11}, \eta_{12}, \eta_{d1}$ are the η values at the points B_1, L_{11}, L_{12} and D_1 respectively. Similarly $\eta_{b1}, \eta_{21}, \eta_{22}, \eta_{d2}$ are the η values at the points B_1, L_{21}, L_{22} and D_2 respectively. The difference between the total Gouy phase shifts is given by

$$\varphi \quad = \quad (921 \quad + \quad \varphi_{22}) \quad - \quad (\varphi_1 \quad 1 \quad + \quad \varphi_{12}) \quad (6.6)$$

This is with the assumption that the Gouy phase along the vertical line is zero. The phase difference (eq.6.6) will change as the lens is moved inside the interferometer because the points representing the lens keep moving. As the lens is moved inside the interferometer one of the circle becomes smaller and smaller while the other becomes bigger and bigger. When the lens reaches the center of the interferometer then the two

circles will become equal resulting in a zero Gouy phase difference. Note that the center of the Sagnac interferometer may not be the beam waist position on the input circle C_o.

If it is assumed that the lens transformation also contributes to the on axis phase then the vertical line representing the lens transformation also contributes to the Gouy phase as calculated below. The Gouy phase for the clockwise beam is equal to the sum of the angles subtended by the arcs B_1L_{11} and $L_{12}D_1$ and the line $L_{11}L_{12}$ at the origin. This sum is given by $\varphi_1 = \eta_{d1} - \eta_{12} + \eta_{12} - \eta_{11} + \eta_{11} - \eta_{b1} = \eta_{d1} - \eta_{b1}$. Similarly for the anti-clockwise beam it is given by $\varphi_2 = \eta_{d2} - \eta_{b1}$. The difference between the Gouy phase of the two beams is given by

$$\varphi = \eta_{d2} - \eta_{d1} \tag{6.7}$$

This means that the Gouy phase difference depends only on the η values of the two beams at the detector. Now we look at variation in both cases i.e., assuming that lens will not contribute to the Gouy phase (eq.6.6) and also that it will contribute (eq.6.7). We plot these as functions of the position of lens L_2. Figure 6.4 shows the Gouy phase difference for different cases. Curves shown in figs.6.4a-d are according to eq.6.6 and the ones in figs.6.4e-h are according to eq.6.7. From the figures it is observed that there is considerable change in the Gouy phase difference between the two beams when the lens is assumed not to contribute compared to the case when lens contributes. The Gouy phase difference when the lens is assumed to contribute is very small compared to the difference in the case when it is assumed that lens does not contribute. This is because in the case where lens does contribute, Gouy phase difference depends only on the η values at the detector on the circles C_1 and C_2. Since the detector is kept at distance $(z \rightarrow \infty)$ far from the beam waists of both the beams, the difference turns out to be very small.

In order to determine the on axis phase experimentally we may examine the interference fringe pattern at the position of the detector, which is a CCD camera. The interference pattern at the detector is given by the expression

$$I_o = I_1 + I_2 + 2\sqrt{I_1 I_2}\ \cos\left[k(z_2 - z_1) - (\eta_2 - \eta_1) + k\frac{r^2}{2}\left(\frac{1}{R_2} - \frac{1}{R_1}\right)\right] \qquad (6.8)$$

where I_1 and I_2 are the intensities, R_1 and R_2 are the radii of curvature of the wave fronts, η_1 and η_2 are the accumulated Gouy phase shift of the two beams respectively at the point of observation. z_1 and z_2 are the distances travelled by the two beams till the point of observation from the beam waist, ω_{io}, of the input beam before the lens L_1. The accumulated Gouy phase for each beam in the output of the Sagnac interferometer is made up of three parts if it is assumed that the lens transformation doesn't add to Gouy phase. $\eta_1 = \varphi_{11} + \varphi_{12} + \varphi_{13}$ and $\eta_2 = \varphi_{21} + \varphi_{22} + \varphi_{23}$. φ_{11}, φ_{12} and φ_{13} are the accumulated Gouy phases of the first beam from the beam waist ω_{io} till the input of the first lens L_1, from the output of the lens L_1 till the input of the second lens L_2 and from the output of the lens L_2 till the point of observation. Similarly φ_{21}, φ_{22}, and φ_{23} are the respective Gouy phase shifts in the three regions for the second beam. Using the above expression for the interference, intensity fringe patterns are generated for different positions of lens L_2. The fringe patterns are generated for both cases i.e., using the eq.6.6 and eq.6.7 so as to provide an immediate check for the experimental data. Figs.6.5a and b show these fringe patterns. On observing, it is found for the case of eq.6.6, when it is assumed that the lens will not contribute to Gouy phase, the fringe pattern (fig.6.5a) has a central bright point. The fringe pattern (fig.6.5b), with the assumption that lens will contribute to the Gouy phase, has a central dark point. This (fig.6.5b) is similar to the output from a Sagnac interferometer without lens L_2 inside. (These fringe patterns (eq.6.6, fig.6.5a) have a central bright spot of varying intensity depending on the position of lens L_2. But when the lens L_2 is at the center of the Sagnac interferometer then the fringe patterns for both cases are exactly same. It is also same as that when no lens is placed inside the Sagnac interferometer.)

Experiment: Qualitative discussion

The setup is as shown in fig.6.1. Incident beam from the He-Ne laser is of beam waist $\omega_{io} = 3.94024*10^{-4}$ meters. Interference fringes are recorded for different cases. It is clear that one observes a central bright fringe of significant and varying intensity in the experimental data (figs.6.6a-h). On comparing these fringe patterns with the theoretical fringe patterns (figs.6.5a and b), one can qualitatively conclude that one has to add the Gouy phase shifts if the beam propagates through different optical systems. Also one can say that lens does not contribute to Gouy phase because the fringe pattern in fig.6.5b has a central dark point compared to the central bright point in the experimental fringes. It is observed from these figures that the intensity at the center varies as the lens L_2 is moved and becomes zero when L_2 is at the center of the Sagnac interferometer. Therefore it can be said that having lens L_2 at the center amounts to having no lens at all in the Sagnac interferometer. Two cases have been studied experimentally.

1. The beam waist of the input beam falls inside the interferometer but they are yet to cross each other.
2. The beam waist of the input is much before the interferometer.

First case is done by placing a lens of focal length, $f_1 = 47.5$cm at distance of l_o from the beam waist of the incident beam. As a result the beam waist of the input counter propagating beams falls inside the interferometer. They are separated from each other but are yet to cross each other. Now a lens (of focal length $f_2 = 6$cm and 10cm) is moved inside the interferometer and the resulting interference fringe pattern is recorded using a CCD camera. In the second case the lens outside the interferometer is removed and a lens (of focal length $f_2 = 6$cm) is moved inside the interferometer. Here also interference fringe pattern is recorded for different position of the lens inside the interferometer.

Quantitative analysis of the experiment

To extract the on-axis phase from these fringe patterns, nonlinear least square fitting of two-dimensional fringe pattern is done according to the eq.6.8. The $\eta_2 - \eta_1$ term is replaced by φ_a in the 'cos' function to take care of the Gouy phase difference and any other phase if present. We call this phase as total additional on-axis phase. The value of φ_a so obtained is plotted in fig.6.7a-d against the position of the lens inside the interferometer. Each interference fringe pattern is fitted by Levenberg-Marquardt method for minimum chi-square for the parameters of the experiment. The parameters of the beams obtained from the best fit are: position of lens L_1 from the beam waist of the input beam; position of lens L_2 for the clockwise as well as the anti-clockwise beams; position of the detector for each beam; center of the spots of the two beams at the detector; intensity of the individual beams (assumed equal); and the additional on-axis phase φ_a. The ten parameters, other than φ_a, can be used to determine the value of Gouy phase for different sections through which the beams travel.

Note that the phase φ_a is a pure number which has been obtained without associating it to any function. To find the function to which the value of φ_a can be attached we calculated the Gouy phase substituting the parameters obtained from the best fits in eqs.6.6 and 7. These values are now compared with the values of φ_a. In figs.6.7a-d we plot the values of φ_a (circles) and the values calculated from eq.6.6 (triangles). The values calculated from eq.6.7 are too small to match with values of φ_a. This shows that the contribution of the lens towards the on-axis phase computed on the basis of Collins chart is incorrect. From the figs6.7a-d, it is clear that the values of φ_a match with the values of phase calculated from eq.6.6 where it is assumed that lens does not contribute to on-axis phase. This match is well enough to prove that the total on-axis phase shift with respect to a reference is obtained by addition of Gouy phase shifts of each section of a multiple optical element system through which the Gaussian beams propagate. This confirms the work in ref.6.5. Though there is good match between the values of φ_a and the calculated values, still there is some difference between them which is left out unexplained. This difference we call as residual phase. Also we ob-

served some scatter in the values of φ_a. This scatter of φ_a in the initial and final stages of the range of L_2 in the Sagnac interferometer is perhaps due to misalignment of beams upto the detector. This misalignment tends to be larger when the two beams travel very different distances after the lens L_2. This scatter may be the cause for the residual phase.

To find whether this residual phase is an error in the fit or it is present in the experiment the fitting is repeated once again with the following expression.

$$I_o = I_1 + I_2 + 2\sqrt{I_1 I_2} \, \cos\left[k(z_2 - z_1) - (\eta_2 - \eta_1) + \varphi_r + k\frac{r^2}{2}\left(\frac{1}{R_2} - \frac{1}{R_1} \right) \right] \qquad (6.9)$$

Here φ_r is the residual phase for which the fitting is done. $\eta_2 - \eta_1$ is the Gouy phase difference between the two beams with the assumption that lens does not contribute to the Gouy phase. The values obtained of φ_r from this fit are plotted in fig.6.7e-h. It is observed that these values are equal to the difference between φ_a and Gouy phase (triangles in fig.6.7a-d). This shows that the residual phase is present in the experimental fringe patterns. The range in which the values of the residual phase are found is (-0.6, 0.6) with some scatter. This scatter is present at the same positions as in the corresponding plots in fig.6.7a-d. The residual phase may be because of the optical path difference created in the beams of the interferometer, which is the cause for the scatter. This can occur in couple of ways.

1. If the two beams are travelling through each other in the interferometer with an angle (as the beams need necessarily not be in the same plane) between them. Because of this the beams coming out can be at an angle with each other resulting in an optical path difference. This can occur when the counter propagating beams are not passing through the center of the lens and lens is not normal to the input beams.

2. If the beams inside are in the same plane and are parallel to each other with a separation between their axes of propagation then also there is a possibility that we end up with some optical path difference.

The beams travel different distances after the lens L_2 in the interferometer. If the beams are at an angle to each other or displaced from one another then the output beams will be at an angle to each other. And since they travel different distances after the lens there will be optical path difference between the two beams. As the lens is moved inside the interferometer this optical path difference also changes because there is a possibility that the beams travel different distances after the lens due to some misalignment of beams. Figure 6.8 shows such a change in the optical path difference for the second case mentioned above. Similarly one can find the difference in the optical path for the first case also and it would not be differing much from the second case. On comparing the curves in fig.6.8 with that of φ_r in fig.6.7e-f one can infer that the residual phase is within the range of experimental error due to optical path difference. We may ask should this phase be treated as an error due to optical path difference or any other unknown experimental error or an effect of lens? We for sure cannot say that it is because of the lens though it appears different in different cases, as we cannot assure that our system is independent of optical path differences. But one can clearly rule out the contribution by the lens to Gouy phase according to the vertical line on Collins chart as this phase difference is larger compared to the residual phase. If one wishes to check whether the lens will have any additional phase difference of the order of the residual phase, in our experiments, then one need to perform a similar experiment making sure that it will not have any errors due to optical path difference, a case we have been unable to achieve.

Thus we have shown that Gouy phase indeed gets accumulated as the beam passes through different optical systems. It is known that a thin lens doesn't contribute to Gouy phase shift. Our experiment confirms this within the experimental errors.

Another case of interest is that of a quadratic index medium which behaves much like a lens but not a thin lens. The study of the effects of quadratic index medium become important keeping in view the changes in nonlinear refractive index in high intensity laser experiments involving phenomenon like self-focusing. Question does arise, is the on-axis phase for a lens of quadratic index medium also zero? Keeping in view eq.6.5 and non-zero value of the element B in the corresponding transfor-

mation matrix one expects that for a quadratic lens the on-axis phase need not be zero. One can obtain the contribution to the on-axis phase in this case by using ABCD matrix [6.1], or the solution obtained by Subbarao [6.7], or by Iwasawa decomposition [6.8] or by disentangling of the operator in the q-representation of the equivalent Schrodinger equation [6.9]. We use ref.6.9 to find the solution of the Schrodinger equation corresponding to a quadratic index medium ($n^2(x) = n_o^2 (1 - k_2 x^2/k)$ where k $= 2\pi/\lambda$ and k_2 is a dimensional constant of the quadratic index medium with dimension [L$^-$]).   The solution is given by the **eq.6.10** where $|\xi_o\rangle$ is the vacuum Gaussian state.

$$|\xi\rangle = \exp[i\gamma\partial^2]\exp[\beta(x\partial)]\exp[i\alpha x^2]\exp[\delta I]|\xi_o\rangle \tag{6.10}$$

$$\alpha = -\frac{-\sqrt{kk_2}}{2}\tan^{-1}\left[-\sqrt{\frac{k_2}{k}}\ z_q\right] \qquad \beta = \ln\left(\cos\left[-\sqrt{\frac{k_2}{k}}\ z_q\right]\right)$$

$$\gamma = \frac{1}{2\sqrt{kk_2}}\tan^{-1}\left[-\sqrt{\frac{k_2}{k}}\ z_q\right] \qquad \delta = \frac{\ln\left(\cos\left[-\sqrt{\frac{k_2}{k}}\ z_q\right]\right)}{2}$$

where z_q is the distance travelled within the quadratic refractive index medium. The distance z_q varies from 0 to L with L being the total length of the quadratic index medium. As a gaussian beam propagates within the quadratic index medium its state can be traced on Collins chart. It is found that the curves representing the gaussian states as the beam propagates are again circles, but the condition of origin to be the common point is no more required. The center of the circle depends on the state just before the quadratic index medium. Figure 6.9 shows these circles for different input states (the states just before the quadratic index medium). Now the Gouy phase is found using eq.6.5. One has to be a little careful in determining the Gouy phase. There is a possibility that the beam can see two foci within the quadratic medium. Going from one

focus to the second, the beam would have completed one full circle. If the beam completes one full circle and then part of a second, then Gouy phase shift should be more than π. But eq.6.5 doesn't give this phase difference as it can at the most show a difference of π. Therefore one has to keep track of the number of foci the beam is going to see as it propagates in the quadratic index medium. From one focus to another focus a full circle is completed and hence one should add a phase difference of n after each full circle. The Gouy phase difference can also be found from the Collins chart. It is given by half the angle subtended by the arc length of the circle describing the propagation of the beam at the center of the circle. One can also use focusing sphere [6.5] in this case to determine the Gouy phase shift. The curves for this case in the plane of ref.6.4 need to be examined to determine the Gouy phase in this case.

References:

6.1 "*Quantum Electronics"* A. Yariv, John Wiley, 1989

6.2 "*Lasers*", A. E. Siegman, University Science Books, California, 1986

6.3 *"Sur une propriete nouvelle **des** ondes **lumineuses**"*, Gouy, C. R. Acad. Sci. Paris 110, 1251,1890

6.4 "***Bargmann** invariant and the geometry of Giioy effect",* R. Simon and N. Mukunda, Phys. Rev. Lett., 70, 880, 1993

6.5 *"Topological phase in Gaussian beam optics",* D. Subbarao, Opt. Lett., 20, 2162, 1995

6.6 *"Accumulated Gouy phase shift in Gaussian beam propagating first-order optical systems",* M. Fatih Erden and Haldun M. Ozaktas, J. Opt. Soc. Am A 14, 2190

6.7 *"Lie optics, geometric phase and nonlinear dynamics of self-focusing and soliton evolution in a plasma",* D. Subbarao et. al., Pramana -J. of Phys., 55, 757, 2000

6.8 "Iwasawa decomposition for SU(1, 1) and *Giioy effect for squeezed states",* R. Simon and N. Mukunda, Opt. Comm., 95, 39, 1993

6.9 "Functional forms for the squeeze and time displacement operators", M. M. Nieto, Quant. Semiclass. Opt., 8, 1061, 1996
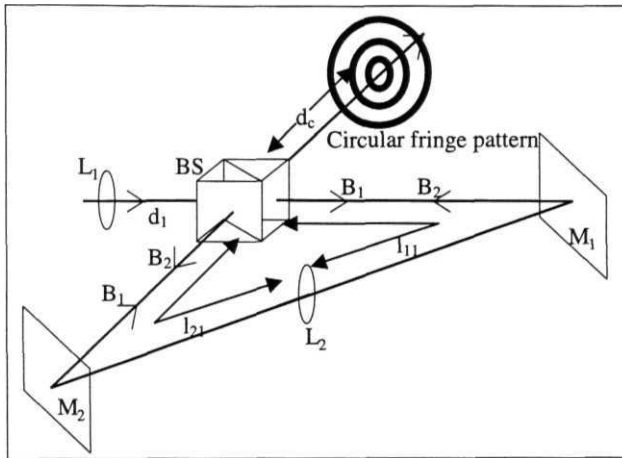
<u>Fig. 6.1</u>: This figure shows the setup to study the effect of a lens inside a three-arm Sagnac interferometer. It consists of lens L_1 placed in the input arm of the Sagnac interferometer and another lens L_2 place in one of the arms of the interferometer. When the beams interfere outside they give rise to circular fringe pattern if the interferometer is aligned perfectly for a zero optical path difference. The distance between the lens L_1 and the beam splitter is d_1. The distance between the BS and the lens L_2 in the clockwise direction is l_{11} and in anti clockwise direction is l_{21} ($l_{21}=l-l_{11}$). The distance between the BS and the point of observation is equal to d_c.
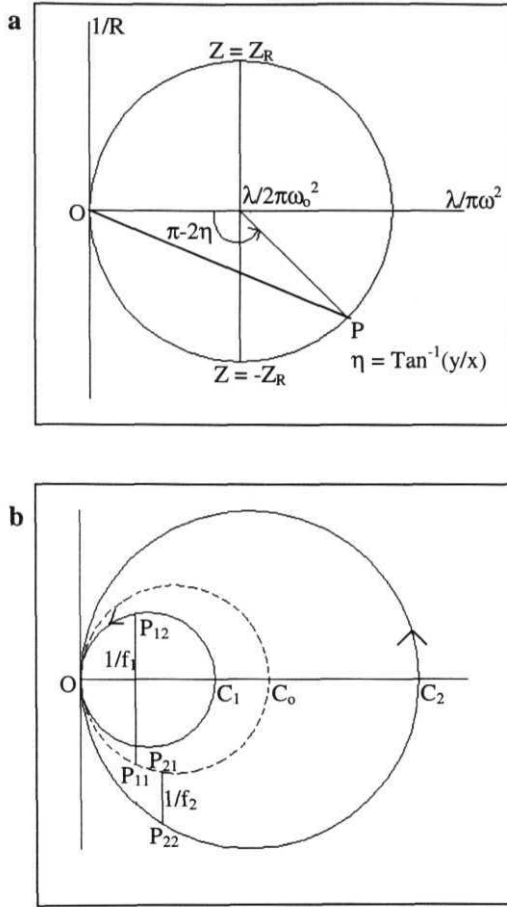
Fig. 6.2a: In this figure we show the Collins chart representation of a Gaussian beam with a beam waist ω_o. The radius of this circle is $\lambda/2\pi\omega_o^2$ and center is $(\lambda/2\pi\omega_o^2, 0)$. The point P represents a point of the Gaussian beam along the propagation direction. The points $Z = Z_R$ and $Z = -Z_R$ are the points of numerically minimum radius of curvature of the Gaussian wave fronts along the direction of propagation. $Z_R = (\pi\omega_o^2)/\lambda$. O is the origin point.

Fig. 6.2b: Here we show examples of the lens transformation on the Collins chart. Circle OC_o represents the input beam. At a point P_{11} a lens of focal length $-f_1$ is placed. This lens transforms the beam into a new beam that starts at the point P_{12} on the circle OC_1. Similarly another lens of focal length $+f_2$ is placed at a point P_{21}. This lens will take the beam to a point P22 on the circle OC_2. O is the origin common to all circles describing different Gaussian beams.
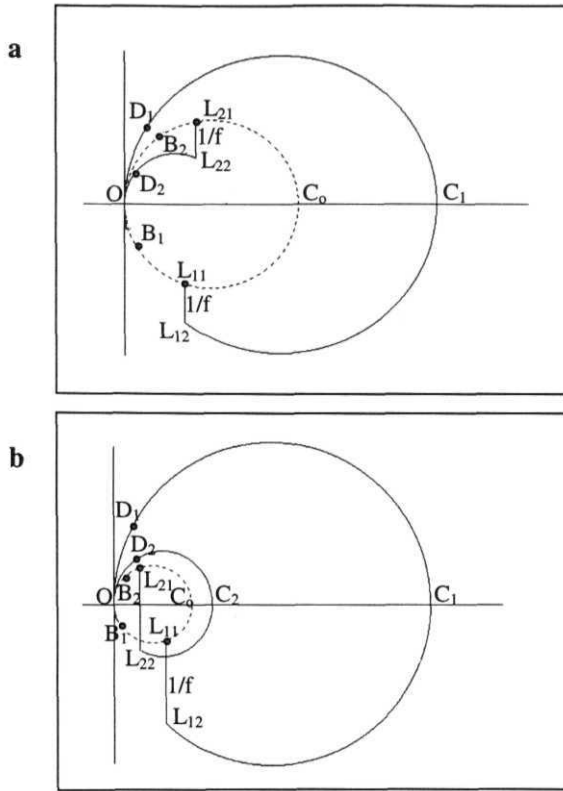
Fig. 6.3: Here we show the Collins chart representing the experiment to study the lens effect in a Sagnac interferometer. The lens transformations take place at different places on the same circle. This occurs naturally in a Sagnac interferometer. B_1 and B_2 are the beam splitter positions on the first and second encounters along the forward path in the Sagnac interferometer on circle OC_0. D_1 and D_2 are the positions of the detector on circles OC_1 and OC_2 respectively.

a: In this figure we show the case when the value of $1/f$ is shorter than the diameter of the input circle OC_0. The circle OC_2 is not shown fully as the path traced by the beam on this circle is in the end of the circle. So one should note that the arc $L_{22}D_2O$ is the circle OC_2. C_2 is not shown in the figure.

b: Here we show the case when $1/f$ is greater than the diameter of the input circle OC_0. Observe that in this case there is a possibility that the beams can trace almost two full circles. Look at the path $B_1L_{21}L_{22}D_2$. The beam travelling along this path almost completed two circles.
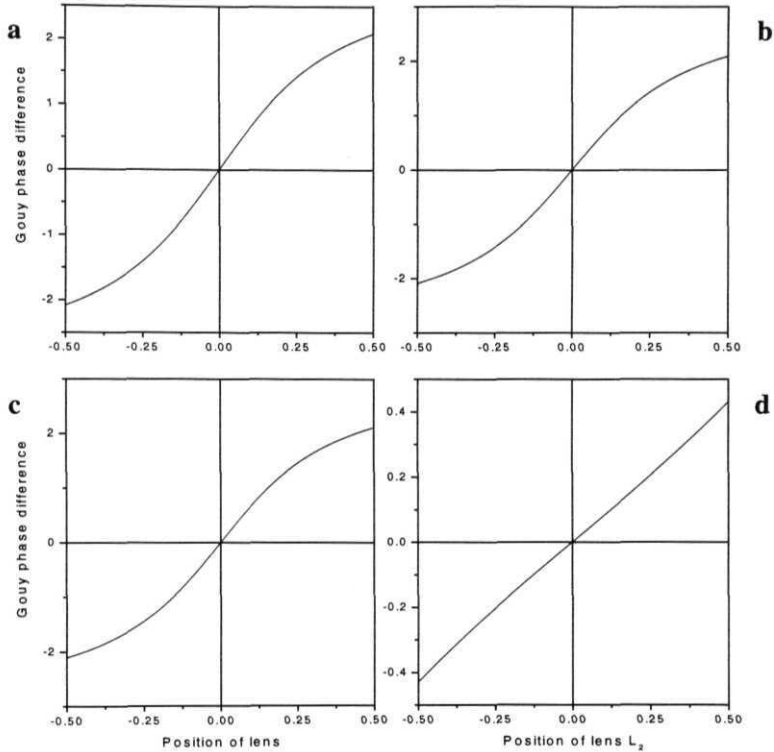
Fig.6.4a-d: In this figure we have shown the theoretical Gouy phase difference between the two beams, for our experimental setup, with the assumption that lens does not contribute to Gouy phase. a) Focal length of outside lens L_1 is 47.5cm. Focal length of inside lens L_2 is 10cm. Distance between lens L_1 and beam splitter is 8cm. b) Focal length of outside lens L_1 is 47.5cm. Focal length of inside lens L_2 is 10cm. Distance between lens L_1 and beam splitter is 10.5cm. c) Focal length of outside lens L_1 is 47.5cm. Focal length of inside lens L_2 is 6cm. Distance between lens L_1 and beam splitter is 8cm. d) There is no outside lens L_1. Focal length of inside lens L_2 is 6cm. Distance between the beam waist of input beam and beam splitter is 71.5cm. Observe that in the first three cases the Gouy phase difference is almost same with values between -2 and 2. In the case 'd' it is less with values between -0.4 and 0.4.
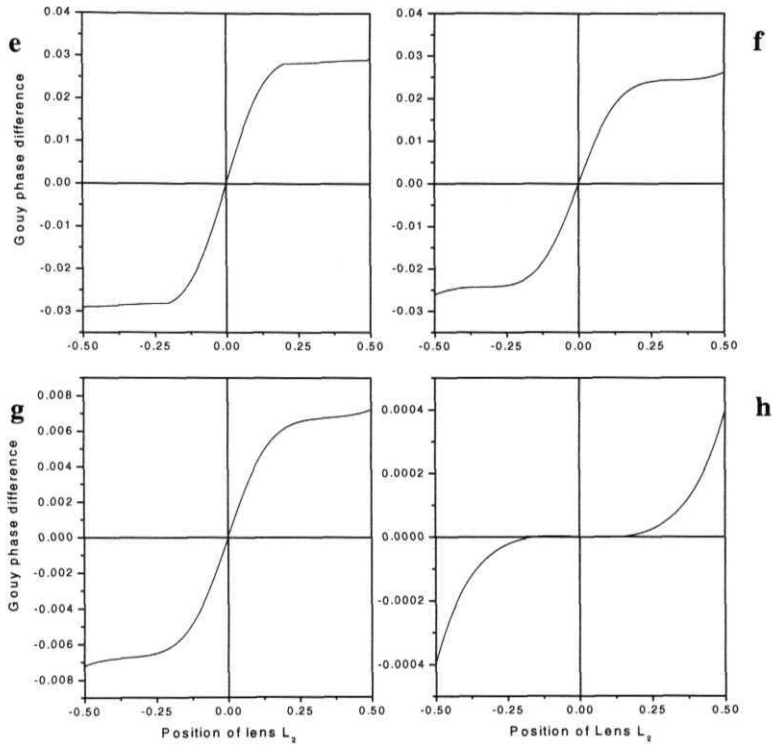
Fig.6.4e-h: In this figure we have shown the theoretical Gouy phase difference between the two beams with the assumption that lens contributes to Gouy phase. a) Focal length of outside lens L_1 is 47.5cm. Focal length of inside lens L_2 is 10cm. Distance between lens L_1 and beam splitter is 8cm. b) Focal length of outside lens L_1 is 47.5cm. Focal length of inside lens L_2 is 10cm. Distance between lens L_1 and beam splitter is 10.5cm. c) Focal length of outside lens L_1 is 47.5cm. Focal length of inside lens L_2 is 6cm. Distance between lens L_1 and beam splitter is 8cm. d) There is no outside lens L_1. Focal length of inside lens L_2 is 6cm. Distance between the beam waist of input beam and beam splitter is 71.5cm. Observe that unlike the cases 'a-d' here, in the first three cases 'e-f the Gouy phase difference is similar but not same. Observe that the difference in the case 'g' is small compared to the cases 'e' and 'f'. In the case 'h' the Gouy phase difference is further small of the order 10^{-4}. Also look at the order of difference in the curves a-d (-2 to2) and in the curves e-f (-0.03 to 0.03).
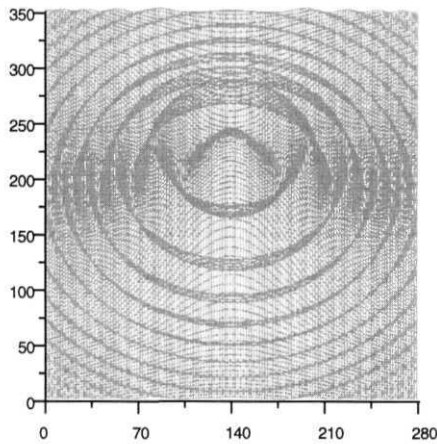
Fig. 6.5a: In this figure we show the intensity fringe pattern generated theoretically using eq. 6.8 assuming that lens does not contribute to Gouy phase. Here we took care of Gouy phase by adding the Gouy phase of different parts of the propagation of the two beams in the interferometer as given in ref. 6.6. Observe the central peak in the fringe pattern. This pattern is generated for a lens L_1 of focal length 47.5cm and a lens L_2 of focal length 10cm when L_1 is placed 8cm before the beam splitter and L_2 is placed 10cm away from the beam splitter along the counter clockwise direction. Detector is assumed to be 40cm away from the beam splitter in the output arm
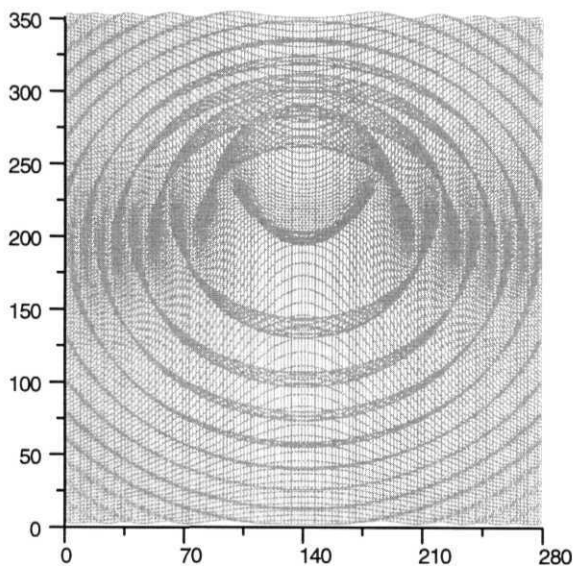
Fig. **6.5b:** In this figure we show the intensity fringe pattern generated theoretically using eq. 6.8 assuming that lens contributes to Gouy phase. Here we assumed that the vertical line representing the lens transformation also will contribute to Gouy phase. As a result the Gouy phase difference will depend only on the η values of the two beams at the detector. Observe the absence of central peak in the fringe pattern. This pattern is generated for a lens L_1 of focal length 47.5cm and a lens L_2 of focal length 10cm when L_1 is placed 8cm before the beam splitter and L_2 is placed 10cm away from the beam splitter along the counter clockwise direction. Detector is assumed to be 40cm away from the beam splitter in the output arm.
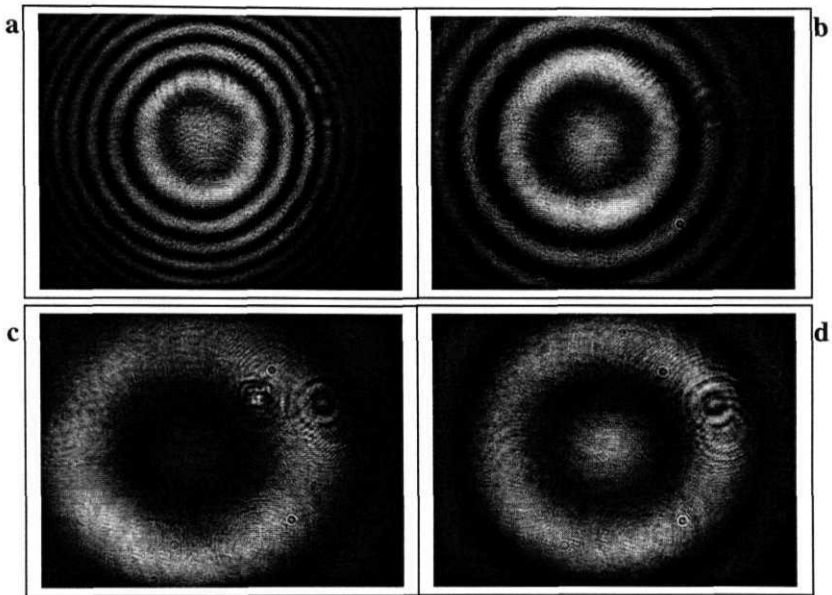
Fig.6.6a-d: Experimental intensity fringe pattern when a 10cm focal length lens is placed inside Sagnac interferometer. A 47.5cm focal length lens L_1 is placed before the interferometer. This is the case when the beam waist after lens L_1 falls short of the center of the Sagnac interferometer. a) The lens L_2 is placed at a distance $l_{11} = 8.7$cm from the beam splitter. b) $l_{11} = 26.2$cm. c) $l_{11} = 41.1$cm. d) $l_{11} = 60.6$cm. Observe the central bright fringe in the fringe pattern. Also note that this bright fringe is having different intensities.
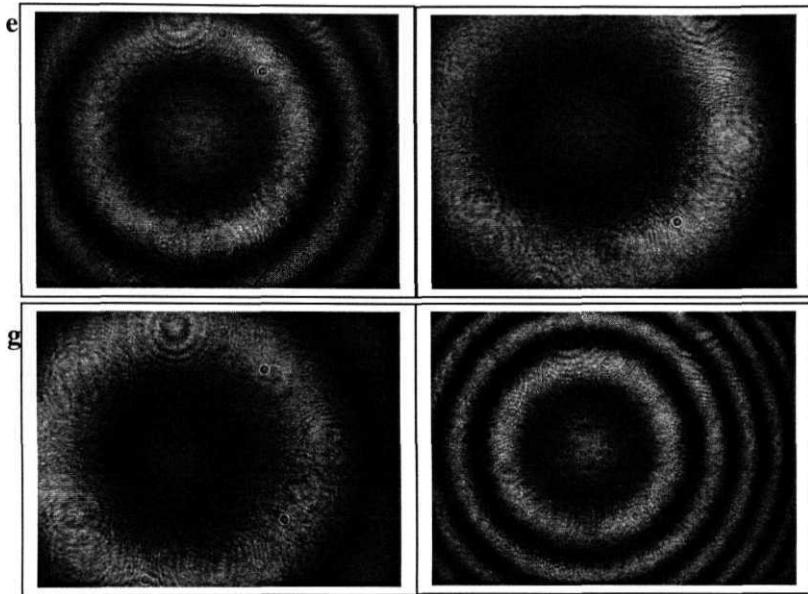
<u>Fig.6.6e-h</u>: Experimental intensity fringe pattern when a 6cm focal length lens is placed inside Sagnac interferometer. A 47.5cm focal length lens is placed before the interferometer. This is the case when the beam waist after lens L_1 falls short of the center of the Sagnac interferometer. This differs from fig.6.6a-d only in the focal length of lens L_2. e) The lens is placed at a distance $l_{11} = 33.2$cm from the beam splitter. f) $l_{11} = 42.2$cm. g) $l_{11} = 57.2$cm. h) $l_{11} = 75.8$cm. Observe the central bright fringe in the fringe pattern. Also note that this bright fringe is having different intensities. The intensity of the central bright fringe decreases as the lens moves towards the center of the interferometer and the size of the fringe increases. When the lens is exactly at the center of the interferometer the central fringe becomes dark as the fringe pattern disappears.
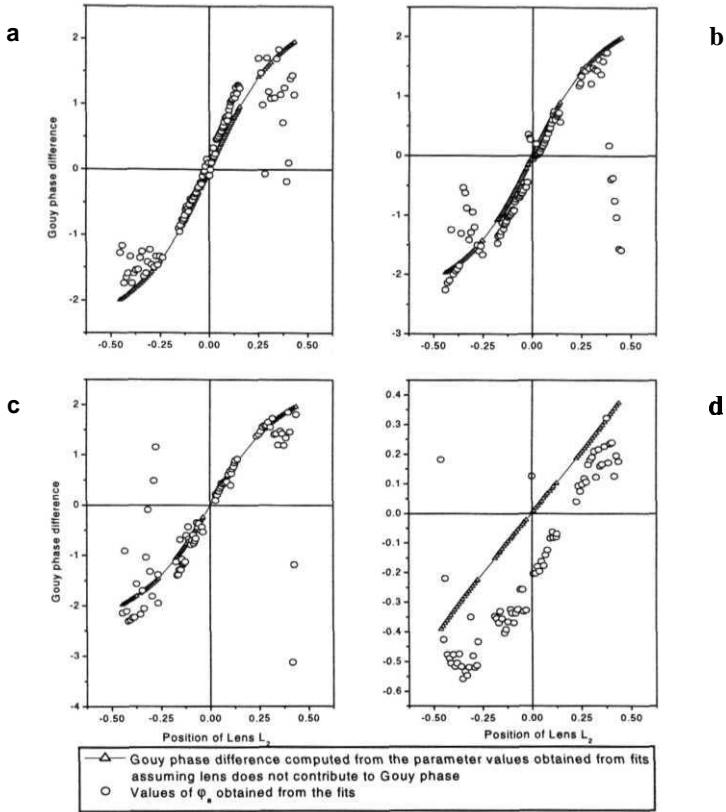
Fig.6.7a-d: In this figure we have shown the value of the phase φ_a (circles) obtained from the fits and the Gouy phase difference (triangles) computed using the values of parameters obtained from the fit. To distinguish squares from circles a solid line overlapping with triangles is **drawn.** a) Focal length of outside lens L_1 is 47.5cm. Focal length of inside lens L_2 is 10cm. Distance between lens L_1 and beam splitter is 8cm. b) Focal length of outside lens L_1 is 47.5cm. Focal length of inside lens L_2 is 10cm. Distance between lens L_1 and beam splitter is 10.5cm. c) Focal length of outside lens L_1 is 47.5cm. Focal length of inside lens L_2 is 6cm. Distance between lens L_1 and beam splitter is 8cm. d) There is no outside lens L_1. Focal length of inside lens L_2 **is** 6cm. Distance between the beam waist of input beam and beam splitter is 71.5cm. Observe the difference between the Gouy phase difference calculated from the fitted parameter values and the phase φ_a obtained directly from the fits. Observe the overlap of φ_a and the theoretical curve. From this one can infer that lens does not contribute to the Gouy phase.
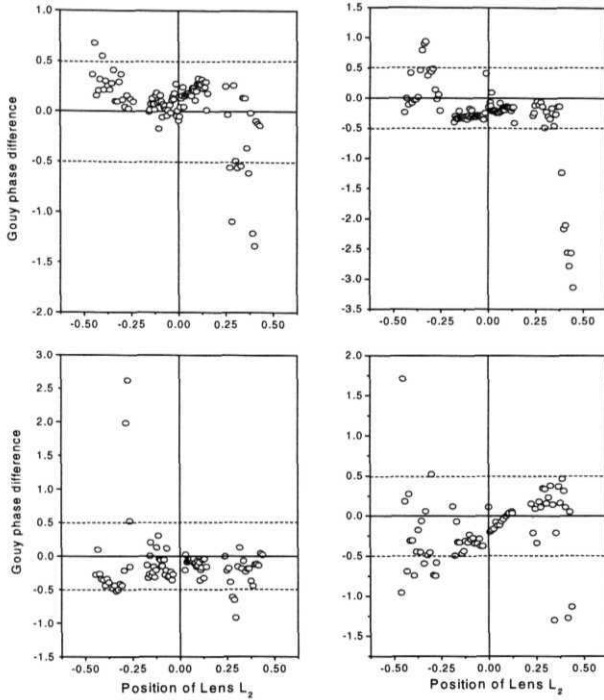
Fig.6.7e-f: In this figure we have shown the additional phase obtained from the fits. This additional phase is the difference between the Gouy phase (triangles in fig.6.7a-d) calculated using the parameter values obtained from the fits with the assumption that lens will not contribute to Gouy phase and the total additional phase φ_a obtained from the fit. Observe that the values of φ_r are within a range of -0.5 to 0.5. a) Focal length of outside lens L_1 is 47.5cm. Focal length of inside lens L_2 is 10cm. Distance between lens L_1 and beam splitter is 8cm. b) Focal length of outside lens L_1 is 47.5cm. Focal length of inside lens L_2 is 10cm. Distance between lens L_1 and beam splitter is 10.5cm. c) Focal length of outside lens L_1 is 47.5cm. Focal length of inside lens L_2 is 6cm. Distance between lens L_1 and beam splitter is 8cm. d) There is no outside lens L_1. Focal length of inside lens L_2 is 6cm. Distance between the beam waist of input beam and beam splitter is 71.5cm.
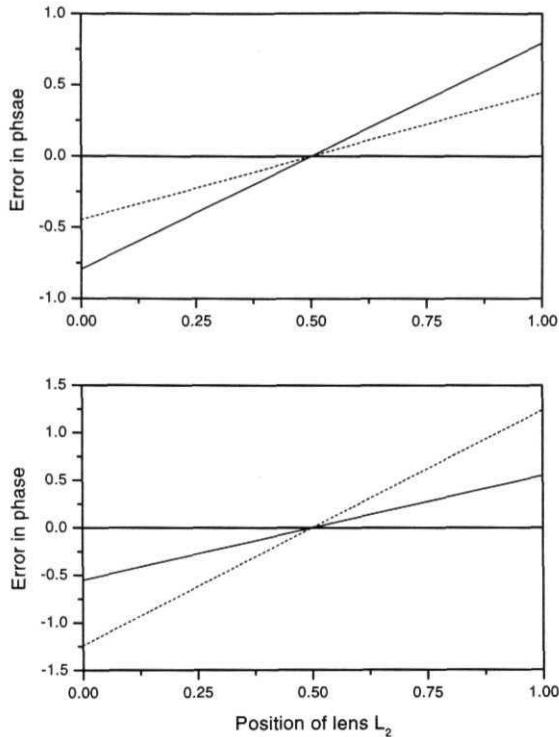
Fig.6.8a and b: In this figure we show the possible error in phase due to optical path difference when a lens is placed inside the Sagnac interferometer. The beams in the interferometer are parallel to each other but have displaced axes of propagation with respect to the center of the lens. As a result there will be some optical path difference at the detector since beams travel different distances after the lens in the interferometer.

a) In this case the focal length of the lens is 10cm. The solid line represents the case when the separation between the two axes is 60microns while the dashed line is for the case when this separation is 80microns.

b) In this case the focal length of the lens is 6 cm. The solid line represents the case when the separation between the two axes is 40microns while the dashed line is for the case when this separation is 80microns.

It is clear that for small displacement in the axes of propagation one can have an error in the phase due to optical path difference.
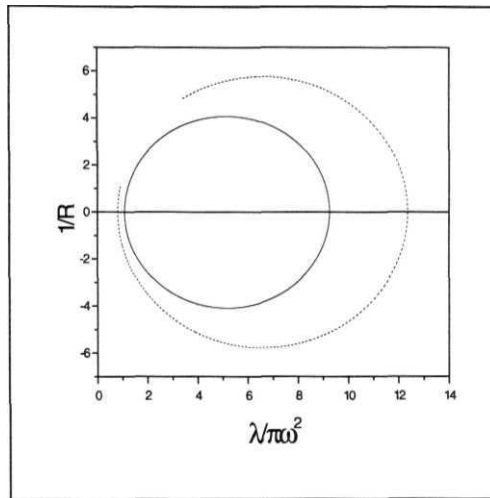
Fig. 6.9: In this figure we show the path taken by a Gaussian beam in a quadratic index medium. A quadratic index medium is placed at two different points along the input Gaussian beam. First at a distance of 5cm from the beam waist of the input beam and second at a distance 50cm from the beam waist of the input. The solid curve represents the path taken by the Gaussian beam in the first case and the dashed curve represents the beam in the second case. Observe that the paths taken by the beam are different when the quadratic index medium is kept at different places along the input beam. Also note that the circle are not touching the origin at all and their centers still lie on the real axis.

Conclusion

This thesis resulted from a study to understand the nonlinear behaviour of Pancharatnam's phase in a Sagnac interferometer and to understand the effect of Gouy phase on the interference pattern of a Sagnac interferometer. We developed three new applications using nonlinear behaviour of Pancharatnam's phase. The three new applications are 1) an interferometric switch, 2) double beam polarimeter and 3) an N-bit signal generator using slowly relaxing medium.

We have shown that Gouy phase accumulated in different sections of a multi-lens system add up. This proves the theoretical result of Erden and Ozaktas. We have also derived a theoretical result for a quadratic index medium using quantum mechanical disentangling procedure.

APPENDIX A

Poincare sphere shown in **fig.A1** is a spherical surface of unit diameter. The points on this sphere are in one-to-one correspondence with different states of polarization of light. This correspondence can be obtained in different methods. For example by using stereographic projection [A1] of a complex plane representation of polarization states onto a sphere of unit diameter or by using Stokes parameters [A2]. We follow the method given in **ref.A1** where the authors project a complex plane onto a sphere of unit diameter.

According to this representation North Pole of the **Poincaré** sphere represents the right circularly polarized light while the South Pole represents the left circularly polarized light. Equator represents all possible linear polarizations. The points on the upper hemisphere represent all possible right elliptic polarizations while the lower hemisphere represents left elliptic polarizations. Any two diametrically opposite states on this sphere are orthogonal to one another and hence can be used as basis states.

We choose linear polarization along the x and y directions (of chapter II) on the equator as the basis states. Let the point X in fig.Al represent the linear polarization in x direction. Then a point Y diagonally opposite to the point X on the equator will represent the linear polarization in y direction. The longitudes are measured with respect to the point X i.e., the longitude (a) passing through X is the 0° longitude and the one passing through the point Y is a $180°$ longitude. North Pole is the 90° latitude ((3) while the South Pole is the -90° latitude with the equator at 0° latitude.

An elliptic polarization with azimuth a and ellipticity β is represented by the point P = (2a, 2β) on this sphere (**figs.A1** and A2). This is because the angle of longitude is double the angle of azimuth and the angle of the latitude is double the angle of ellipticity. The point X is given by (2a, 2β) = (0°, 0°) and the point Y by $(180°, 0°)$. Thus each point represents a unique polarization state. Equi-azimuth lines

are the longitudes and the **equi-ellipticity** curves are the latitudes. Now one can trace the changes in the polarization of a light wave as it propagates in optical systems.

When an optical element OE, with preferential axis, like wave plate or polarizer is placed in the path of polarized light, its position with respect to the reference point X, is determined by the angle made by the preferential axis with the x-axis. If the preferential axis is making an angle y with the x direction then the point representing OE will be at an angle 2y from the point X (fig.A2) on the equator.

We now give some examples explaining how one can use a Poincare sphere. Consider a polarizer to be placed in the path of an elliptically polarized light with azimuth a and ellipticity β (represented by the point $P_1 = (2\alpha, 2\beta)$ on the Poincare sphere shown in fig.A2). Let the polarizer be represented by the point P on the equator, which is at an angle 2y from the point X and hence lies on the longitude 2y. The component of P_1 passing through the polarizer is given by the shortest arc connecting the two points P_1 and P. This will lie on the great circle passing through these two points. A great circle passing through points on a sphere is the circle passing through the points on the sphere such that the plane of the circle divides the sphere into two hemispheres. The sphere and great circles are concentric.

Now consider (in **fig.A3**) a wave retarder placed in the path of an elliptically polarized light represented by a point P on the Poincare sphere. Let the fast axis of the retarder make an angle γ with the x-axis. Therefore, it is represented by a point R on the equator at an angle 2y from the point X. This retarder changes the polarization of the light wave. To determine the change occurring due to it we connect the points R and P by the shortest possible arc, which lies on the great circle passing through the point R and the point P. The transformation due to the retarder takes place along the arc PP'. P' is the polarization of the light after the retarder. This arc PP' is in a plane, which is perpendicular to the plane containing the points R, P and the center, C of the Poincar6 sphere. The length of the arc PP' (in angles) is equal to the retardation strength. The lengths of the arcs RP and RP' are equal. Thus a quarter wave retarder

will take the point P to the point P_q, which is at an angle 90° from P along the arc PP_q. A half wave retarder will take the point P to a diagonally opposite point P_h, which is at an angle of 180° from the point P. Note that the paths taken are in the anti-clockwise direction with respect to the position of the optical element (wave retarder in this case).

We have given examples, which help to understand the different processes considered in the present thesis.

References:

A1. **R. M.** A. Azzam and N. M. Bashara, Ellipsometry and polarized light, North-Holland, 1977.

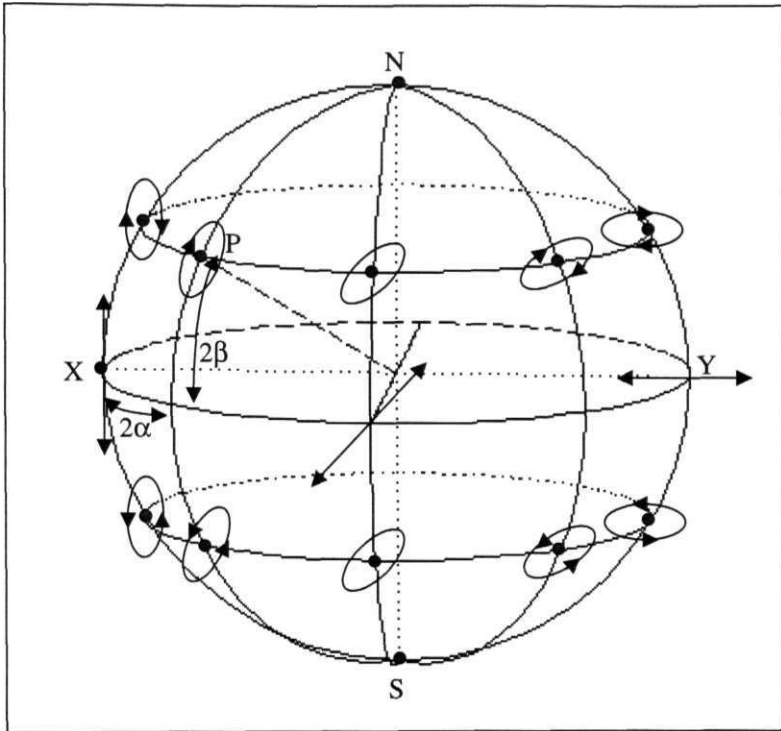A2. M. Born and E. Wolf, Optics, Pergamon press, Sixth (Corrected) edition, 1989

Fig.A1:This figure shows the Poincare sphere representation of polarization states. N represents the right circularly polarized light, S represents the left circularly polarized light. Equator represents all possible states of linearly polarized light. Point P represents elliptically polarized light when the angles are measured from the point X representing the horizontal linear polarization. Point P is on the longitude 2a and on the latitude 2β. Equi- azimuth lines are the longitudes and equi-ellipticity curves are the latitudes. Note we may not have shown the ellipticities to the scale. The ellipses on the latitudes and longitudes are shown just to show the equi-ellipticity and equi-azimuth curves. The points in the upper hemisphere represent right elliptic polarizations while the points in the lower hemisphere represent the left elliptic polarizations.
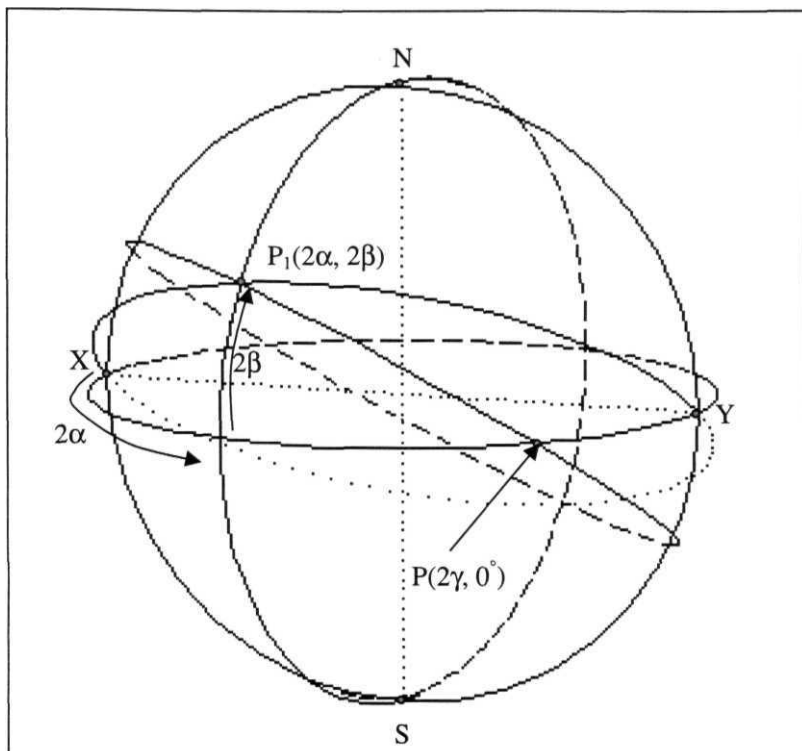
Fig.A2: This figure shows an elliptic polarization state P_1 (2a, 2(3). This state is of azimuth a and ellipticity β. This state may be described as a linear superposition of the two orthogonal polarizations namely X and Y, which are the chosen basis set for all possible polarizations. The arc P_1X gives the X-component of P_1 and the arc P_1Y gives the Y-component. In this figure we also show a polarizer on the Poincare sphere. P is the point representing the polarizer and is at an angle 2γ from the point X on the equator. The component of P_1 passing through P is given by the arc P_1P.
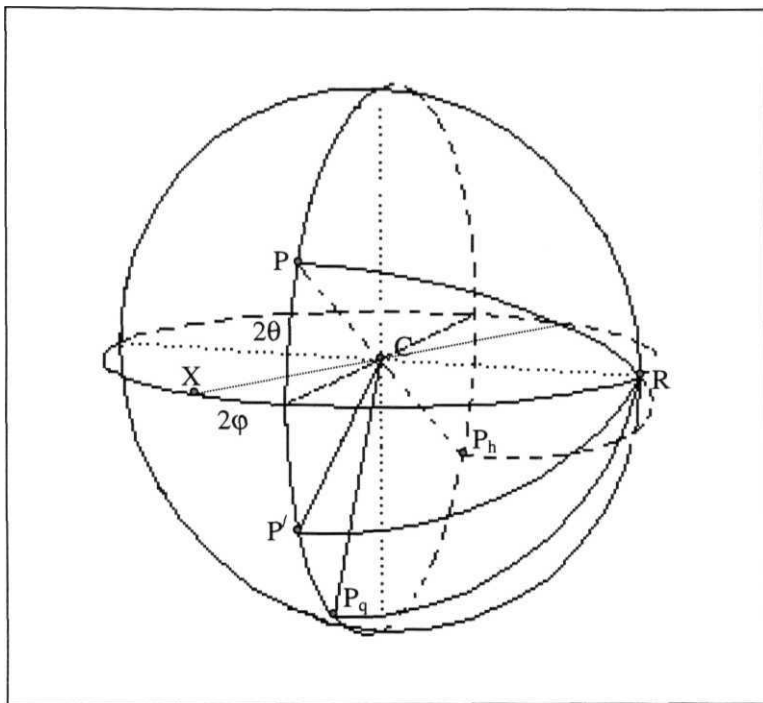
<u>Fig.A3</u>: in this figure we show the transformation of polarization by a wave retarder. P is the input polarization. R is the position of the wave retarder on the equator. The path, which the beam traverses on the sphere, is in the anti clockwise direction with respect to R. Therefore it moves along the arc $PP'P_qP_h$. If the retarder strength is 8, then the polarization changes to P', which is at an angle 2δ from P. If the $\tilde{\delta}$ = rc/2, then the final polarization state will be P_q, which is at an angle 90° from P. Similarly for $8 = \pi$ the polarization changes from P to P_h along the arc $PP'P_qP_h$. Note that the arc $PP'P_qP_h$ is in a plane perpendicular to the plane containing the points R, P and C where, C is the center of the Poincare sphere. The arcs RP, RP', RP_q and RP_h have same length.

APPENDIX B

We have used a 4x4 matrix method for doing the calculations in the thesis. All the intensity expressions are obtained from these calculations. We have not shown the matrices used in the chapters. Here, in this appendix, we give the matrices used in deriving the expressions in different chapters of the thesis. Recall that we have introduced a right handed Cartesian coordinate system attached to the beams in chapter II. The x-axis in that system is perpendicular to the plane of interferometer and y-axis is parallel to the plane of interferometer while, z-axis is the direction of propagation. The input matrix is given by $E_i = (E_\parallel^1, E_\perp^1, E_\parallel^2, E_\perp^2)^T$ as explained in Introduction

I. Four-arm Sagnac Interferometer:

Consider the case of a four-arm Sagnac interferometer in which an optical element is placed as shown in fig.B.l. The beam encounters the beam splitter twice and there are two beams passing through the interferometer in opposite directions. This beam splitter is a 50:50 non-polarizing beam splitter. Following the procedure given in the introduction the following matrices are constructed. The matrices representing the optical path include the effect of mirrors encountered within that path length.

The beam splitter matrix is given by, $\mathbf{B_s} = \begin{bmatrix} r_\parallel & 0 & it_\parallel & 0 \\ 0 & r_\perp & 0 & it_\perp \\ it_\parallel & 0 & r_\parallel & 0 \\ 0 & it_\perp & 0 & r_\perp \end{bmatrix}$.

Here r's and t's are the reflection and transmission coefficients of the beam splitter. The II component represents the component parallel to the x-axis and the $\perp$ component is the y-component. This notation is same through out.

For optical path matrix before optical element we have

$$
P_{41} \;=\; \begin{bmatrix}
e^{i\Delta_1} & 0 & ie^{i\Delta_1} & 0 \\
0 & -e^{i\Delta_1} & 0 & ie^{i\Delta_1} \\
ie^{i\Delta_2} & 0 & e^{i\Delta_2} & 0 \\
0 & ie^{i\Delta_2} & 0 & e^{i\Delta_2}
\end{bmatrix}
$$

Here Δ_1 is the phase due to optical path from the beam splitter till the optical element for the anti-clockwise beam, while Δ_2 is for the clockwise beam.

The optical element matrix is given by

$$
E \;=\; \begin{bmatrix}
oe_{11} & oe_{12} & 0 & 0 \\
oe_{13} & oe_{14} & 0 & 0 \\
0 & 0 & oe_{21} & oe_{22} \\
0 & 0 & oe_{23} & oe_{24}
\end{bmatrix}
$$

Here oe_{1i} are the elements of the transformation matrix of the optical element for the anti-clockwise beam and oe_{2j} are the elements of the transformation matrix for the clockwise beam.

1) For the retarder plate the transformation matrix elements are given by

$oe_{11} = oe_{21} = \cos^2\varphi + e^{i\delta}\sin^2\varphi$; $\qquad oe_{14} = oe_{24} = \sin^2\varphi + e^{i\delta}\cos^2\varphi$

$oe_{12} = oe_{13} = -oe_{22} = -oe_{23} = \cos\varphi\,\sin\varphi\,(1 - e^{i\delta})$

where, δ is the retardation strength. $\delta = \pi/2$ represents a quarter wave plate while $\delta = \pi$ represents a half wave plate and φ is the angle made by the fast axis of the wave plates with the x-axis.

2) For a linear polarizer the transformation matrix elements are

$oe_{11} = oe_{21} = \cos^2\varphi \qquad\qquad oe_{14} = oe_{24} = \sin^2\varphi$

$oe_{12} = oe_{13} = -oe_{22} = -oe_{23} = \cos\varphi\,\sin\varphi$

where (p is the angle made by the axis of the polarizer with the x-axis.

3) For optically active medium the transformation matrix elements are

$oe_{11} = oe_{21} = oe_{14} = oe_{24} = \cos\varphi;$ $oe_{12} = -oe_{13} = oe_{22} = -oe_{23} = \sin\varphi$

where (p is the angle by which the input polarization is rotated.

Optical path matrix after the optical element: P_{42} =
$$\begin{bmatrix} e^{i\Delta_2'} & 0 & ie^{i\Delta_2'} & 0 \\ 0 & e^{i\Delta_2'} & 0 & ie^{i\Delta_2'} \\ ie^{i\Delta_1'} & 0 & e^{i\Delta_1'} & 0 \\ 0 & ie^{i\Delta_1'} & 0 & -e^{i\Delta_1'} \end{bmatrix}$$

Here Δ_2 is the phase due to optical path, for the anti-clockwise beam, after the optical element till the beam splitter, while A/ is for the clockwise beam.

The total matrix for the four-arm Sagnac interferometer is

$$S4 = \mathbf{B_s}\, P42\, E\, \mathbf{P_{41}}\, \mathbf{B_s}.$$

n. Three-arm Sagnac interferometer:

Consider the case of a three-arm Sagnac interferometer in which an optical element is placed as shown in fig.B.2. The beam splitter matrix will be same as the $\mathbf{B_s}$ for the four-arm case as the beam splitter used in this case also a 50:50 non-polarizing beam splitter.

Optical path matrix before optical element: $\mathbf{P_{31}}$ =
$$\begin{bmatrix} e^{i\Delta_1} & 0 & ie^{i\Delta_1} & 0 \\ 0 & -e^{i\Delta_1} & 0 & ie^{i\Delta_1} \\ ie^{i\Delta_2} & 0 & e^{i\Delta_2} & 0 \\ 0 & ie^{i\Delta_2} & 0 & -e^{i\Delta_2} \end{bmatrix}$$

Where Δ_1 is the phase due to optical path, for the anti-clockwise beam, before optical element from the beam splitter, while Δ_2 is for the clockwise beam.

Optical element matrix:
$$E = \begin{bmatrix} oe_{11} & oe_{12} & 0 & 0 \\ oe_{13} & oe_{14} & 0 & 0 \\ 0 & 0 & oe_{21} & oe_{22} \\ 0 & 0 & oe_{23} & oe_{24} \end{bmatrix}$$

Here oe_{1i} (i=1, 4) are the elements of the transformation matrix of the optical element for the anti-clockwise beam and oe_{2j} (j=1, 4) are the elements of the transformation matrix for the clockwise beam and are same as for the four-arm case.

Optical path matrix after optical element:
$$P_{32} = \begin{bmatrix} e^{i\Delta_2'} & 0 & ie^{i\Delta_2'} & 0 \\ 0 & -e^{i\Delta_2'} & 0 & ie^{i\Delta_2'} \\ ie^{i\Delta_1'} & 0 & e^{i\Delta_1'} & 0 \\ 0 & ie^{i\Delta_1'} & 0 & -e^{i\Delta_1'} \end{bmatrix}$$

Here Δ_2' is the phase due to optical path, for the anti-clockwise beam, after the optical element till the beam splitter, while A/ is for the clockwise beam.

The total matrix for the four-arm Sagnac interferometer is

$$S_3 = B_s\, P_{32}\, E\, P_{32}\, B_s.$$

We have also considered four-arm and three-arm Sagnac interferometer cases with polarizing beam splitters. These polarizing beam splitters are not represented by the matrix B_s.

Polarizing Beam splitter matrix:
$$B_s' = \begin{bmatrix} r & 0 & 0 & 0 \\ 0 & 0 & 0 & t \\ 0 & 0 & r & 0 \\ 0 & t & 0 & r_\perp \end{bmatrix}$$

Where r's and t's are the reflection and transmission coefficients of the beam splitter

HI. Sagnac Interferometric Switch

In this case we have a three-arm setup as shown in fig.B2. In the output arm of this interferometer we place a linear analyzer. Note that the matrices representing the optical elements placed in the output arm will be slightly different from the matrix of the same element placed in the interferometer. This is because when the element is inside the counter propagating beams see the element differently, whereas here, both the beams see the element in the same way. The matrix for this linear analyzer is

$$
L = \begin{bmatrix}
\cos^2 \eta & \cos \eta \sin \eta & 0 & 0 \\
\cos \eta \sin \eta & \sin^2 \eta & 0 & 0 \\
0 & 0 & \cos^2 \eta & \cos \eta \sin \eta \\
0 & 0 & \cos \eta \sin \eta & \sin^2 \eta
\end{bmatrix}
$$

Here η is the angle made by the axis of the polarizer with the x-axis.
The total matrix for the interferometric switch

$$
S_w = L\, S_3
$$

IV. Double Beam Polarimeter.

In this case we have a four-arm **Sagnac** interferometer (fig.Bl) with optically active medium as the optical element and along with that we have a quarter wave plate and a linear analyzer in the output arm. The linear analyzer matrix is same as in the above case. The matrix for the quarter wave plate placed in the output is

$$
Q = \begin{bmatrix}
\cos^2 \varphi - i \sin^2 \varphi & \cos \varphi \sin \varphi (1-i) & 0 & 0 \\
\cos \varphi \sin \varphi (1-i) & \sin^2 \varphi - i \cos^2 \varphi & 0 & 0 \\
0 & 0 & \cos^2 \varphi - i \sin^2 \varphi & \cos \varphi \sin \varphi (1-i) \\
0 & 0 & \cos \varphi \sin \varphi (1-i) & \sin^2 \varphi - i \cos^2 \varphi
\end{bmatrix}
$$

The total matrix in this case is given by $\qquad S_p = L\,Q\,S_4$

V. N-bit Signal:

Consider the fig.B3. Here we have two nonlinear retarders placed between two quarter wave plates inside the Sagnac interferometer. The quarter wave plates are at ±45 for a beam going through them. The construction of the matrices here will be slightly different. The matrices representing the optical elements here will not represent a single element. Let us label the elements in the order in which the anti-clockwise beam sees them. The first quarter wave plate is labeled as '1', then the first nonlinear retarder as '2', the second nonlinear retarder as '3' and the second quarter wave plate is labeled as '4'. These elements are placed symmetrically inside the Sagnac interferometer. We will not consider the optical paths between these elements but include them in the optical path matrices representing the paths before and after this 1-4 element set.

Now lets look at the construction of the matrices. Refer to the construction of optical path matrices in the introduction. In a similar way we construct the matrices here. As there is no reflection from the optical elements we will have only block diagonal matrices. The anti-clockwise beam first sees element 1 while the clockwise beam sees the element 4. Therefore our first matrix will have 2x2 matrices representing the elements 1 and 4 for the two beams respectively arranged along the diagonal of the matrix shown below.

$$E_{14} = \begin{bmatrix} oe1_{11} & oe1_{12} & 0 & 0 \\ oe1_{13} & oe1_{14} & 0 & 0 \\ 0 & 0 & oe4_{21} & oe4_{22} \\ 0 & 0 & oe4_{23} & oe4_{24} \end{bmatrix}$$

Where $oe1_{1j}$ (j=1, 4) are the elements of the transformation matrix of the element 1 for the anti-clockwise beam and $oe4_{2j}$ are of element 4 for the clockwise beam. These elements are same as those given in the four-arm case.

The second matrix is given by

$$E_{23} = \begin{bmatrix} oe2_{11} & oe2_{12} & 0 & 0 \\ oe2_{13} & oe2_{14} & 0 & 0 \\ 0 & 0 & oe3_{21} & oe3_{22} \\ 0 & 0 & oe3_{23} & oe3_{24} \end{bmatrix}$$

Where $oe2_{1j}$ (j=1, 4) are the elements of the transformation matrix of the element 2 for the anti-clockwise beam and $oe3_{2j}$ are of element 3 for the clockwise beam.

The third matrix is given by

$$E_{32} = \begin{bmatrix} oe3_{11} & oe3_{12} & 0 & 0 \\ oe3_{13} & oe3_{14} & 0 & 0 \\ 0 & 0 & oe2_{21} & oe2_{22} \\ 0 & 0 & oe2_{23} & oe2_{24} \end{bmatrix}$$

Where $oe3_{1j}$ (j=1, 4) are the elements of the transformation matrix of the element 3 for the anti-clockwise beam and $oe2_{2j}$ are of element 2 for the clockwise beam.

The fourth matrix is given by

$$E_{41} = \begin{bmatrix} oe4_{11} & oe4_{12} & 0 & 0 \\ oe4_{13} & oe4_{14} & 0 & 0 \\ 0 & 0 & oe1_{21} & oe1_{22} \\ 0 & 0 & oe1_{23} & oe1_{24} \end{bmatrix}$$

Where $oe4_{1j}$ (j=1, 4) are the elements of the transformation matrix of the element 4 for the anti-clockwise beam and $oe1_{2j}$ are of element 1 for the clockwise beam.

After the Sagnac interferometer we have a linear polarizer in the output arm. **Its** matrix is same as L given earlier. Therefore the final output matrix is given by

$$S_s = L \; B_s \; P_{32} \; E_{41} \; E_{32} \; E_{23} \; E_{14} \; P_{31} \; B_s$$

APPENDIX C

In chapters III and IV nonlinear change in the area of spherical triangle on Poincare sphere is discussed. A calculation of how this nonlinear change occurs is given below. Consider a spherical triangle P_1AP_2 (fig. C.1). P_1 and P_2 are on either side of the equator and A is on the equator of the Poincare sphere. The change in the area of this spherical triangle as the point A moves along the equator is of interest to us.

According to spherical trigonometry on a sphere of radius R, the area of a spherical triangle P_1AP_2 is given by

$$\text{Area} = R^2 \left(\angle P_1 + \angle P_2 + \angle A - \pi \right) \tag{C.1}$$

where $\angle P_1$, $\angle P_2$ and ZA are the inner angles. Let the points P_1, P_2 and A be given in terms of longitude and latitude by $(-a,, \beta_1)$, $(\alpha_1, -\beta_1)$ and $(a, 0)$ respectively. The longitude of 0 is taken to be passing through the midpoint I (of P_1P_2) on the equator. (The point I represents the polarization state of the input beam of the experiments in chapters III and IV). This (fig. C.1) is the case studied in chapter HI. The inner angle of the spherical triangle at A is given by the dot product of the vectors at A. The vectors are, respectively, normal to the planes containing the great circles passing through P_1A and P_2A.

$$\angle A = \cos^{-1}\left[-\frac{\sin^2\beta_1 - \sin(\alpha - \alpha_1) \sin(\alpha + \alpha_1) \cos^2\beta_1}{\left(\sin^2\beta_1 + \sin^2(\alpha - \alpha_1) \cos^2\beta_1\right)^{1/2} \left(\sin^2\beta_1 + \sin^2(\alpha + \alpha_1) \cos^2\beta_1\right)^{1/2}} \right] \tag{C.2}$$

Similarly the angle at P_1 (P_2) is given by dot product of the vectors at P_1 (P_2), normal to the planes containing the great circles passing through P_1P_2 and P_1A (P_1P_2 and P_2A). These are given by

$$\angle P_{1} = \cos^{-1}\left[\frac{\cos\alpha\,\sin^{2}\beta_{1} - \sin\alpha_{1}\,\sin(\alpha - \alpha_{1})\,\cos^{2}\beta_{1}}{\left(\sin^{2}\beta_{1} + \sin^{2}\alpha_{1}\,\cos^{2}\beta_{1}\right)^{1/2}\left(\sin^{2}\beta_{1} + \sin^{2}(\alpha - \alpha_{1})\,\cos^{2}\beta_{1}\right)^{1/2}}\right]$$

(C3)

$$\angle P_{2} = \cos^{-1}\left[\frac{\cos\alpha\,\sin^{2}\beta_{1} + \sin\alpha_{1}\,\sin(\alpha + \alpha_{1})\,\cos^{2}\beta_{1}}{\left(\sin^{2}\beta_{1} + \sin^{2}\alpha_{1}\,\cos^{2}\beta_{1}\right)^{1/2}\left(\sin^{2}\beta_{1} + \sin^{2}(\alpha + \alpha_{1})\,\cos^{2}\beta_{1}\right)^{1/2}}\right]$$

(C.4)

The case $\alpha_1 = 0$ represents the experiment of chapter IV.

The variation in the area of the spherical triangle obtained by using eqs.C.2-4 in eq.C.l, for different positions of A is shown in fig.C.2 for two cases: 1) $\beta_1 = -5$ and 2) $\beta_1 = -90°$. The variation in area is nonlinear in the first case and linear in the second case. First case is relevant to chapter HI and IV. The exact linear variation of area for $\alpha_1 = 0°$ and $\beta_1 = 90°$ is easy to grasp as in this case the movement of A on the equator corresponds to the linear movement of a longitude connecting the North Pole to the South Pole. Nonlinear behaviour is pronounced for $\beta_1 \approx 0$. Now the rate at which P_1A and P_2A move to cover the area on the sphere for a change in the position of A near the diametrically opposite point to I is not linear.
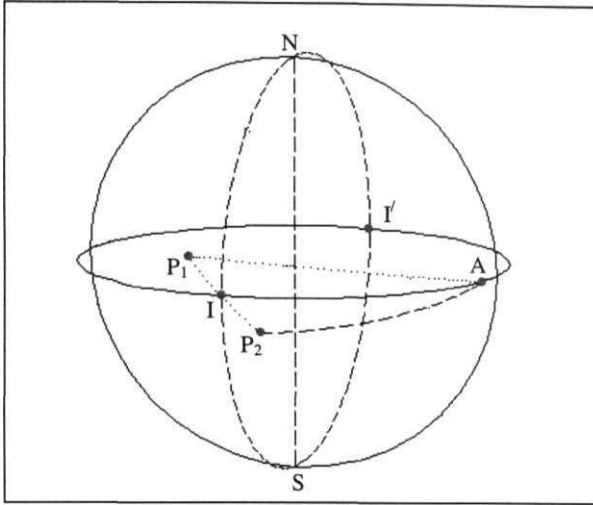
Fig.Cl: Poincare sphere showing the area of the spherical triangle P_1AP_2, on the surface of the sphere. $P_1(-\alpha_1, \beta_1)$, $P_2(+\alpha_1, -\beta_1)$ and $A(\alpha, 0)$.
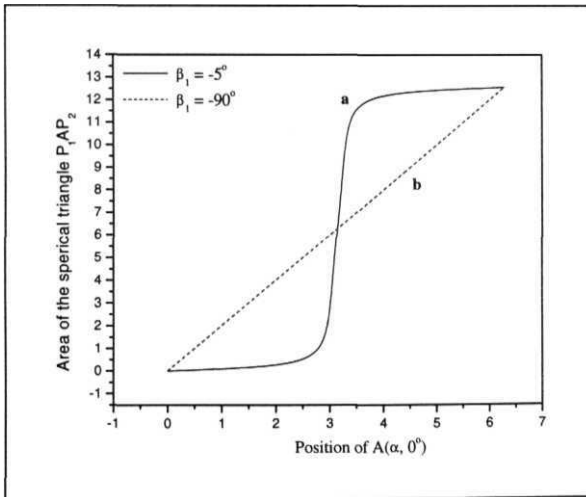

Fig.C2: Variation in the area of the spherical triangle P_1AP_2 in fig.Cl as the point A moves on the equator. a) is for $\beta_1 = -5°$ and b) is for $\beta_1 = -90$.